OPTIMIZATION OF THE WARM UP PROCESS OF THE COMPRESSION MOULDS FOR THE TYRE MANUFACTURING INDUSTRY.

Submitted in fulfilment of the requirements of the degree of Master of Engineering: Mechanical Engineering in the Faculty of Engineering and the Built Environment at the Durban University of Technology

Happy Christian Tshimbiluni

2016

Supervisor: Prof. P. Tabakov

Co-Supervisor Mr G. Thurbon

Declaration

I, Happy Christian Tshimbiluni, declare that:

I. This dissertation has not been submitted for any examination at any other university.

II. The research work presented in this dissertation besides where otherwise indicated, is my original research work.

III. This dissertation does not contain graphics, text, or tables that are copied from the internet, unless specifically acknowledged, and the source being indicated in the dissertation and in the bibliography.

Student: Happy Christian Tshimbiluni

Signature: ..... Date: .....

As the student's supervisor I agree to the submission of this thesis.

Supervisor: Prof. P. Tabakov

Signature: ..... Date: .....

As the student's co-supervisor I agree to the submission of this thesis.

Co-Supervisor: Mr G. Thurbon

Signature: ..... Date: .....

ACKNOWLEDGEMENT

Behind every success, there is an inspiration or support of at least one person. In my case, it was a group of people including my mentor, my co-supervisor, Apollo-Dunlop staff and my family. First and foremost, I would like to acknowledge the guidance, wisdom and support of my mentors, Prof P. Tabakov and Mr G. Thurbon. I have been very fortunate to have had the opportunity to work so closely with mentors that have so much to offer and are willing to share it so freely. This dissertation would not have been possible without their valuable suggestions throughout the duration of this study. Their vast experience and keen input has been a motivational support for me. Second of all, I do not think many mentors would go to Apollo-Dunlop tyres (Pty) Ltd manufacturing factory to help their student with running an experiment. Whenever I had any problem, I knew I could talk to them and they would help me to find the solution.

I would like to express my thanks to all personnel from the truck bus radial (TBR) workshop at Apollo-Dunlop tyres (Pty) Ltd. Mr T. Govender and Miss P. Mhlongo have greatly contributed to the outcome of the study, and have provided extremely beneficial technical and educational knowledge and experience. In addition, I would like to especially thank Mr B. Ngema and Mr E. Baloyi for their support - technical, educational, and moral.

Last and certainly not least, I have to thank my parents for their unconditional support and encouragement. I would also not ever have been in a position to complete this dissertation without the support of my family. They played a crucial part throughout my educational journey. My parents supported and understood my long periods of my absence as I worked long and hard to bring this study to its completion.

ABSTRACT

Pneumatic tyres are of major importance in the modern life. It is estimated that over one billion tyres are manufactured worldwide annually. The manufacturing process is rather power consuming one, mainly to a curing operation taking place in a press dome. The tyre compression mould warm up process is a powerful heat transfer technique. Saturated steam is fed into a press dome to directly transfer heat energy into the prismatic container through convection and conduction heat transfer.

This dissertation concerns the work done at Apollo-Dunlop tyres, the tyre compression mould warm up process was optimised to reduce the high energy cost. A heat transfer numerical analysis was carried out to investigate the steam quantity required to warm up the tyre compression mould from an ambient temperature ($_1 = 25^0$ C) to operational temperature ($_2 = 151^0$ C). Thereafter, an experimental work was performed to investigate the actual duration required to warm up the tyre compression mould to the operational temperature. This was achieved by establishing a temperature profile of the tyre compression mould during the warm up session. The numerical analysis and the experimental results were correlated to create a new warm up process with reduced steam consumption and warm up duration. The new warm up process was tested and the results are furnished in this study (see ***Appendix B*** for the performance results sheet). Apollo-Dunlop tyres (Pty) Ltd reduced a five hour tyre compression mould warm up process to a three hour process. The implementation of the proposed reduced warm up process occurred after the research work in this paper was presented to Apollo-Dunlop tyres (Pty) Ltd board members. This work was acknowledged by the company management and a new technological process has been implemented (***Appendix A*** for the relevant documents, note: the specifications sheet show the warm-up duration as four hours, but the actual operational warm up duration is five hours). A cost saving analysis on energy usage was carried out to indicate that Apollo–Dunlop tyres will currently save approximately around about 0.64 million per year after implementing this study.

Table of Content

Nomenclature

Q	Heat energy	[kW]
c_p	Specific heat capacity of water	[kJ/kg.k]
M	Mass	[kg]
ΔT	Temperature difference	[T^0 C]
Q_T	Total heat energy	[kJ]
h_{fg}	Specific enthalpy change of evaporation	[kJ/kg]
ρ	Density	[kg/m^3]
V	Volume	[m^3]
T_1	Initial temperature	[T^0 C]
T_2	Operational temperature	[T^0 C]
Q_{pm}	Heat energy of the plated mould adjuster	[kJ]
M_p	Platen mass	[kg]
Q_{pc}	Prismatic container	[kJ]
Q_{PB}	Prismatic bars	[kJ]
M_m	Mould mass	[kg]
Q_{CM}	Heat energy of the compression mould	[kJ]
R	Thermal resistance	[K/W]

λ	Thermal conductivity	[W/mK]
ε	Surface emissivity	
t	Insulation thickness	[mm]
A	Solid surface area	[m^2]
t_w	Wall thickness	[mm]
$\propto$	Heat transfer coefficient	[W/m^2K]
δ_A	Thickness of fluid A film	[mm]
δ_B	Thickness of fluid B film	[mm]
U	Overall heat transfer coefficient	[W/m^2K]
V	Potential difference	[v]
I	Current	[A]
A_0	Outside surface area	[m^2]
α_0	Heat transfer coefficient for the outside surface	[W/m^2K]
A_i	Inside surface area	[m^2]
α_i	Heat transfer coefficient for the inside surface	[W/m^2K]
r	Radius	[mm]
r_m	Geometric mean radius	[mm]
$R_{PD\ WALL}$	Thermal resistance of the pressure dome	[K/W]

$R_{AIR\ GAP}$	Thermal resistance of the air gap	[K/W]
$R_{GALV\ COVER}$	Thermal resistance of the galvanized cover	[K/W]
$R_{AIR\ FILM}$	Thermal resistance of the air film	[K/W]
R_T	Total thermal resistance	[K/W]
$R_{PD\ WALL}$	Thermal resistance of the pressure dome wall	[K/W]
m_s	Steam mass	[kg]
m_T	Total steam	[kg]
F_X	Tangential force variation	[N]
F_Y	Lateral force variation	[N]
F_Z	Radial force variation	[N]
G_r	Grashof number	
P_r	Prandtl number	
$\bar{h}$	Heat transfer coefficient for the inside surface	[W/m^{2}K]

List of Figures

List of Tables

1. INTRODUCTION

1.1. Apollo – Dunlop Tyres History

John Boyd Dunlop created the first practical pneumatic tyre for his son's tricycle in 1888 (Best, 2004). The result was the beginning of the Dunlop tyres industrial empire and the revolution of the automobile industry. Dunlop was the founder of the rubber company 'Dunlop Pneumatic Tyre Company'. Dunlop officially opened the first tyre factory in Durban, South Africa in 1935 and manufactured the first car tyre in South Africa that year.

The Dunlop Ladysmith factory began producing radial textile belted tyres in 1973. The textile belted tyres were generally sidewall-over-tread construction with two casing plies. Initial moulds were a two-piece construction. During the 1980's the car tyres were mainly steel-belted and moulded in centripetal moulds instead of two-piece moulds. As material technologies improved, the casing ply material was changed from rayon and nylon to polyester. Rayon is still used solely for 17 and 18-inch truck radial tyres. In the late 1990's to 2002 the tyre building machines were also changed from two stage machines to more advanced uni-stage building machines (Best, 2004). The high field performance demands necessitated conversion of the ring machine from the bandage construction to a joint reduced bandage wrap. This was done to improve the uniformity and high-speed performance of the ring machine. Furthermore, the tyre curing process has improved from an all-steam process to a nitrogen process. This improved the tyre's performance and reduced the energy costs. The tyre compound changes were mostly done on the tread ply in order to improve the dynamic cord adhesion in the casing cover of the sidewall.

The tyre grip and rolling resistance were improved by introducing the silica-silage technology. The inner liner material was converted to halo-butyl polymer in order to improve the casing air permeability. The modifications of the tyre material compounds were carried out in order to comply with international regulations such as REACH (Registration, Evaluation, Authorisation and Restriction of Chemicals) and ISO 14001 (Safety and Health Standard).

In 2006, Dunlop tyres was bought by an Indian tyre manufacturing giant Apollo tyres which took over the trademark rights to the Dunlop tyre brand in South Africa. Apollo-Dunlop tyres output has risen from about 5000 a day in 1990 to 97 000 a day (Best, 2004).

1.2. Problem Statement

Apollo-Dunlop tyres use saturated steam to warm up the tyre compression mould from the initial temperature, 25^0C to the operational temperature of 151^0C. The warm up process duration is five hours, this process is standardised throughout all the curing presses, regardless of the tyre compression mould size. Apollo-Dunlop tyres have been carrying out a five-hour pre-warm up process on the curing presses for more than hundred years. Therefore, there has been countless optimization studies performed on the geometry of the tyre compression moulds.

The optimizations aim was to reduce the mass of the tyre compression mould. However, optimizations of the warm up process remained neglected over the years. The compression moulds energy consumption decreased because of their mass being reduced over the years. The warm up process was never optimised to be suitable for the new mass reduced tyre compression moulds. Therefore, the warm up process remained five hours long. This negatively affected Apollo-Dunlop tyres because it is very energy inefficient and costly to the business due to

excessive steam usage during the warm up process of the tyre compression moulds. Given the recent high steam generation costs, it is a vital factor in modern tyre manufacturing business sector to reduce energy cost. The tyre price becomes a differentiator in the market, low cost manufacturing makes product very competitive in the tyre manufacturing business sector.

Apollo-Dunlop tyres cannot keep up with the tyre compression moulds high steam demand during the warm up process due to the increased number of moulds. This has led to several boiler trips at the Apollo-Dunlop tyres (Pty) Ltd plant. Such trips, can be characterized by a two-hour loss opportunity in the production process because of an insufficient amount of steam. Certain other inefficiencies such as steam pressure fluctuations and curing cut-offs were a consequence of a steam shortage. Steam cut-offs during the curing process of the green tyre normally result in the compression mould producing under-cured tyres that are considered as scrap.

1.3. Problem Solution

The objectives of this study are:

1.3.1. To determine the minimum required steam quantity

A numerical analysis of heat transfer is applied to determine the required steam quantity to warm up the tyre compression mould from the initial to the operational temperature. This will enable Apollo-Dunlop tyres to install a steam flow-rate regulating system on the steam feed line on each curing press. The analysed required steam quantity is used as a set point in the flow rate regulating system.

1.3.2. To determine the minimum required time

The required steam quantity can be analysed but the warm up process cannot be reduced without knowing the actual time required for the tyre compression mould to reach the operational temperature. Hence, warm up evaluations are carried out to investigate the required warm-up duration for the tyre compression mould to heat up from $25\ to\ 151^0$ C operational temperature. The tyre compression mould temperature profile is analysed using the Personal Daqview 55^{TM} system. This system enables K-227 thermocouple wires to be mounted into the tyre compression mould drilled holes to monitor the temperature profile of the compression mould throughout the warm up process.

1.3.3. To test the optimized warm up process on sample tyres

The sample tyres cured with the tyre compression mould warmed up using the reduced warm up process are rigorously evaluated to check if they meet the minimum Apollo – Dunlop tyre's performance requirements. The performance test will be composed of evaluation of the tyre's durability (wear resistance/life span) and effectiveness (braking ability) through quantitative tests carried out in testing laboratory.

1.4. Literature Review

This chapter provides a critical review on a segment of a published body of current knowledge including substantive findings through summary, classification and comparison of prior research studies and theoretical articles. The main purpose of this literature review is to develop an understanding of the topic at hand through previous work done on the heating treatment of metals. The scope of this chapter includes heat transfer numerical analysis, heat treatment and

experimental methods on metals. A fundamental theory on the tyre compression mould warm up process is briefly discussed with the focus on the known heating method utilised.

1.4.1. Heat Transfer Numerical Analysis

The numerical solution of heat transfer, and other related processes were made possible when the laws governing these processes had been expressed in a mathematical form. This is generally in terms of differential equations. In 1701 a review of the background of "Newton's Law of Cooling" leaded to the conclusion that it is appropriate to credit Newton with the concept of the conductive heat transfer coefficient (HTC). Furthermore, because his early experiments with heat were eluded too in the Principia, the 300th anniversary of this volume should honour him as a pioneer in heat transfer as well as in solid and fluid mechanics. Isaac Newton is widely credited with the convective heat transfer coefficient equation (Cheng and Schulenberg, 2001).

$$Q = h\ A\ (T_{sur} - T_{surr}) \qquad (1.1)$$

Where:

$\dot{Q}$ = Heat transfer rate (kW)

h = Heat transfer coefficient $(^{W}/_{m^2C})$

A = Surface area (m^2)

T_{sur} = Surface temperature (^0C)

T_{surr} = Surroundings temperature. (^0C)

1.4.2. Heat Transfer Experimental Methods

According to Kulkarni and Radhakrishna (2005), the students from the Department of Mechanics of B.M.S College of engineering used two methods to measure the HTC at the metal–mould interface during the casting process. The 1st method measured the size of the gap formed between the metal and the mould during the casting process and estimated the value of the HTC based on the gap size. The second method measured the temperature of the metal and the mould at certain surfaces, and the reverse method was used to derive the HTC at the gap. A procedure was also developed to use the temperature measurement data in order to obtain the HTC as a function of the casting temperature near the interference.

Garcia (2005) attempted to quantify the transient interfacial metal mould heat transfer coefficient by emphasizing different factors affecting the heat flow across such interface during a solidification stage. These are, the thermo-physical properties of the contacting materials, the casting geometry, the orientation of the casting-mould interface with respect to the gravity (contact pressure), the mould temperature, the pouring temperature, the roughness of mould contacting surface and the mould coatings. It was proven that the heat flow is controlled by the thermal resistance at the curing-mould interface during rubber curing and casting in the metallic moulds. Thus, heat transfer coefficient at the metal mould interface has a predominant effect on the rate of heat transfer. The effect of pressure on molten metal will only affect the heat transfer rate at least at the initial steps of solidification in some processes such as low pressure and die casting (Fardikhchy et al, 2011).

There are various theories on the nature of heat that were developed by Scottish chemist Joseph Black 1761. These include discovering that ice can absorb heat without changing its temperature when melting (Guerlac and Henry, 1980). This led Black into concluding that the heat must have

combined with the ice particles and become latent, henceforth the theory of latent heat energy was formulated. In 1797, a cannon manufacturer Sir Benjamin Thompson demonstrated through the use of friction that it was possible to convert work to heat. He designed a special shaped cannon barrel that was thoroughly insulated against heat loss (Rumford, 1804). Furthermore, he used a dull drill bit to replace the sharp boring tool and immersed the front part of the gun in a water vessel. Thereafter he heated up the water in the vessel from ambient to a boiling point within 2.5 hours without the use of fire.

Eastop (1993) proved by using a hot burner that heat energy can be conductional transferred from one molecule to another molecule within a substance touching a hot burner. He also proved that heat energy can be conventionally transferred by the mass movement of liquid or gas, and heat energy can be transferred by waves through radiation. When heat is transferred the thermal energy always moves from warmer to cooler objects. The heat never flows from cooler object to warmer object. The warmer object loses the thermal energy and becomes cooler as the cooler object gains the thermal energy and becomes warmer (Bergles, 1986). The heat energy conversion in general and specific heat capacity in particular, has been the main topic in energy saving research for the last 30 years. The energy enhancement techniques studies were successfully conducted in the past. The thermal energy is dependent on the total amount of molecules in motion therefore, the thermal energy absorbed increases as the volume of the component under warm-up increases. The thermal heat energy is directly proportional to the specific heat capacity, c_p of a substance that is required to raise the temperature of a given mass of the substance by some amount. The heat capacity varies from substance to substance (Eastop, 1993). It was proven that the heat is the thermal energy that is transferred from one object to another when the objects are at different temperatures. The amount of heat that is transferred

when two objects are brought into contact depends on the difference in the temperature between the objects. The heat transfer continues until both objects are at the same temperature (Zalba and Marin, 2003).

Heat transfer research and studies were done successfully in the past through experiments and research work done by various researchers. Cheng and Schulenberg (2001) proved that heat transfer at supercritical pressures is mainly characterized by the thermal physical properties which vary strongly near the pseudo-critical line. The steam heating efficiency of a rapid heat cycle moulding (RHCM) can be effectively improved by increasing the thermal conductivity of the cavity or core material. This situation is diametrically opposite for an electric heating RHCM. The thermal response of a new electric heating mould was also simulated. The simulation results showed that the cooling plate can significantly improve the cooling and heating efficiency (Wang and Zhao, 2010).

1.4.3. Heat Treatment of Metal

According to Osmond and Austen (2012) generally there would be an organizational change in steel when it is quenched into a hard phase during heating and cooling. Six different microstructures of steel under a microscope were used to prove this. The above two achievements initially lay the theoretical foundation for the modern heat treatment process. From 1850 to 1880 a number of innovations were turned into patents for the application of various gases (such as hydrogen, carbon monoxide gas, etc.) to protect the heating process. In 1960s the heat treatment technology made the use of plasma field and developed the ion nitrating process was developed. The application of the laser and the electron beam technology made the metal to gain a new surface and chemical heat treatment method in the carburizing process (Castle, 2000).

Single cell ovens, nitrogen atmosphere and even induction heating have been the recent developments in the die heating technology over the last 10 years (Castle, 2000). However, the majority of the manufacturing factories are still dependant on the basic air circulating chest furnace. Most factories now realize the necessity of controlling the temperature in the aluminium extrusion process hence it is rare today to find an extruding machine without the output temperature measurement. The extrusion industry uses a single cell oven with no air circulation fan. The set temperature is 460^0 C and the furnace control system requires the operator to input the die dimensions or weight. The control system then calculates and display the required heating time. The furnace design has two banks of heating elements on either side of the die. The heating elements provide the radiant heat. The set temperature is reached after two hours and there is a temperature differential of about 25^o C between the surface and the core (Castle, 2000).

An innovative steam moulding system was designed by Terry Pearson who was a principle director in a Britain based company that was formed in 2007. Pearson had been involved with gas moulding for more than 25 years (Merril, 1955). Since then, the steam moulding system has moved to automotive applications and is widely used to improve the surface finish of television frames in Asia. In the rapid temperature cycling (RTC) process, the mould is heated by flowing saturated steam through groove channels located close to the cavity surface. After the mould warm up process, the saturated steam is replaced with cooling water in the same mould channels to cool the mould. The RTC process uses steam as a heating media because it releases latent heat energy when it condenses to water. Therefore, the higher the steam temperature the more heat is released (Merril, 1955). The condensation heat transfer coefficients decrease as the saturation temperature decreases, however it increases with the mass flux of the refrigerants (Dalkilic and Wongwises, 2009). The region of common down flow has higher heat transfer rates than the

region of common upper flow. Non-linear instability of the cylindrical interface between the vapour and liquid phases of a magnetic fluid was analysed with a method of multiple time scale expansion (Goldstein and Eckert, 2005). Strategies to enhance the underground heat collection low energy density of ground heat source requires to be covered by efficient heat transfer, mixing highly conductive substances is one of well approved strategies to accelerate the heat transfer (Baeyer, 1998).

2. PNEUMATIC TYRE MANUFACTURING PROCESS

This chapter provides an understanding of the pneumatic tyre history and current manufacturing process. The scope of this chapter includes tolerances that outline the geometric accuracy that must be achieved in the tyre manufacturing process and the manufacturing steps through which raw materials are transformed into a final product. A fundamental theory of the relationship between the process used and the properties of the finished product is briefly discussed. It is a necessity to know what influence a particular process will have on the tyre's response to different conditions (i.e. stress, heat). In order to conduct this experimental work one must understand well the manufacturing process and the required operational characteristics of the tyre.

2.1. Pneumatic Tyre History

At first, tyres were made out of leather and then with steel cords. Forge fire was used to heat the metal for contraction and to fit tightly onto the wheel. This used to be carried out by a skilled worker, known as a wheelwright. But the origin of a pneumatic tyre can be traced back to 1845 when Robin William Thomson a Scottish engineer invented the pneumatic (inflatable) tyre. Thomson's design consisted of a number of thin inflated tubes inside a leather cover (Thomson, 1851). **Fig. 2.1** shows the first design of the leather tyre.

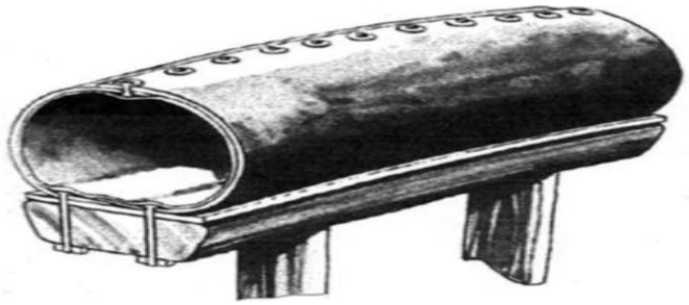

Fig. 2.1: Thomson's leather tyre (Thomson, 1851)

Thomson's design main advantage over later designs was that it would take more than one puncture to deflate the whole tyre. His design was only applied on hoarse drawn carriage since neither bicycles nor automobiles were invented when Thomson introduced his tyre. In 1885 this idea was abandoned because of severe difficulties encountered during manufacturing and fitting (Thomson, 1851).

In 1887 Scottish inventor John Boyd Dunlop designed the first practical pneumatic tyre (bicycle tyre). Dunlop's patent application was filed at the Oriel House, Westland Row in Dublin in 1888 but it was declared invalid because of prior work of fellow Scot Robin William Thomson (Thomson, 1851). In terms of tyre materials, John Dunlop is credited with introducing rubber into a tyre since it could withstand wear and tear while retaining its resilience. The most significant of this was a design by W.E. Bartlett, an American working in his uncle's company, a North British Rubber Company based in Edinburgh. In 1890, Bartlett patented his design. This is what is now known as the Beaded edge tyre (Thomson, 1851). The main difference between the beaded edge tyre and the 'Welch' Rim tyre was that the bead core was formed from very strong vulcanised rubber. This increased the stretching ability of the tyre and enabled the tyre bead to be stretched over the rim flange.

In 1920, synthesis rubber was invented in Bayer laboratories in Bayern, German. Ever since, one billion tyres are manufactured annually in more than 400 factories using same design and materials that Welch invented (Edwards, 2001). **Figs. 2.2-5** illustrate the structural development of the tyre over the years.

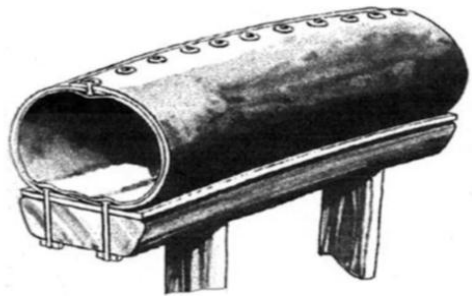

Fig. 2.2: Thomson's patent 1845.

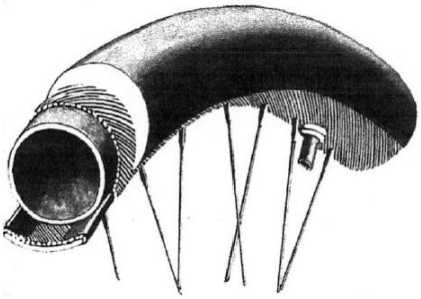

Fig. 2.3: Dunlop's composite tyre, patent 1888.

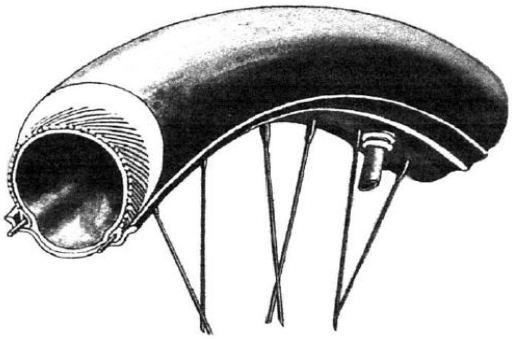

Fig. 2.5: The Bartlett patent 1890.

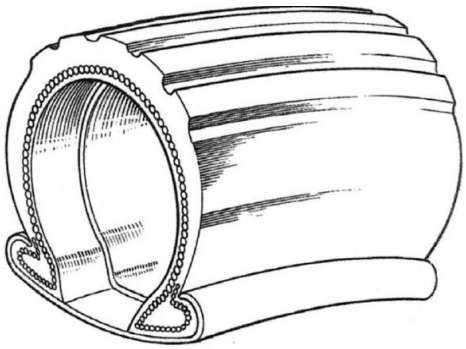

Fig. 2.4: The Welch, well based rim patent 1890.

(All above figures are sourced from a paper written by Thomson (1851)

According to Tompkins (1981) it has been hundred years since the invention of the first practical pneumatic tyre by Scottish inventor John Boyd Dunlop. Since then the tyre manufacturing processes are optimized every year to maintain or reduce the tyre mass, operations cost while maximizing the tyre production. Apollo-Dunlop modern tyres are made of nine different components and layers that have different mix of ingredients since their tyre road applications

require various material properties. The biggest tyre that Apollo-Dunlop tyres produce is a 255/75 R15 and the smallest tyre is a 275/344 R15, which uses the original moulds from 1980.

2.2. Pneumatic Tyre Components

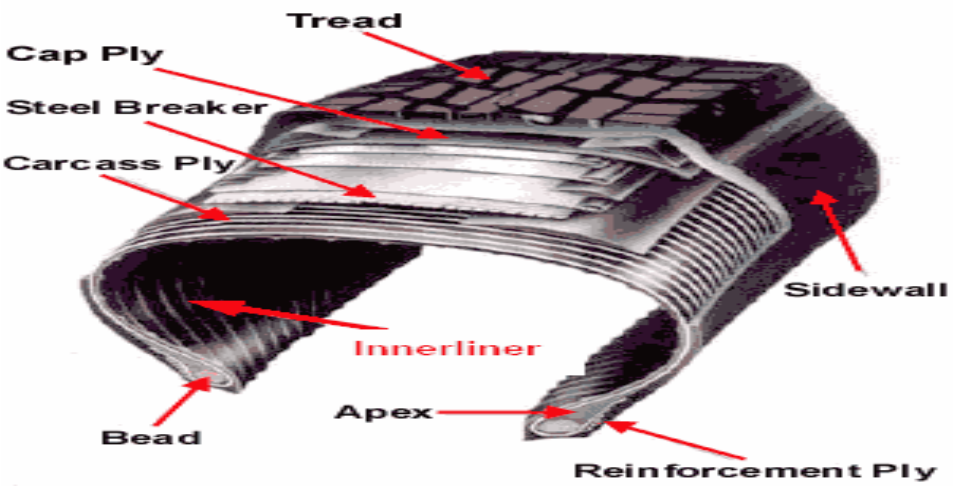

Fig. 2.6: A tyre carcass showing layers that build up a tyre (Spiegelhalder, 1983).

2.2.1. The Tread

A tyre tread is a thick extruded rubber profile that surrounds the tyre carcass and makes contact with the tar road and ground surface. The grooves in the tread rubber are designed to allow water to circulate and expel from beneath the tyre during contact with the road surface. Tyre traction efficiency is directly affected by the proportion of rubber to air space on the road surface. The air circulation restriction through the tread limits the tyre's effectiveness in providing proper traction. More additives are introduced into tread compound to impart wear resistance, traction ability and environmental resistance. However, this development is compromise since soft compounds have poor wear characteristics but good traction whereas hard compounds have poor traction but good wear characteristics. The tread pattern is designed to provide varying degrees

of traction, wear and heat resistance. Hence, the tread pattern selection of a proper on/off road tyres depends on the application and environmental conditions.

According to Messrs and Firestone (1971) there are three tread thickness classifications for off-road tyres, namely: regular, deep and extra deep. The deep and extra-deep treads are 1.5 and 2.5 times thicker than the regular tread. The thicker treads have greater wear and cut resistance. The tread codes are as follows:

- Extra-Deep tread, L5, L5S.
- Deep tread, E4, L4 and L4S.
- Regular tread, E2, E3, G2, G3, L2 and L3.

Size identification and Aspect ratio of the off-road tyre is normally indicated by tyre width, rim diameter and ply rating. The nomenclature for this is as follows:

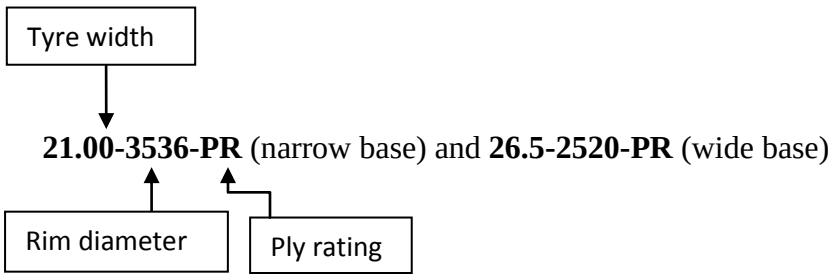

A narrow base tyre has an aspect ratio (tyre height/tyre width) of 96 – 98% and a wide base tyre has an aspect ratio of 80-82%. Apollo-Dunlop tyres main focus is on passenger steel radial, light-truck, truck-bus steel radial and tractor tyre. Hence, manufactured tread patterns are mainly: rock, traction, block and rib pattern. **Figs. 2.7-10** illustrate various tread patterns produced by Apollo-Dunlop tyres.



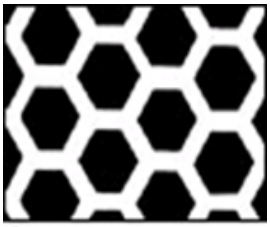


Fig. 2.7: Rock pattern **Fig. 2.8:** Traction pattern **Fig. 2.9:** Block pattern **Fig. 2.10:** Rib pattern

Figs.2.7-10: Five tread patterns manufactured at Apollo-Dunlop Tyres. (Messrs and Firestone, 1971)

Rock pattern is an off-road pattern specially designed to prevent cuts caused by sharp objects such as rocks, broken bottles and etc. the excellent wear resistance is provided by maximum contact area which has grooves running across the direction of the travel mark. ***Traction pattern*** is a terrain pattern with lugs on the tyre and large voids in-between the lugs. The lugs provide plenty of bite in low traction conditions whilst voids in-between allow the tyre to disperse mud off tread grooves. ***Block pattern*** is a heavy load pattern that consists of wide tread width and rounded shoulders for good flotation properties, block pattern is characterized by large ground contact area that creates low good contact. Therefore, block pattern is mostly used for operating with heavy loads on soft and muddy ground. ***Rib pattern*** is mainly used on free-rolling tyres with minimal friction. Rib pattern possess high directional stability hence its grooves are running parallel to the direction of travel. The design of a tyre tread has a direct effect upon noise generated especially at high speeds. Therefore, deeper tread patterns often enhance safety while shallow patterns are less costly to produce, but becomes noisy as speed increases. Normally tyres intended for dry weather use are designed with minimal pattern in order to increase the road contact pitch.

2.2.2. The Sidewall

The sidewall is composed of a crack-resistant, flexible and non-reinforced extruded profiles mixed with additives such as antioxidants and antiozonants. Both additives provide sidewalls with abrasion resistance and environmental resistance. A thick rubber area is provided on sidewall extrusions to enable moulding of raised prints. The sidewalls main function is to give the tyre the abrasion resistance against harsh environmental conditions.

2.2.3. The Inner-liner

The inner liner is a halobutyl rubber sheet that is extruded and compounded with various additives in order to possess low air permeability. The use of halobutyl rubber as inner-liners in tyres allows significant improvement in air retention properties, tyre durability and maintains proper inflation pressure. Therefore, main function of the inner-liner is to ensure that the tyre holds high pressure air inside without gradually diffusing through the rubber structure. The pneumatic tyre needs sufficient pressure to ensure good performance under safe conditions, therefore it is a basic requirement that inner-liner must be made of Halobutyl elastomers such as Exxon chlorobutyl and bromobutyl rubber.

2.2.4. The Body Plies (carcass and reinforced)

The body plies are calendared sheets that are composed of polyester or fibre cords wound together and sandwiched in rubber. The fibre cords are used for their flexibility and inelasticity. The body plies allow the tyre to flex but prevent it from deforming or losing its original shape under excessive pressure. The body plies are configured in a manner that they all run perpendicular to the direction of the tyre's rotation to enhance radial strength. Truck, off-road and aircraft tyres consist of more body plies since they constantly exposed to harsh

environmental conditions. The main purpose of the body plies is to provide the tyre with structural strength. The pneumatic tyre normally fails under high pressure if rubber compound is unable to resist high air pressure if the body plies are damaged or cut.

2.2.5. The Apex

The apex is a tyre component that is extruded into a triangular profile. The main purpose of the apex is to support the bead. The apex provides cushion between the body ply, flexible inner-liner and rigid bead assembly.

2.2.6. The Bead

The bead is a batch of bronze coated steel wire with high tensile strength and combined with a rubber compound. The special alloys of bronze are used to coat steel to prevent corrosion. The bead is inflexible and inelastic component that provides mechanical strength by supporting the load when the rim is fixed into the tyre.

2.2.7. The Steel Breaker

The steel breaker is a strip of steel cords covered with rubber compound. The steel cords breaker provides the tyre with very high cut resistance when running on sharp rocks. It is very difficult to re-tread the steel breaker tyres. Hence, steel breaker tyres should not be subjected to excessive heat.

2.2.8. The Cap Ply

The cap ply is an extruded component fitted in between steel breakers and the tread to prevent mechanical wear on the tread and the breaker that might be caused by rubbing friction between both components.

2.3. Tyre Processing

There are relative standardized processes that govern the pneumatic tyre manufacturing process and the machinery in more than 400 tyre manufacturing factories worldwide. The production process consists of five sub-processes such as raw material mixing, component preparation, tyre building, vulcanization or moulding, and performance evaluation. Although today, large efficient factories use automation to guide many of the steps in the tyre manufacturing process, highly skilled workers are still required to assemble components of the tyre.

2.3.1. The mixing Process

According to Tadmor and Gogos (2006) Edwin Chaffee developed a two-roller machine to mix additives into rubber. Since then, the twin roller machine has been used to carry out mixing of additives with rubber. Raw material mixing is the operation of blending together additives and raw material ingredients to form a rubber compound. A ban-bury press machine is used to blend all required ingredients to mix a batch rubber compound. The first stage compounding is composed of standard chemical formulation for all batch rubber compounds. The chemical formulation is characterized with natural rubber, carbon black (standard), synthetic rubber, stearic acid, sulphur (20% oil) and continuous polarization tandem (CPT) accelerator. **Fig. 2.11** illustrates the Banbury machine with raw materials.

Fig. 2.11: Banbury machine withdraw materials (Courtesy from Apollo-Dunlop tyres).

The tyre manufacturing process use natural rubber as the primary raw material and the synthesis rubber is used as the secondary raw material. The primary rubber forms in a Hevea Brasilliensis tree (rubber tree) which occurs naturally. The synthesis rubber is a petroleum by-product that has a high elastic deformation which enables the tyre to retain its original state after stretching under high stresses and its thermal stability distinguishes it from natural rubber. The carbon black is a material produced by incomplete combustion of heavy petroleum product such as fluid catalyst cracking (FCC) tar, coal tar and ethylene cracking tar. Carbon black hardens rubber compound and sustains its black colour during compounding. Stearic acid softens the natural rubber for the tyre not to be brittle. Sulphur oil is used to dilute suffocating rubber odour and to soften mixture flow. CPT accelerator is used to regulate cooling rate in the rubber compound.

2.3.2. Raw Material Compounding

Raw material compounding is a mixing process where ingredients are mixed at a specific temperature by a machine called a ban-bury. A hydraulic ram exerts pressure onto raw ingredients until the rubber compounds and additives are fully compounded together. The mixed rubber compound is dipped in a Rhenodiv solution that minimizes rubber compound adhesion properties to prevent rubber compounds from sticking to each other during processing. Second

stage, rubber batch compound has a different mix of ingredients that are determined by required properties for various operational applications. The descriptions of all raw materials that differentiate rubber compounds used in the mill are as per Table 1.

Table 1: Coded raw material (Courtesy from Apollo-Dunlop tyres).

RAW MATERIAL	*OLD CODE*	*NEW CODE*
SMR10	01-9710	129710
SMR10 HOCK HIN	01-9700	129710
SIR10	01-9750	129710
SBR AFPOL 1502	02-5025	135025
OESBR AFPOL 1783	02-5461	131783

2.3.3. Additives Mixing

Mechanical work is applied on compounded rubber with continuous polarization additives in order to blend into a homogeneous substance. The mixing process is performed using internal mixers that are equipped with two counter-rotating rotors that shear the rubber compound along with the additives. The mixing machine is called a twin mill. The mixing order of ingredients incorporates whether mixing is done in three or four stages. The mixing rate is dependent on considerable heat generated by shearing action of both rotors and housing. The vulcanization of the rubber compound is prevented by water-cooling rotors that maintain low temperature along the twin mill. The rubber charge is fed onto an open mill batch-off system for further mechanical

work so to produce a thick rubber sheet. **Figs. 2.12–15** illustrate rubber charge fed into the mill batch-off system.

Fig. 2.12: Batch rubber compound from the Banbury.

Fig.2.15: Prepared strip awaiting extrusion.

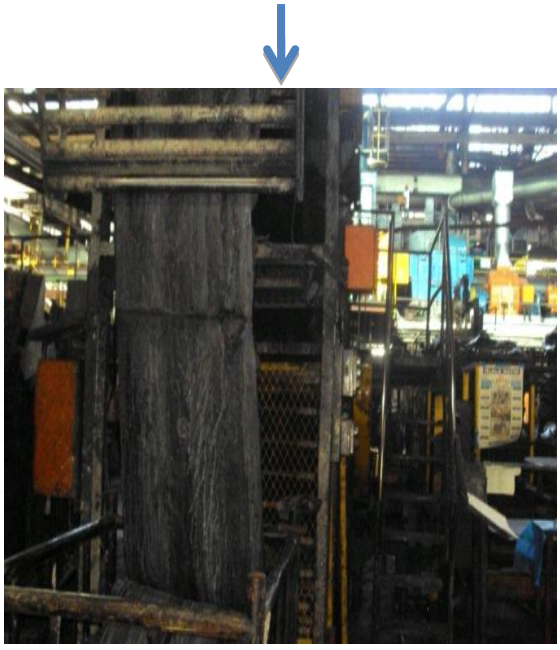

Fig. 2.13: Batch compound Rhenodiv dipping.

Fig. 2.14: Twin-mill mixing prepared rubber.

(All above images are a Courtesy from Apollo-Dunlop tyres).

A twin mill machine consists of twin counter-rotating rolls, one of the roll is serrated in order to maximize the mechanical work done. The strip is laid down into a pallet bin to cool down, after the sheet is pulled off the rollers in a form of a strip and dusted with talc.

2.3.4. Component preparation

Component preparation is divided into three manufacturing processes namely: bead building, extrusion and calendaring.

a) Bead building

The bead components of the tyre is a non-extensible composite loop that connects body plies and clamps the tyre onto the wheel assembly so it will not slip on the rim. The pneumatic tyre bead is made up by combining the steel wire loop, apex and bead filler using a bead tendering machine. The continuous steel wire covered in rubber and wound around with several continuous loops is used to make bead wire loop. The bead filler is made out of tough extruded rubber compound for forming a wedge. The pneumatic tyre mounting can be a problem if bead circumference is too small, or if too loose, the tyre can separate from the rim easily under loading. Therefore, the precision of the bead circumference is highly important.

b) Extrusion

According to Tadmor and Gogos (2006), Thomas Hancock invented a rubber "masticator" designed to reclaim processed rubber scraps but the first thermoplastic extrusion was in 1935 by Paul Troester and his wife Ashley Gershoff in Hamburg, Germany. Two years later, Roberto Colombo of LMP developed the first twin screw extruders for rubber extrusion in Italy. The extrusion process is an operation where the rubber strips of the mixed rubber compound are fed into the extruder through a shearing action of an extruder screw, where additional mixing of

compounds is provided. The extrusion process is often used to form the tyre treads but also used for sidewall profiles and inner liners. The extruder machine consists of two feeders, hot and cold feed extruders. Both extruders have a screw and barrel-drive that feeds the rubber compound into a common die. The extrusion die is a tool that shapes the compound into a desired shape.

Figs. 2.16 –19 illustrate the extrusion process.

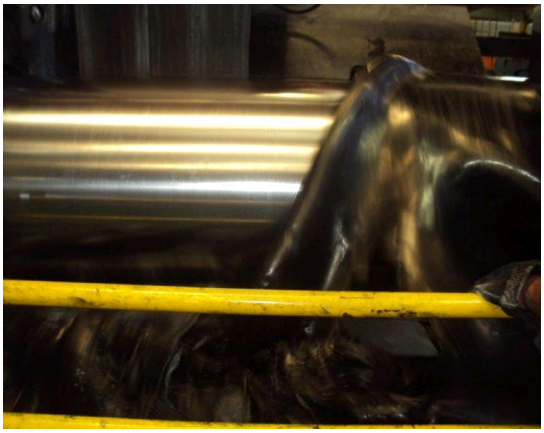

Fig. 2.16: Rubber strips fed into roller feed.

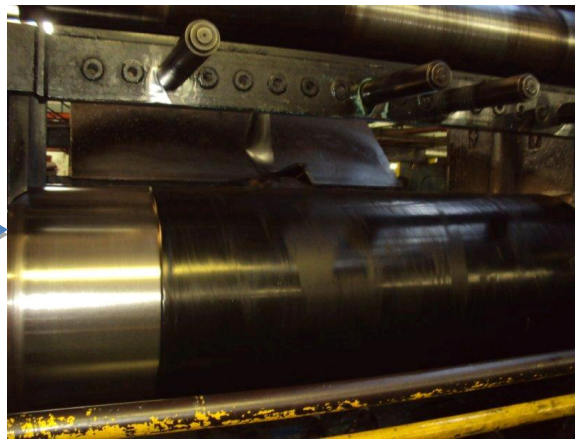

Fig. 2.17: Mixed rubber compound rolling.

Fig. 2.19: Extrusion die profile.

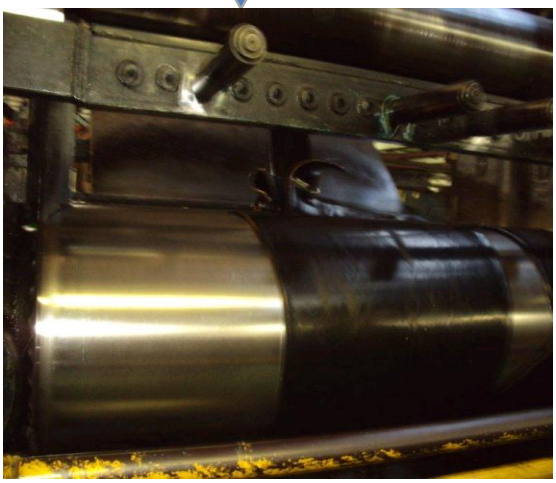

Fig. 2.18: Mixed rubber into extruder screw.

(All above images are a Courtesy from Apollo-Dunlop tyres).

The rubber compound is warmed up by three mill machines, namely, the cracker mill, the warm-up mill and the feed mill before extrusion takes place. The extruder screw agitates the rubber compound before feeding mixed rubber strips into a continuous oven where extruded profile is vulcanized and cooled to terminate the vulcanizing process. After termination of vulcanizing process rubber compound is fed into a die. The extruded tread or sidewall is cooled in a refrigeration system before pantograph and masters tests, pantograph is a test where a meter of a tread or sidewall compound is cut-out for weight per meter measurement. The tread or sidewall is cut to length and rolled up on a spool.

c) Calendaring

According to White and Lindsay (1990) in 1836 Edwin M. Chaffee patented a four-roll calender to make a rubber sheet and he worked with Charles Goodyear with intention to produce a sheet of rubber laminated to a fabric base. The design of the calenders developed at high rate with the expansion of rubber industry. The calenders were also used for fabrics and paper long before later applications for thermoplastics. Calendering is a process that form and smoothen a rubber compound into thin sheets called body plies and belts. There are two types of calendering machines namely, fabric and steel calendering machines. Fabric calender produce upper and lower rubber sheet with a layer fabric in between and steel calendar do so with steel cords. A calender is series of large-diameter rolls that hard-pressure rubber compound into thin sheet, usually of 2 meters wide order. Multiple fabric and wire spools are housed and fed into a calender using a facility called, Creel room. A Creel room is a heavy duty frame work that supports wire spools up to 50 kg. The calendered components are sheared and spliced by calendars utilizing downstream equipment. **Figs. 2.20-21** illustrate the calender machine with wire spool.

Fig. 2.20: Wire spool mounted on machine.

Fig. 2.21: Steel calendar machine.

(Both above images are a Courtesy from Apollo-Dunlop tyres).

2.3.5. Pneumatic Tyre Building

According to Miller (1985) in 1909 W.C State of Goodyear Tyre Company invented and patented a tyre building machine (TBM) that dramatically increased worker's productivity. Before 1910, the plies and the beads of the pneumatic tyre used to be manually built by workers. Each ply and bead was stretched, cemented and stitched around an iron core. The TBM could carry plies, beads and tread on the rollers carried on a central turret. The worker had to pull the appropriate material over the core while the machine's electric motor held the proper tension for the worker to finish cementing and stitching.

The tyre building is the process of assembling all the prepared components of the pneumatic tyre into a green cover or raw cover, green cover refers to uncured state of the pneumatic tyre. Tyre building machine (TBM) is used to build up green covers through manually and automatically operation. The tyre building process consists of two stages namely, drum wrapping and drum shaping. Drum wrapping is the process where the sidewalls, inner-liner, body plies and apex are wrapped around the drum and the beads are placed on the sides. The drum shaping operation is where the outer components that interact with tar road are applied to the drum. The outer

components are belt breakers (belt packages), tread and then the drum is inflated for shaping. All components are spliced in order to make both sides of the green tyre equivalent. The sidewall and tread are joined with a skived splice, where both joining ends are bevel cut to prevent overlapping. The breakers (belts) both ends are joined. The body plies and inner liners are spliced with a square-ended overlap, because if both sides of the green tyre are not symmetrical, these may result in producing defected tyres. The prepared raw cover is called a green cover. **Figs. 2.22-23** illustrate the TBM machine and a prepared raw cover ready for curing process.

Fig. 2.22: TBM machine with inflated drum

Fig. 2.23: Green tyre before the curing process

(Both above images are a Courtesy from Apollo-Dunlop tyres)

2.3.6. The tyre curing process

The tyre curing process is an 18th century invention. However, the history of rubber cured by various means dates back to 17th century. Although, identifying the inventor of the curing process proved to be difficult, Charles Goodyear is generally credited as the first who formulated the curing process. However, Goodyear never fully understood the curing process. According to

Best (2004), Goodyear's earlier work inspired Thomas Hancock, hence he furthered the curing process experiments and was the first to patent the rubber curing machine.

The tyre curing process is moulding of the green cover into a desired final shape of the pneumatic tyre. The heat and compression pressure are applied to the green cover in a mechanical mould to ensure rubber elasticity to develop the desired pneumatic tyre shape. A green cover is automatically placed on the lower compression mould using hydraulic arms and a flexible balloon called a bladder. The bladder is inflated inside the green tyre. The bladder is expanded by filling in the saturated steam at 55 kPa for 8 minutes to shape the green cover and force the blank tread rubber against raised interior of the mould. A nitrogen gas is fed into the bladder at 2700 kPa pressure to cure the green cover into a pneumatic tyre by moulding it into desired shape through compression and high temperature. The curing duration depends on the characteristics desired for the tyre. Hence, there are different types of cures used in Apollo-Dunlop tyres. The cures used are namely: N1, N2 and N3 (see ***Appendix C*** for a cure sheet).The main variation amongst the cures is the moulding pressure and the presence of nitrogen.

Figs 2.24–26 illustrate the condensate pegging of the compression mould and the cured tyre waiting for offloading.

Fig. 2.24: Condensate pegging on the bladder.

Fig. 2.25: 55 kPa inflated bladder

Fig. 2.26: Press opening after curing round

(All above images are a Courtesy from Apollo-Dunlop tyres)

The nitrogen gas is bled off after the curing cycle and the compression mould opens for the tyre to be off-loaded. **Fig. 2.27** illustrates the schematic mould layout during the curing process.

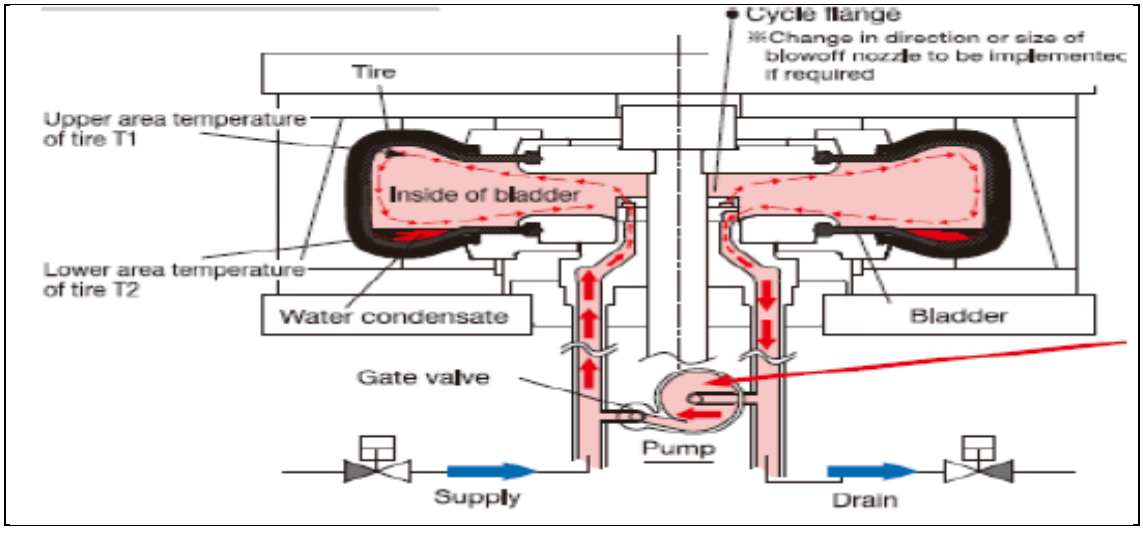

Fig. 2.27: Schematic mould layout during the curing process. (Messrs and Firestone, 1971)

2.3.7 Quality Control

The accuracy of all factors involved in production is reviewed at the final stage of the pneumatic tyre production. A quality control inspector (QCI) ensures that the manufacturing process of the pneumatic tyres adheres to prescribed quality and safety standards as required by *ISO 9000.* The quality control inspector ensures that every component from raw materials to pneumatic tyres meets the quality and safety standards as specified in the purchasing documentation.

Apollo-Dunlop tyres also inspect products purchased from competitors and maintain records of the supplier's performance. These sets of data are important in assisting Apollo-Dunlop tyres to improve their tyre performance and to remain competitive in the tyre industry. Most of the quality control tests are routinely and quick, therefore automated systems are often used to test thousands of tyres. Apollo-Dunlop tyres keep records of all the tests carried out and use statistics to analyse their results. The quality control tests conducted on tyres at Apollo-Dunlop tyres are as follows:

a) Defect inspection

Inspections are an important part of the quality assurance process in the pneumatic tyre manufacturing industry. Apollo-Dunlop tyres management system of defects is composed of two related challenges, firstly, being able to carry out inspections efficiently and quickly identifying and communicating any defects. The second challenge is correcting the defect in a timely manner whilst reducing negative effects on the rest of the operation process. Defects are a serious threat to the performance and can have negative effects on quality of the product. Hence, all the pneumatic tyres are rigorously tested in order to identify and correct defects. Tyre inspection is the last step in the tyre manufacturing process. The tyre inspection includes:

- Trimming (Sipping).
- Visual inspection.
- Uniformity inspection.
- Balance inspection.
- X-ray inspection.
- Performance analysis.

2.3.7.1 Trimming (Sipping)

Tyre trimming is the pre-production inspection performed on the cured tyre. The excessive mould flash and micro-vents, are trimmed from the tyre tread, before a final inspection is undertaken to ensure the tyre conform to specifications and it come up to the rigorous standards set. The tyre trimming method was proposed by Sipe (1923). In the 1920s Sipe worked in a slaughter house and grew frustrated of slipping on the wet floors. He found out that cutting slits in the tread of the bottom of his shoes resulted in a better traction than the uncut tread (Sipe 1923). Sipe's invention was unsuccessful, hence, it was only applied to solid rubber tyres, rather than pneumatic tyres since the tyres had poor wet grip anyway, owing to their limited contact patch. According to Tompkins (1981) in 1939 John’s son, Harry E. Sipe, popularised the use of the tyre trimming method in the USA for the new low-pressure balloon tyres. **Fig. 2.28** illustrates tyre trimming after the curing process.

Fig. 2.28: Tyre trimming after curing process (Tompkins, 1981).

2.3.7.2 Visual inspection

Visual inspection is carried out to identify visible signs of damage that could necessitate repairing or scraping of the defected tyre. The cured tyre is rotated on a machine and all surfaces of the tyre are scanned by a camera system called Auto Vision. The necessity of the visual inspection stems from the fact that the damages can be defected on the surface areas.

2.3.7.3 Tyre Uniformity Testing

Tyre uniformity inspection is a quantitative measure of variations within a tyre. Apollo – Dunlop tyres utilises an axis system to measure the dynamic mechanical properties of the pneumatic tyres as defined by the measurement standards and test conditions approved by global car and tyre makers. These measurement standards considers the following parameters, radial run-out, lateral run-out, conicity radial force variation, lateral force variation, tangential force variation, plysteer and sidewall bulge.

According to Tompkins (1981), in 1979 the Motor Vehicle Manufacturers Association (MVMA) together with the Rubber Manufacturer Association (RMA) founded a research program at the University of Michigan Transportation Research Institute (UMTRI). The research programme aim was to investigate the truck ride effects resulting from non-uniformities in the tyre. The research programme created a tyre uniformity testing machine called MTS Model 860. **Fig. 2.29** illustrates the MTS Model 860 tyre uniformity machine testing a pneumatic tyre.

Fig. 2.29: MTS Model 860 tyre uniformity machine testing a pneumatic tyre.

(Above figure is a Courtesy from Apollo – Dunlop tyres).

Apollo – Dunlop tyres use the MTS Model 860 machine to measure uniformity and balancing on tyres, the axis system of the uniformity machine bisects the tyre center and forces are measured along the axes. **Fig. 2.30** illustrates forces measured along the tyre axis:

- F_Z - Radial force variation
- F_Y - Lateral force variation
- F_X- Tangential force variation

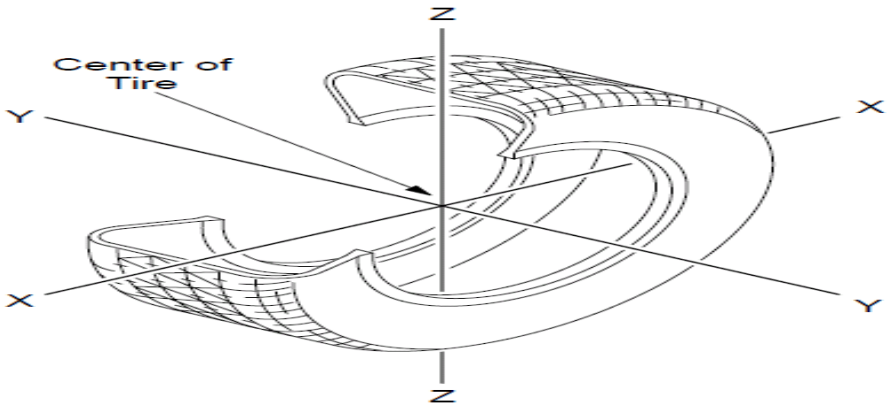

Fig. 2.30: Axis measurement systems (Pacejka, 2006).

The tyre uniformity parameters measured by the MTS Model 860 machine are as follows:

a) Radial force variation

The radial force is the vertical force between the tyre and the road. The vertical force acts upwards to support the vehicle. This vertical force is perpendicular to the road. This is the axis where radial force F_Z is applied to the tyre. **Fig. 2.31** shows the radial force acting on the pneumatic tyre.

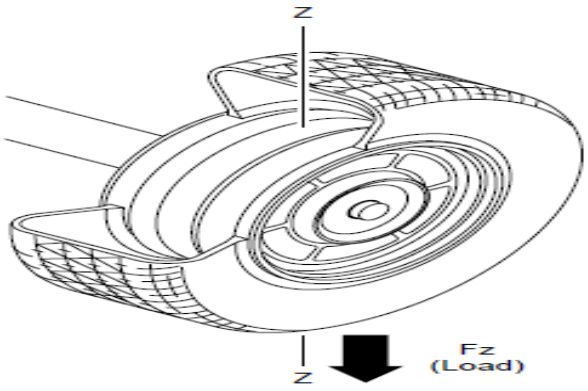

Fig. 2.31: Radial force acting on the tyre (Pacejka, 2006).

The radial force variation (RFV) describes the change in this force as the tyre rotates under load. As the tyre rotates, a spring elements with various spring constants enter and exit the contact area, the radial force changes. Once the tyre is inflated, loaded and rotating, the radial force becomes periodic. There is a slight difference in radial force variation when the tyre is rotated in either direction. The RFV, as well as all other force variation measurements can be expressed as a complex waveform. This waveform can be expressed in terms of its harmonics by applying *Fourier Transform* (FT). The Fourier transformation permits one to parameterize various aspects of the tyre dynamic behaviour (Thomas, 1986). **Figs. 2.32-33** illustrate the force variation and harmonic waveforms on the pneumatic tyre.

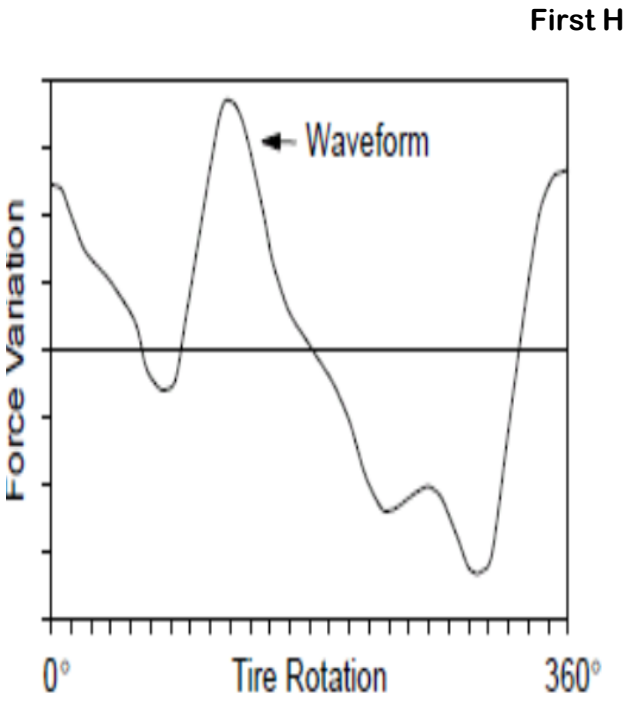

Fig. 2.32: Force variation waveform.

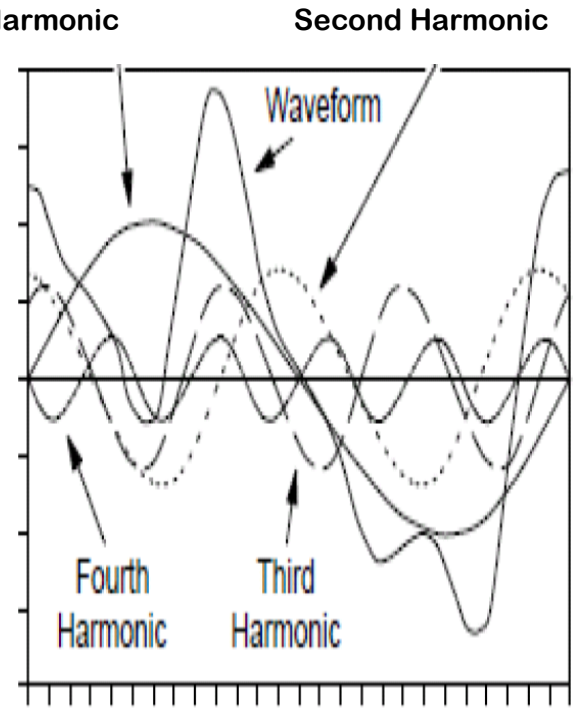

Fig. 2.33: Harmonic waveforms.

(Both figures are sourced from a paper written by Pacejka (2006)).

b) Lateral force variation

The lateral force variation is a property of the tyre that characterizes its dynamic behaviour of the steering, the traction and the braking load by transmitting the lateral forces between the vehicle and the road. As the tyre rotates it may exert a lateral force on the order of ± 25 kg, causing steering pull in one direction. It is typical for the force to vary up and down from ± 25 kg. A variation between 22 and 26 kg would be characterized as a 4 kg lateral force variation (LFV).The circumference of the tyre can be modelled as a series of very small spring elements with spring constants that vary according to the manufacturing conditions. These spring elements are compressed as they make contact with the road surface, and they recover as they exit the footprint. The variation of the spring constants in the lateral direction cause fluctuations in the compressive and restorative forces as the tyre rotates. This variation is the source of various disturbances during a ride. Both tyre and car makers seek to reduce such disturbances for dynamic performance improvement of the vehicle. **Fig. 2.34** illustrates the lateral force acting on the pneumatic tyre.

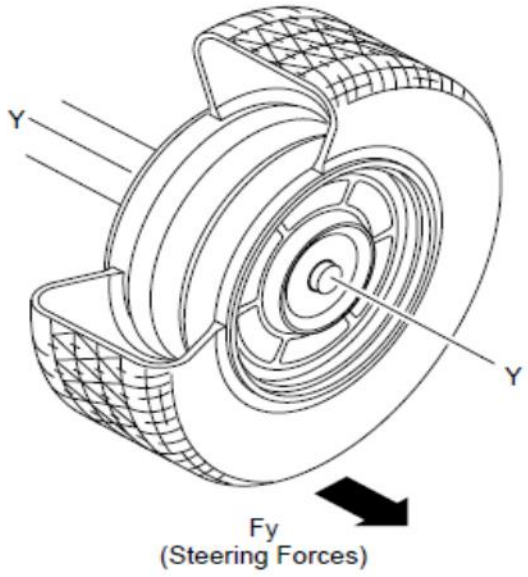

Fig. 2.34: Lateral force acting on the pneumatic tyre (Pacejka, 2006).

c) Tangential force variation

The tangential force is the load acting in the direction of rotation. The tangential force variation expresses the change in this force as the tyre rotates under the load. As the tyre rotates and spring elements with various spring constants enter and exit the contact area, as the tangential force changes. As the tyre rotates it applies a high traction force in order to accelerate the vehicle and maintain its speed under constant velocity. The driving force between the tangential axis and the tyre is parallel to the road in the direction of rotation. The driving force F_x is applied to the tyre in this axis. **Fig. 2.35** illustrates the tangential force acting on the pneumatic tyre (Pacejka, 2006).

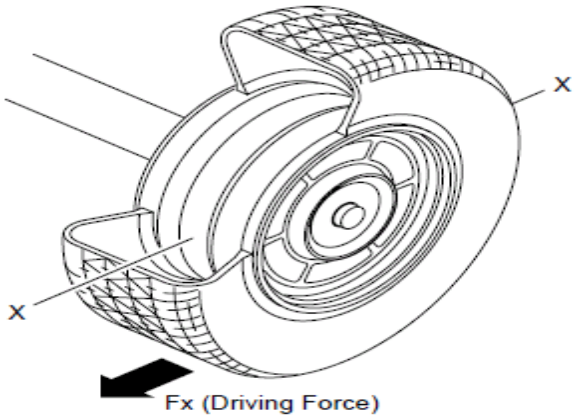

Fig. 2.35: Tangential force acting on the pneumatic tyre (Pacejka, 2006).

d) Conicity

Tyre conicity is a lateral force defined as lateral shifts due to the clockwise rotation. It is a parameter based on the lateral force behaviour. Tyre conicity is used as an indicator of steering pull caused by off-center belt (about 30 N/mm offset). It is the characteristic that describes the tyre's tendency to roll like a cone. A properly inflated tyre causes a vehicle to pull sideways when driven due to conicity. The lateral force is exerted in the same direction, clockwise or counter-clockwise. **Fig. 2.36** illustrates the conicity on a Pneumatic tyre.

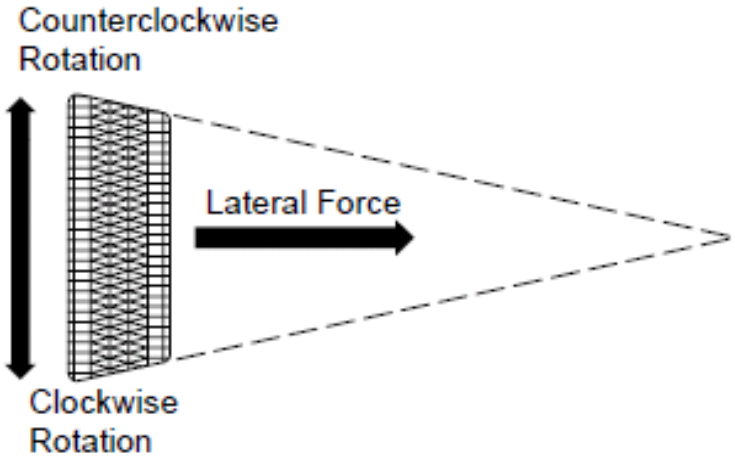

Fig. 2.36: The conicity on a pneumatic tyre (Pacejka, 2006).

e) Plysteer

The ply steer describes the lateral force that the tyre generates due to the symmetries in its carcass as it rolls forward with zero slip angle and may be called pseudo side slip. It is the characteristic that is usually described as the tyre's tendency to move sideways while maintaining the straight-line orientation. This tendency affects the steering performance of the vehicle. Ply steer is determined by measuring the lateral force generated as the tyre rolls both forward and backward. The ply steer force depends on direction of rotation and the outer-most ply has the dominant effect. The ply steer is not measured in production testing, but it is measured during performance review inspections. **Fig. 2.37** illustrates the ply steer on a pneumatic tyre (Pacejka, 2006).

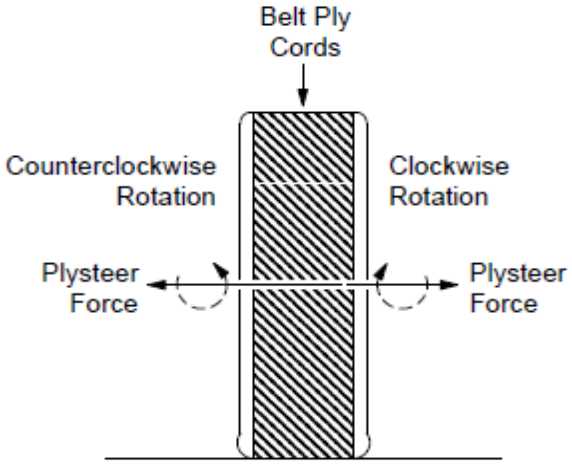

Fig. 2.37: The ply-steer on a pneumatic tyre (Pacejka, 2006).

f) Radial Run-Out

Radial Run-Out (RRO) is the deviation in roundness, or change in distance from the center of the tyre outward to the tread, as the tyre is rotated. This means that the pneumatic tyre rotates about a secondary axis instead of being centrally aligned. Severe RRO causes an excitation into the vehicle in a manner similar to radial force variation and can cause up and down vibrations that result in hopping of the tyre while on rotation. The RRO is most often determined by measuring the radial displacement of the pneumatic tyre surface as the tyre rotates. **Figs. 2.38-39** illustrate the measurement of the RRO on the pneumatic tyre (Pacejka, 2006).

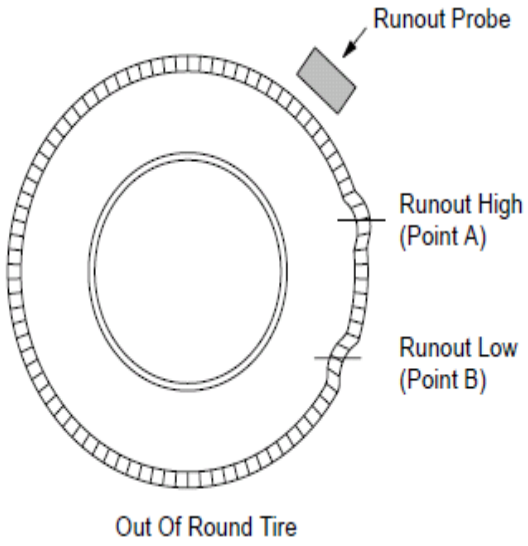

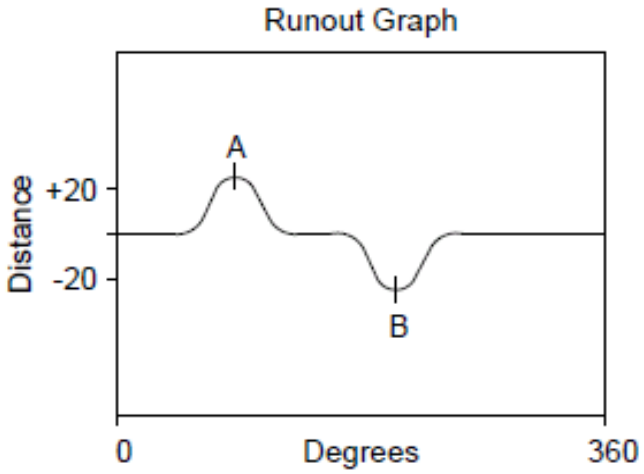

Fig. 2.38: Pneumatic tyre with radial run-out. **Fig. 2.39:** RRO measurement.

(Both figures are sourced from a paper written by Pacejka (2006)).

g) Lateral Run-Out

The lateral run-out (LRO) is the amount "wobble" and sideways motions generated due to dynamic imbalance problems as the pneumatic tyre rotate. The LRO causes an excitation into the vehicle in a manner similar to lateral force variation. The sensitivity of a vehicle to wobble vibration from lateral run out is eight to four times that of radial run out. Apollo-Dunlop tyres use a dial indicator to measure lateral run-out on pneumatic tyres. A dial indicator is placed on the tyre sidewall to measure the sidewall thickness uniformity.

h) Sidewall Bulge and Depression

A sidewall bulge is a weak spot in the tyre due to a lack of cord material and defected fabric in sidewall ply. The mistakes that affect the outside appearance of the finished sidewall can happen during tyre building. An overlap or a gap, in a cord material will show up in the finished tyre as bulges or depressions. Sidewall depression is a brittle spot that does not inflate in equal measure

as the surrounding area. Both visual defects are deemed scrap. The tyres are measured during the production process so to identify those with severe visual defects. The bulges may also indicate defective construction conditions such as missing cords, which is regarded as a safety hazard. As a result, tyre makers impose stringent inspection standards to identify tires with bulges. The tyre sidewall bulge and depression are measured by using a dial indicator to monitor the sidewall thickness uniformity. **Fig. 2.40** illustrates the pneumatic tyre with a bulged sidewall (Pacejka, 2006).

Fig. 2.40: Pneumatic tyre with a bulged sidewall (Pacejka, 2006).

2.3.7.4 Tyre Balance Testing

Tyre balance is the uniform distribution of tyre mass about the axis of its rotation, where the tyre center of gravity is located in the same point as the center of rotation. A balanced tyre is one with a mass that is uniformly distributed around its center of rotation when mounted on the axle of the balancing machine. An out-of-balance tyre leads to noticeable vibrations, degrades ride quality and shortens the tyre life span, bearings, shock absorber, and other suspension components.

Apollo–Dunlop tyres use an axis system to measure the dynamic mechanical properties of the pneumatic tyres as defined by a set of measurement standards and test conditions accepted by the global tyre and car makers. These measurement standards include the parameters of static, dynamic and run-out imbalances. Apollo – Dunlop tyres use the MTS Model 860 machine to measure these three imbalance parameters generated during tyre operation due to vibrations.

Fig. 2.41 illustrates the static and dynamic imbalanced tyres with a heavy spot (Pacejka, 2006).

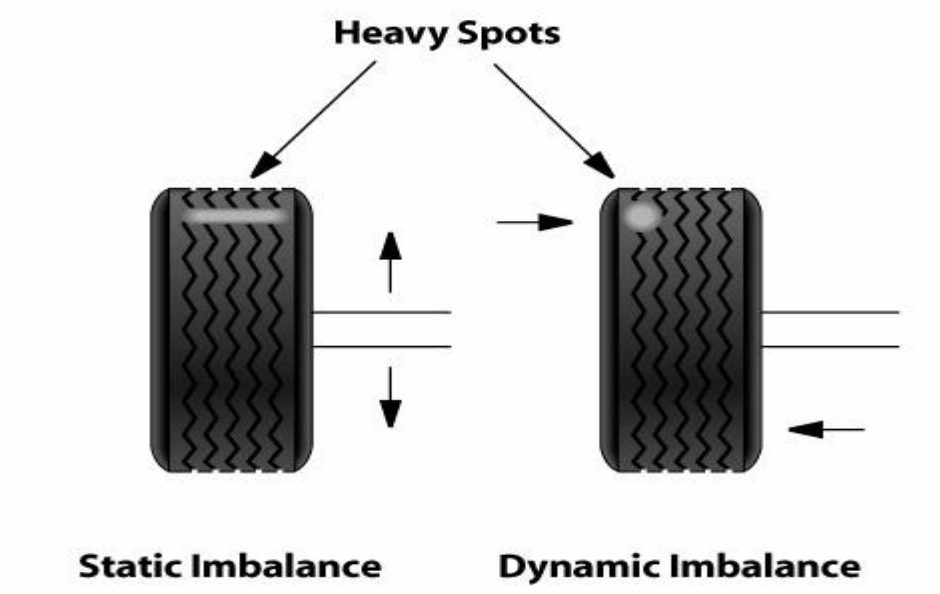

Fig. 2.41: Static and dynamic imbalanced tyres with a heavy spot (Pacejka, 2006).

a) Static Imbalance

Static imbalance is the upwards and downwards motion of the tyre caused by a heavy or light spot in the tyre. The static balance of a tyre is measured by using a static balancing machine where the tyre is clamped in its vertical axis on a non-rotating spindle tool. The heavy spot on the tyre is acted upon by gravity to deflect the tooling downward. The deflection magnitude indicates the severity of the imbalance. The angular location of the imbalance is indicated by the angle of the deflection.

b) Dynamic Imbalance

Dynamic imbalance is the lateral movement generated due to unequal weight on both sides of the tyre and wheel assembly's circumferential center-line. At Apollo-Dunlop tyres, the tyre and the wheel are mounted on a balancing machine test, the tyre – rim assembly is accelerated up to a speed of 100 rpm (20 to 25 km/h with recent high sensitivity sensors) or higher, 300 rpm (85 to 90 km/h with typical low sensitivity sensors).The imbalanced forces are measured by sensors as the tyre rotate, these forces are resolved into static and their compared to the imbalance tolerance (the maximum allowable manufacturing limits).

c) Run Out Imbalance (ROI)

Improper bead seating of the tyre-wheel assembly cause excessive radial and lateral movement resulting from the tyre non-uniformity. The Run-out balance can be achieved by balancing the radial and lateral imbalances. The radial run-out balancing is achieved by rotating the two bolts positioned at 180^{0} on the wheel. The lateral run out is achieved by using a run out gauge to check both the tyre and wheel. The highest point of a run-out on both the tyre and wheel is chalk marked. The out of specification component (tyre, wheel, or both) get replaced. This is corrected by measuring the amount of the tyre - rim assembly run out with a gauge, and the component having excessive run out is replacing. **Fig. 2.42** illustrates the lateral and radial imbalance measurement on pneumatic tyre.

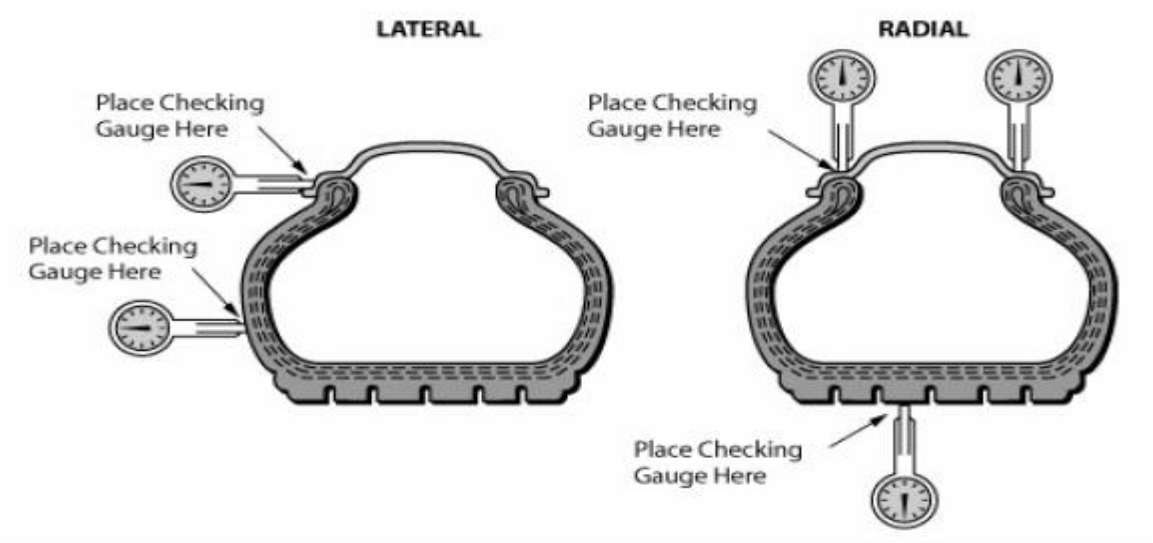

Fig. 2.42: Lateral and radial imbalance measurement on a pneumatic tyre (Pacejka, 2006).

2.3.7.5 X – Ray Inspection

The tyre X-ray inspection is the most common and proven quality control method available today in the tyre manufacturing sector. Tyres are subjected to high safety standards, hence a thorough quality check has to be carried out during the tyre production. Apollo-Dunlop tyres use a SS-X1006SMI Collman machine to carry out X-ray inspections. This enables a high-grade quality control and can directly be integrated into the production process because of its high scanning rate. The common defects that are normally produced at Apollo-Dunlop tyres are namely: open ply joint (OPJ), distorted ply and foreign objects. **Fig. 2.43** illustrates an open ply joint defect.

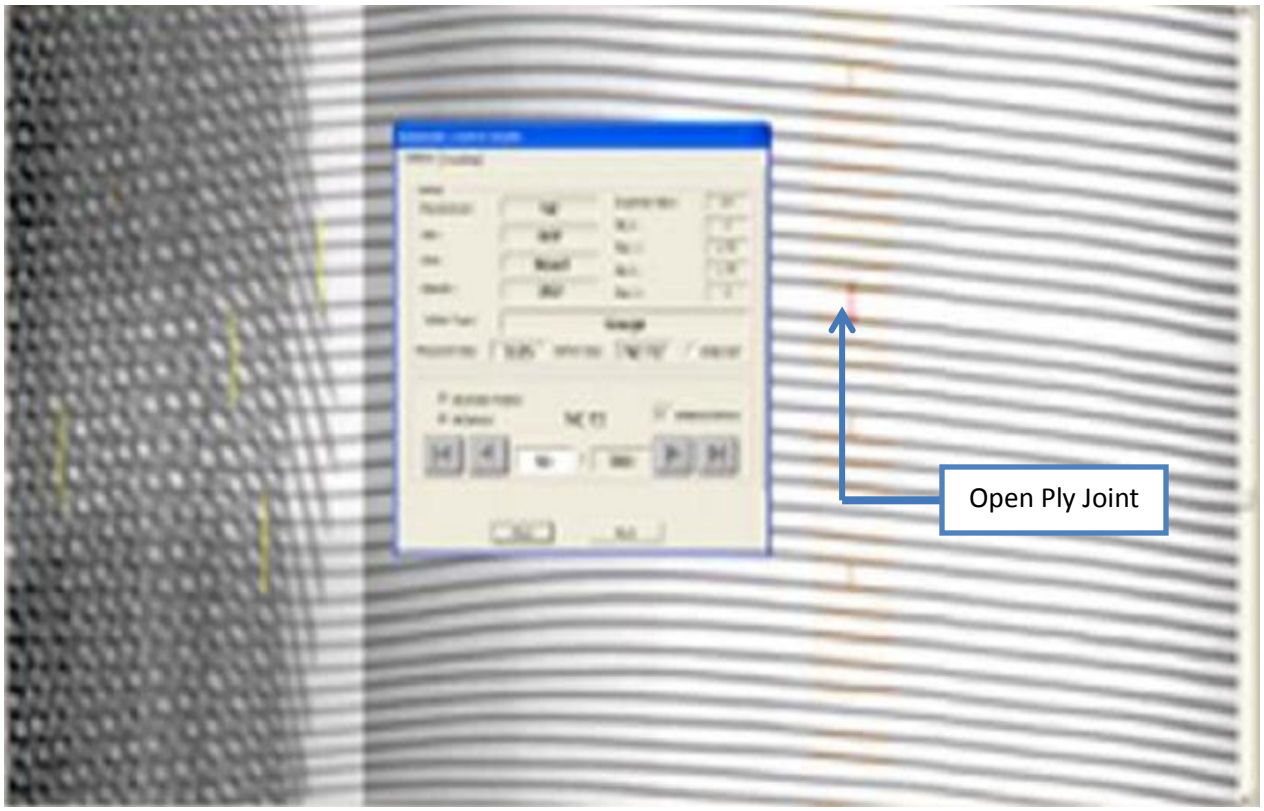

Fig. 2.43: An open ply joint defect (Courtesy from Apollo-Dunlop tyres).

The open ply joint (OPJ) is considered as the first degree defect because it cannot be repaired. Therefore, the damaged plies necessitate tyre scrapping. The OPJ defect is generated during plies splicing on the bias cutter or during the first stage of the tyre building. The splice dimensions can vary according to the ply tension, the slippage, the cutting accuracy and the heavy or open splices which are a potential source of defects in the finished tyre. **Fig. 2.44** illustrates a distorted ply defect.

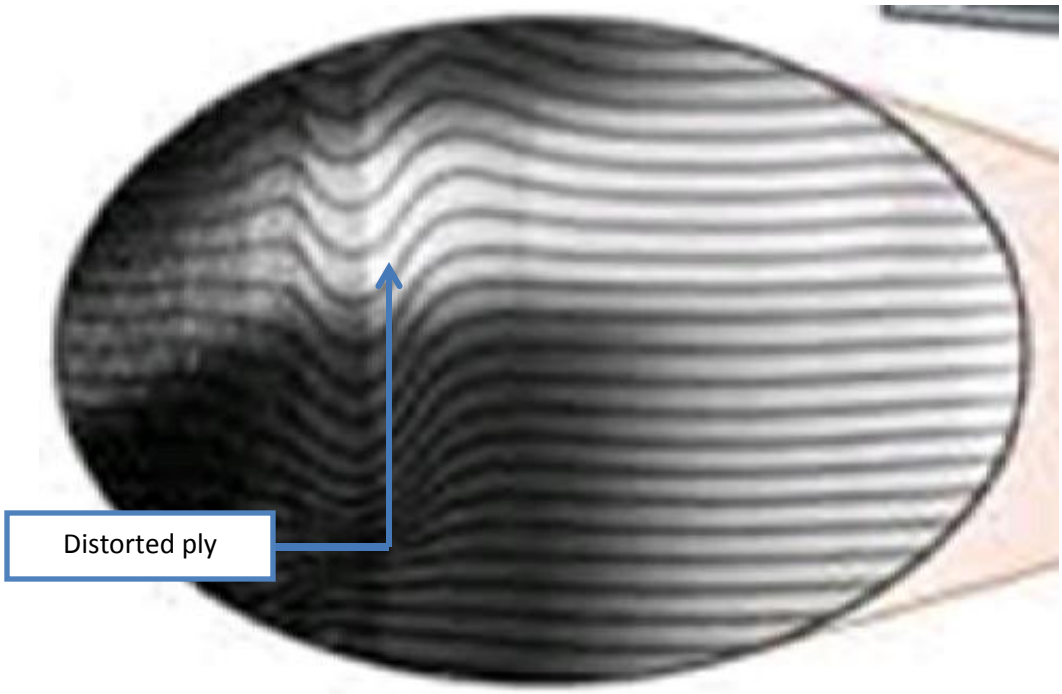

Fig. 2.44: Distorted ply defect (Pacejka, 2006).

The plies are layers made out of inextensible cords embedded in the rubber to hold its shape by preventing the stretching of the rubber in response to the internal pressure. The distorted ply defect is mainly formed during the curing process. The bladder is inflated to 26 bars to compress or pressurize the green cover against the mould tread pattern to form the desired tyre shape (see **Fig. 2.25** for inflated bladder awaiting the green cover). The distorted plies form with excessive curing pressures over 27 bars. The SS-X1006SMI Collman machine has given the industry a more versatile method of verifying the integrity of the tyre construction. **Figs. 2.45-46** illustrate the SS-X1006SMI Collman machine carrying out an X-ray inspection on a pneumatic tyre and the G03 vertax eye scanning the tyre inner liner.

Fig. 2.45: The tyre-tread X-ray inspection. **Fig. 2.46:** The tyre inner-liner inspection.

(Both figures are a Courtesy from Apollo-Dunlop tyres)

2.3.7.6 Tyre performance evaluation

The tyre performance evaluation is a process of determining the durability, effectiveness and the life-span of a tyre through quantitative tests carried out in testing lab. This process demonstrates if the pneumatic tyre meets Apollo-Dunlop tyres performance requirements. Apollo-Dunlop brand tyres are tested together with competitor's tyres to demonstrate areas that require improvement. This enables tyre optimization studies to be carried out in order to remain competitive in the industry. Apollo-Dunlop tyres test tyre designs against performance criteria such as, the aquaplaning resistance, the braking ability and the tyre wear-rate.

a) Braking ability

Braking ability is the time the tyre takes to maintain the traction and the braking performance on wet road surfaces before it comes to a complete stop when the brakes are applied. A 4.28 ton load is exerted onto the axle of the tyre and the tyre is run at 120 km/h before a sudden stop.

Fig. 2.47 illustrates the braking performance test carried out on the DL526ATL (5 Ton) ATL machine.

Fig. 2.47: Braking performance test carried out in the DL526ATL machine (Tompkins, 1981).

b) Aquaplaning Resistance

The tread grooves of a pneumatic tyre are designed to remove water from underneath the tyre, in order to provide high friction even in wet conditions. The aquaplaning occurs when the pneumatic tyre encounters excessive water that it cannot dissipate, this lead to poor traction that prevents the vehicle from responding to control inputs. If it occurs to all four tyres simultaneously, the vehicle becomes uncontrollable and loss of stability occurs. The pneumatic tyres are tested in a patch of water using the primacy MXV4 machine to measure aquaplaning resistance.

c) Wear Resistance

The tyre wear is a complicated phenomenon that depends on numerous parameters such as the tyre compound, design, vehicle type, road conditions and environmental conditions. The tyre wear has negative effects on the economy and ecology of the tyre industry, therefore, tyre wear prediction is of higher importance to tyre manufacturers. Apollo-Dunlop tyres utilises a hydraulic driven indoor wear tester capable of testing tyres at high speeds (± 250 km/h). It simulates loads, accelerations and cornering – to reproduce what a tyre experiences on the road. The radial load and lateral force are measured through strain gauge sensors for the ability to control lateral force by slip angle motion.

3. The warm up process

This chapter provides an understanding on the mould warm up process. The scope of this chapter includes the procedure and importance of the tyre compression mould warm up process. A fundamental theory of the relationship between the required steam volume and the warm up duration for the tyre compression mould to reach operational temperature is briefly discussed. It is a necessity to know what influence a particular process will have on the tyre's response to different conditions (i.e. stress, heat).

The mould warm up is a process of preheating the tyre compression mould so the rubber material can be softened by the heat. The green cover is placed directly into a heated metal mould, whilst the bladder inflates to compress the cover against the tyre compression mould to force the green cover to conform to the shape of the mould. Apollo-Dunlop tyres use saturated steam to warm up the tyre compression moulds to the operational temperature. Saturated steam is utilised due to its ability to transport controllable amounts of energy from boiler house to the point of use. Steam use as heating media is popular throughout the industry for mechanical power generation and process applications, reasons for using steam are as follows:

- Steam is easy to generate.
- Steam is cost efficient and it is easy to manage.
- Good heat transfer coefficients and energy is easily transferred to media.

The use of saturated steam as an energy media can be traced back to the early age of industrial practices. The heat transfer continues to be a field of major interest to scientific and engineering researchers, as well as developers, designers and manufacturers. Steam provides means of

transporting adjustable amounts of heat energy from a central, automated boiler house, where it is efficiently and economically generated, to the point of use. It was in the late 1970s when the electrical heating system was implemented in moulding industry (Laughton and Say, 2013). However, it was later realized that the electrical heating system was economically inefficient with recent power generation and distribution problems encountered in South Africa.

Apollo-Dunlop tyres efficiently and economically generate steam from an 11KV electrical boiler and a HFO oil boiler. **Fig. 3.48** illustrates Apollo-Dunlop steam distribution system for the curing process.

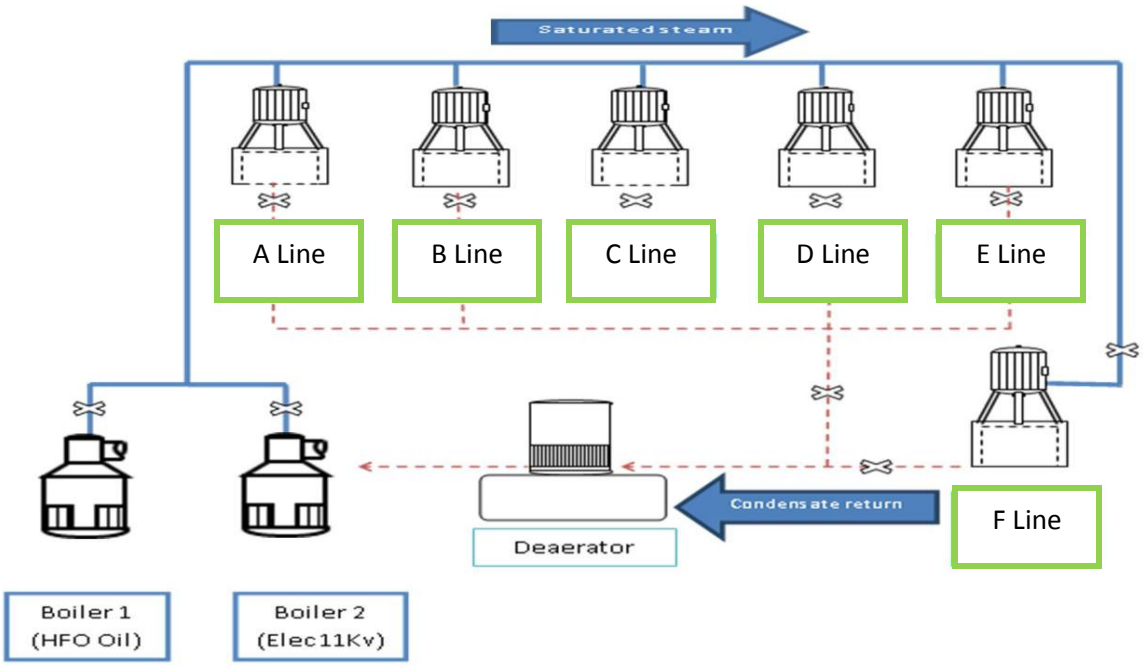

Fig. 3.48: Steam distribution system (Courtesy from Apollo-Dunlop tyres).

3.1 The warm up procedure

Four bar saturated steam is fed into the press dome at 151^0C temperature, to heat up the prismatic container that eventually transfers the heat energy to the tyre compression mould through convection heat transfer. The temperature and pressure probes are mounted inside the

press dome to monitor saturated steam conditions. Unfortunately, the tyre compression mould profile temperature cannot be directly monitored, since there is no temperature probe mounted onto the tyre compression mould. It proved to be difficult to have a permanent temperature probe mounted on tyre compression mould, since, tread sectors keep opening and closing during operation.

3.1.1 The warm up process start-up

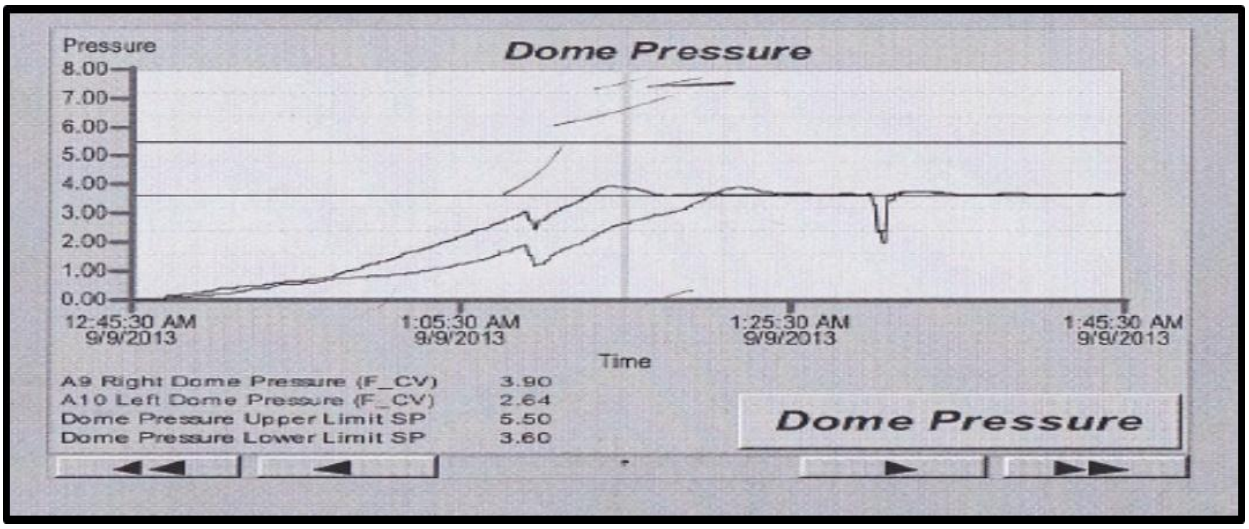

Fig. 3.49: The start-up time of the tyre compression mould warm-up process

(**Fig. 3.49** is a courtesy from Apollo-Dunlop tyres)

As shown above, saturated steam is introduced into the press dome at 4 bars and 151^0 C. Saturated steam is continuously introduced into the press dome for a period of five hours. As the press dome is pressurised, steam transfers heat energy to the prismatic container through convection heat transfer, while the prismatic container transfers heat energy to the tyre compression mould through conduction heat transfer.

3.1.2 The warm up process end-time

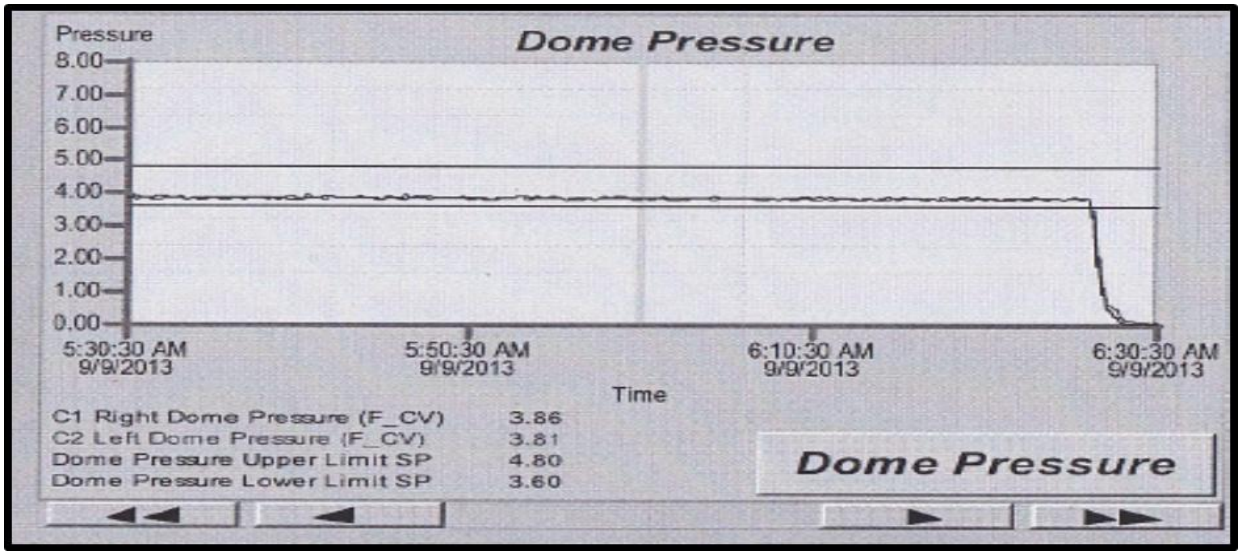

Fig. 3.50: The end-time of the tyre compression mould warm-up process.

(**Fig. 3.50** is a courtesy from Apollo-Dunlop tyres)

The warm up duration determines if the tyre compression mould is ready or not to proceed with the curing process. Saturated steam is normally fed into the press dome for five hours before the tyre compression mould is declared ready to start with curing process. The tyre compression mould mass has been gradually reduced throughout the years but focus was never on optimizing the warm up process.

3.2 Steam usage during warm-up

Apollo-Dunlop tyres moulding plant is composed of 85 curing presses. The curing presses steam feed-lines do not possess mass flow-meters, therefore, it is difficult to regulate or measure the steam quantity used on each curing press during the warm up process. The 85 curing presses are divided into 6 sections (A-F). The existing mass flow-meters are mounted on the main steam-line towards every two sections of the curing presses.

Hence, the moulding plant only has 3 mass flow-meters. It was found to be difficult to quantify steam flow into each curing press due to a shortage in measuring equipment. The steam mass flow-meter on A and B curing sections was monitored for 10 months in order to approximate the steam consumption during warm up period for A and B curing sections. It was discovered that the steam consumption across A and B curing sections varied with calendar seasons. Graph 1 illustrates the steam consumption of A and B curing sections during the warm up process, throughout the 10 months period.

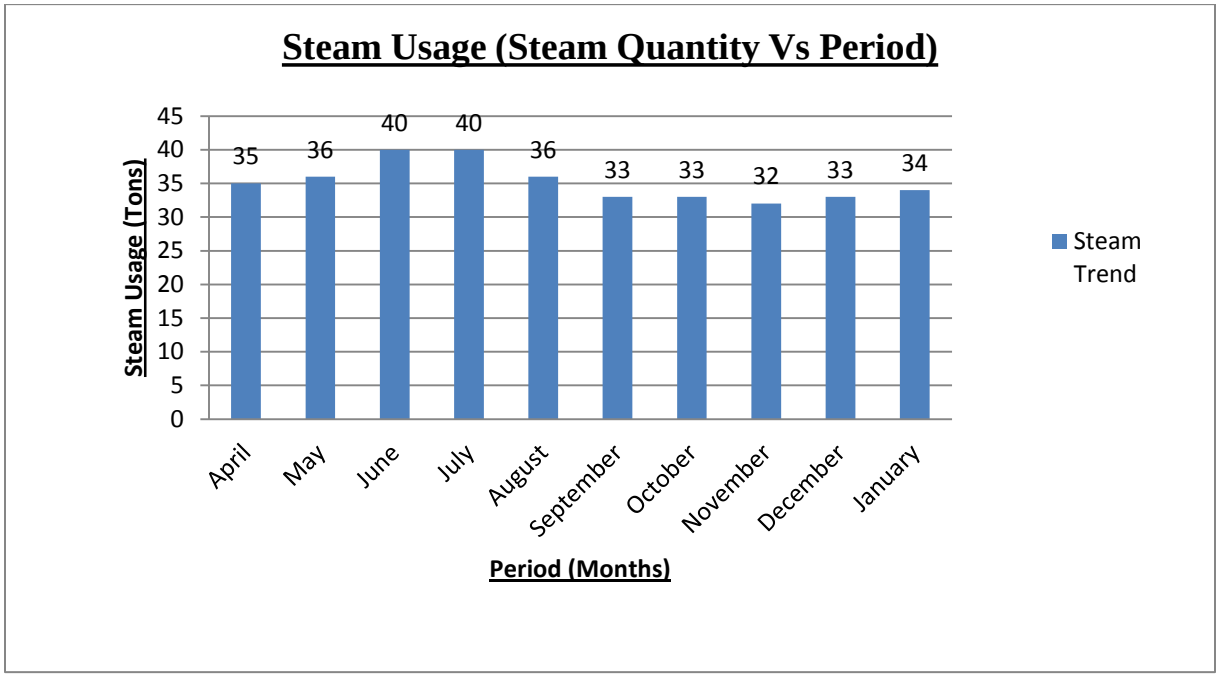

Graph 1: The steam consumption of A and B curing sections during the warm up section.

(Graph 1 is a Courtesy from Apollo-Dunlop tyres).

Apollo-Dunlop tyres warm up the tyre compression moulds once per week. Therefore, it is critical that the press dome preserve the steam temperature during the warm up process, hence, the press dome is insulated with a 30 mm air gap covered with 10 mm galvanised sheet for capsulation. The winter season (June - August) has high steam consumption due to a temperature gradient, in this case it is the temperature difference between the press dome and its

surroundings. The steam demand is high during winter since high heat losses occurs due to radiation heat transfer. Graph 1 show that an average steam usage for A and B curing sections is 35 tons per month. Curing sections, A and B are each composed of 5 curing presses, therefore, 35 tons is used on ten presses to warm up the tyre compression moulds in the A and B curing sections. This entails that each curing press use 0.875 tons saturated steam per warm up session. Therefore, the reduction of the steam usage during the warm up process of the tyre compression moulds is very beneficial considering high costs of producing saturated steam.

4. Steam consumption numerical evaluation

This chapter contains an overview of the type of the method carried out to investigate the steam consumption of the tyre compression mould during the warm up process. The significance of the numerical analysis method is highlighted and the scope it presents as a solution to further problems. This study aims at presenting a basic application of heat transfer analysis to demonstrate the heat energy required and heat losses during the warm up process.

The steam quantity required to warm up a moulding the plant can be determined using three methods, namely: numerical analysis, direct measurement and thermal rating. In this case, numerical analysis has been utilised to determine the steam consumption of the tyre compression mould during the warm up process. The numerical analysis method has been utilized instead of the direct measurement method, due to Apollo-Dunlop tyres financial constraints. The direct measurement method is recording the steam flow rate across the inlet pipe of each curing press, Apollo – Dunlop tyres does not possess steam flow meters on the curing presses. Therefore, numerical analysis has been used to determine the minimum steam amount required to warm up the tyre compression mould to reach the operational temperature.

4.1 Numerical analysis

The four bar saturated steam is fed into the press dome. The press dome is a split vessel with an oblate spheroid upper half and cylindrical bottom-half. The press dome houses the metallic components such as the prismatic container, the platen mould adjuster, the support bars and the tyre compression mould. The latent heat energy of the saturated steam is conventionally

transferred into the press dome internals as soon as it enters the press dome. However, the prismatic container transmits heat energy molecules into the tyre compression mould through conductional heat transfer. 1st law of thermodynamics is applied to determine the required thermal heat energy for the tyre compression mould to heat up from the ambient to the operational temperature. The 1st law of thermodynamics is given as follows:

$$Q = Mc_v\Delta T \qquad (4.1)$$

Where Q is the thermal heat energy, M is the mass of media, c_v is the specific heat capacity and ΔT is the change in the initial and the final temperature.

The steam quantity required for the tyre compression mould to reach the operational temperature can be determined by dividing the required total sensible heat energy Q_T with the enthalpy h_{fg}. **Fig. 4.51** illustrates an assembled compression mould in a prismatic container (without the platen adjuster and the support bars).

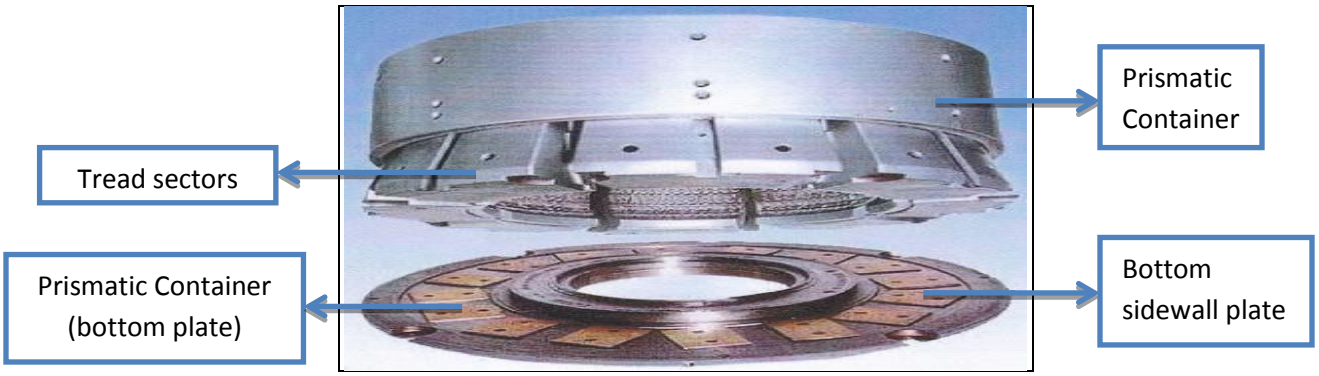

Fig. 4.51: Assembled tyre compression mould with prismatic container (Tompkins, 1981).

4.1.1 Platen Mould Adjuster

The platen mould adjuster is a metal plate mounted on the curing press. The mould adjuster compresses the upper and lower moulds into position in order to create an even seal of the prismatic container during the curing process. **Fig. 4.52** illustrates a stripped platen mould adjuster on top of the prismatic container.

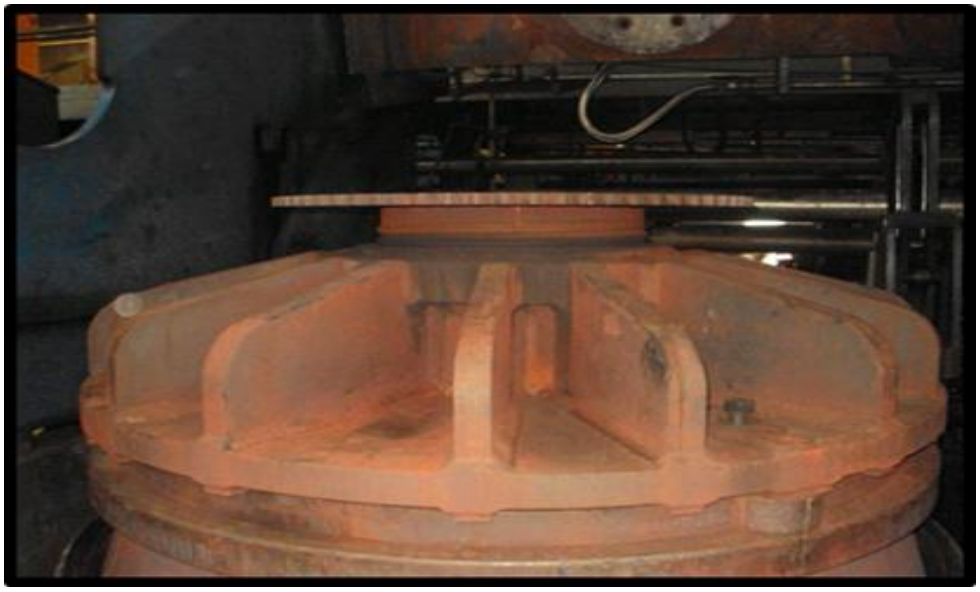

Fig. 4.52: Stripped platen mould adjuster mounted on the prismatic container

(**Fig. 4.52** is a Courtesy from Apollo-Dunlop tyres)

The platen adjuster is composed of plain carbon steel, Grade-350WA. The plain carbon steel density is $\rho = 7860\ \text{kg}/m^3$ (see ***Appendix D***) and the platen volume is $V = 0.182\ m^3$ (see ***Appendix E*** for calculations).The initial temperature T_1 of the platen is 25^0C, this was measured with a temperature gun. The operational temperature of $T_2 = 160^0\text{C}$ was used instead of required 151^0C since allowances were made for unforeseen losses. The specific heat capacity of Grade-350WA plain carbon steel is $c_v = 0.49\ {}^{\text{kJ}}/_{\text{kg. k}}$ (see ***Appendix F***).

The platen adjuster mass is found to be:

$$\rho = {}^{M_p}/_{V}, M_p = (0.182)(7860) = 1430.5\ kg \quad (4.2)$$

Therefore the thermal heat energy required by platen plate (mould adjuster) is given as follows:

$$Q_{pm} = mc_v\Delta T \quad (4.3)$$

$$Q_{pm} = mc_v(T_2 - T_1) \quad (4.4)$$

$$Q_{pm} = 94.6\ \text{MJ (heat energy)} \quad (4.5)$$

The thermal heat energy required by the platen adjuster to warm up from the initial to the operational temperature is 94.6 MJ.

4.1.2 Prismatic container

The prismatic container is a plain carbon steel container that houses the tyre compression mould. It is made of segments that provide the tread sectors with the compression movement. The prismatic container is the heaviest component in the press dome. Hence, it consumes more steam when compared to the other press dome internals. **Fig. 4.53** illustrates an assembled prismatic container.

Fig. 4.53: An assembled prismatic container (Courtesy from Apollo-Dunlop tyres).

The prismatic container mass was physically measured to be $M_p = 3900\,\text{kg}$. Apollo-Dunlop tyres use one standardised container for all the curing presses. The initial temperature T_1 used for the prismatic container is 15^0C due to its frequent removal from the curing presses. The prismatic container is stored in a room with low controlled temperatures and it is replaced more often. Therefore the operational temperature of $T_2 = 160^0\text{C}$ was used instead of required 151^0C since allowances were made for unforeseen losses. The prismatic container is made of Grade-350WA plain carbon steel, therefore, the specific heat capacity is $c_v = 0.49\ {}^{\text{kJ}}/_{\text{kg. k}}$. The thermal heat energy required by the prismatic container is given as follows:

$$Q_{pc} = mc_v\Delta T \tag{4.6}$$

$$Q_{pc} = mc_v(T_2 - T_1) \tag{4.7}$$

$$Q_{PC} = 277.1\ \text{MJ (heat energy)} \tag{4.8}$$

The thermal heat energy required for the prismatic container to warm up from the initial to the operational temperature is 277.1 MJ which is significantly higher due to the material mass of the container.

4.1.3 Prismatic Bars

The prismatic bars secure and align the prismatic container. **Fig. 4.54** illustrates the prismatic container support bars.

Fig 4.54: Prismatic container support bars (Courtesy from Apollo-Dunlop tyres)

The prismatic support bars are composed of Grade-350WA plain carbon steel. Thus, the specific heat capacity and density are 0.49 $^{kJ}/_{kg.k}$ and 7860 kg/m^3, respectively. The combined volume of each prismatic support bar was physically measured and found to be $0.019\ m^3$(see ***Appendix E*** for calculations).The prismatic bars are fixed to the curing press, therefore, they are always warm when compared to the other components. Hence, the ambient temperature T_1 used is 25^0 C and the final temperature T_2 is 160^0C. The mass of the support bars is found to be:

$$\rho = {}^{M_S}/_{V}, M_S = (7860)(0.019) = 149\ kg \quad (4.9)$$

Therefore the thermal heat energy required by the support bars is given as follows:

$$Q_{PB} = mc_v\Delta T \quad (4.10)$$

$$Q_{PB} = mc_v(T_2 - T_1) \quad (4.11)$$

$$Q_{PB} = 9.85\ \text{MJ (heat energy)} \quad (4.12)$$

The thermal heat energy required for the prismatic support bars to warm up from the initial to the operational temperature is 9.85 MJ.

4.1.4 Tyre Compression Mould

The tyre compression mould cures the green cover into the pneumatic tyre through a vulcanization process. The tyre compression mould is first preheated up to the operational temperature of 151^0C before the vulcanization process occurs. The tyre compression mould is preheated so to apply the pressure and heat energy onto the green cover in order to stimulate the chemical reactions between rubber and other tyre construction materials. The tyre compression mould is composed of the upper sidewall plate, the lower sidewall plate and the tread sectors. As the tyre compression mould closes, the bladder inflates in order to apply the pressure to force the rubber material into contact with all mould cavities, while heat and pressure are maintained until the rubber material has cured into a pneumatic tyre. The bladder inflation enables the rubber material to take the tread pattern prints and sidewall lettering engraved into the green tyre.

Figs. 4.55-57 illustrate the stripped compression mould.

Fig. 4.55: Tyre compression mould (Best, 2004).

Fig. 4.56: Tread sectors of the mould.

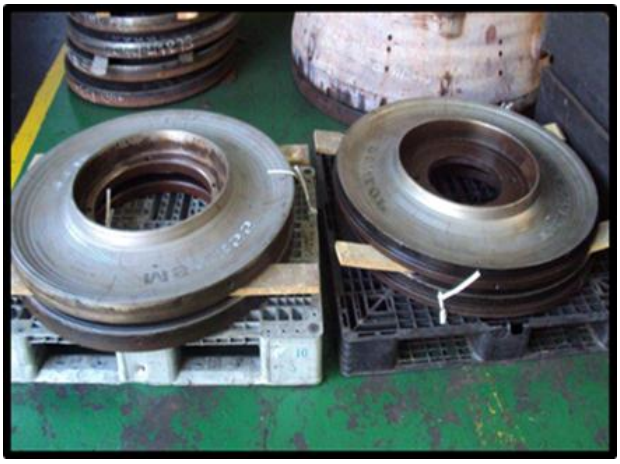

Fig. 4.57: Sidewall plates of the mould.

(**Figs. 4.56-57** are a Courtesy from Apollo-Dunlop tyres).

Apollo - Dunlop tyres manufacture various types of tyres, but this study focus is on truck bus radial (TBR) plant. The TBR plant builds and mould tyres ranging from R17- 275/344 to R34-295/355. The tyre compression mould size varies but the prismatic container has a standard size. Therefore, the mould thickness is the only dimension that varies since the prismatic container has a standard geometry. This makes the smallest size tyre to have more mould flesh to warm up. The thicker the tyre compression mould the more the thermal energy required to warm it up to

the operational temperature. The numerical analysis is applied to determine the minimum amount of energy required to heat the mould material of the R17- 275/344 tyre compression mould. The minimum thermal heat energy required to warm up the R17- 275/344 tyre compression mould was determined as follows:

The mass of the tread sectors and sidewall plates of the tyre compression mould were physically measured using a scale:

Tread sectors = 665 kg (The tyre compression mould consists of 10 tread sectors)

Sidewall plates = 707 kg (The tyre compression mould consists of 2 sidewall plates)

M_m = sectors + sidewall plates + additional mass (4.13)

M_m = 665 + 706+ 50 (i.e.: 50 kg represent unforeseen masses)

M_m = 1422 kg (4.14)

The tyre compression mould ambient temperature T_1 is assumed to be the same as the prismatic container temperature since both components get replaced and stored in the same room. The tyre compression mould is composed of Grade350WA plain carbon steel therefore the specific heat capacity and density are 0.49 $^{kJ}/_{kg.\,k}$ and 7860 kg/m^3, respectively.

$$Q_{CM} = mc_v\Delta T \quad (4.15)$$

$$Q_{CM} = mc_v(T_2 - T_1) \quad (4.16)$$

$$Q_{CM} = 101\ \text{MJ (heat energy)} \quad (4.17)$$

The thermal heat energy required for the 275/344 compression mould to warm up from the initial to the operational temperature is 101 MJ.

4.1.5. Vacant dome volume

The vacant dome volume is the open space in the press dome that requires a certain saturated steam amount to pressurise the dome for high convection heat transfer rate to occur into the metal components inside the press dome. **Fig. 4.58** illustrates the vacant space inside the press dome that saturated steam must circulate before convection heat transfer occurs.

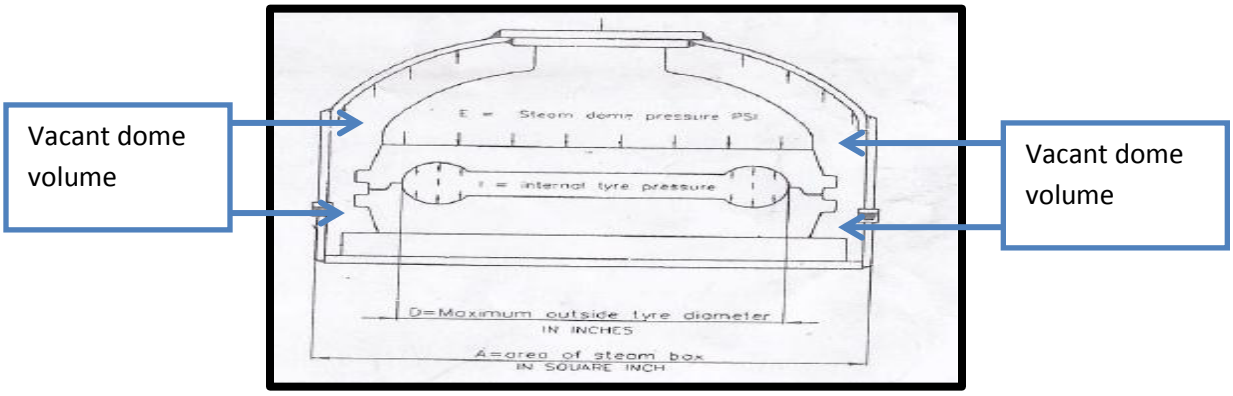

Fig. 4.58: The press steam dome with vacant dome space.

(**Fig. 4.58** is a Courtesy from Apollo-Dunlop tyres)

The vacant dome volume was determined by subtracting the volume occupied by components inside the press steam from the overall press dome volume. The press dome dimensions were physically measured off the press dome. **Fig. 4.59** illustrates press dome dimensions.

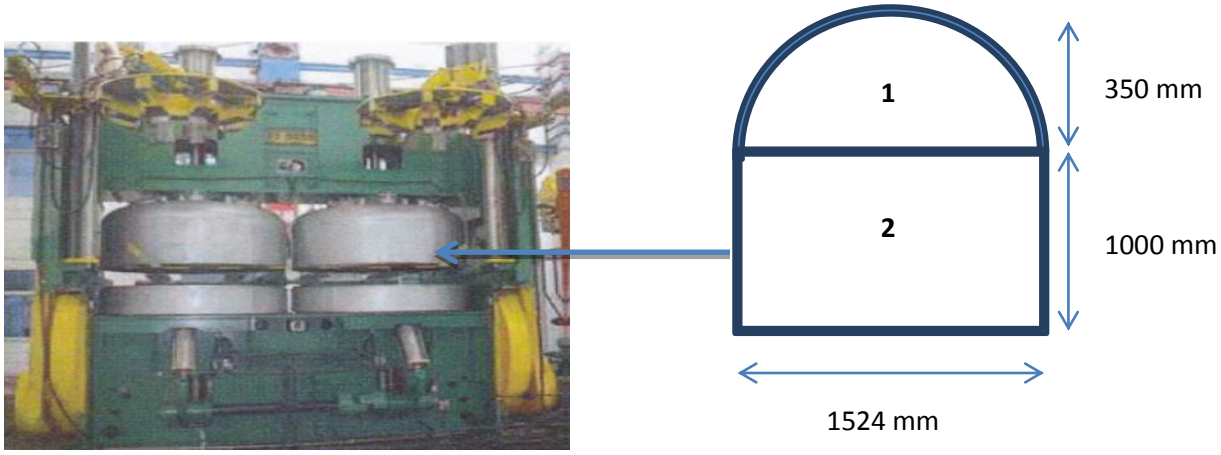

Fig. 4.59: Slightly open press (Courtesy from Apollo-Dunlop tyres).

The total press dome volume is found to be 2.67 m^3 (see ***Appendix E*** for calculations) and mostly occupied by the platen mould adjuster, the prismatic container and prismatic support bars, but a small volume of the press dome is still vacant. The vacant dome volume is found to be:

Vacant volume = Press-dome volume – prismatic container – prismatic bars – platen adjuster

The dimensions of the prismatic container, prismatic bars and platen were physically measured (see ***Appendix E*** for the volume calculations of some of the press dome internals).

$$\text{Vacant volume} = 2.67 - 1.025 - 0.019 - 0.182 \quad (4.18)$$

$$\text{Vacant volume} = 1.45\ m^3 \quad (4.19)$$

Therefore, the steam quantity required to occupy and pressurise the vacant dome volume can be determined as follows:

$$\rho = {}^{M_v}/_{V}$$

The density was found to be $2.669\ kg/m^3$ with gauge pressure of 4 bars (5.01 absolute pressure) at a temperature of 151^0C (see ***Appendix G*** for the density table).

$$\rho = {}^{M_v}/_{V}, M_v = (2.669)(1.45) = 3.86\ kg \quad (4.20)$$

The total thermal heat energy required to warm up the press dome equipment from the initial to the operational temperature is given as follows:

$$Q_T = \text{Dome} + \text{container} + \text{mold} + \text{platen} + \text{supports} \quad (4.21)$$

$$Q_T = 277.1 + 101 + 94.6 + 9.85$$

$$Q_T = 482.55\ \text{MJ} \quad (4.22)$$

The total thermal heat energy required to warm up the tyre compression mould to the operational temperature in the press dome is $Q_T = 482.55$ MJ. Therefore, the actual steam quantity required to supply such heat energy can be determined by dividing the total required thermal energy with the specific enthalpy h_{fg} at the operational absolute pressure and temperature. The required steam quantity is found to be:

The specific enthalpy h_{fg} was found to be $2107\ {}^{kJ}/_{kg}$ at a gauge pressure of 4 bars at a temperature of 151^0C (see ***Appendix G*** for the steam table). Therefore, required steam quantity is given as follows:

$$\text{Steam amount} = \frac{\text{Total thermal heat energy}}{\text{Specific ethalpy } (h_{fg})} \qquad (4.23)$$

$$\text{Steam amount} = \frac{482.55\text{x}10^6}{2107\text{x}10^3} = 229 \text{ kg}$$

20% (45.8 kg) of the required minimum steam quantity was added to counter high steam demand during extremely cold weathers. Therefore minimum required steam is 274.8 kg per dome. However, this required steam quantity is not inclusive of the thermal heat loss through insulation inefficiencies.

4.2 Heat Loss Due to Insulation Inefficiency

Apollo-Dunlop tyres have been using the same press dome material for more than 70 years. The performance of a thermal insulation may vary over time due to change of environmental conditions and ageing of material. Thermal insulation reduces heat energy flow between objects in range of radiation influence or in thermal contact. The heat flow is a consequence of thermal contact between objects with different temperatures. Thermal insulation can be achieved with

special engineered methods or processes, as well as with suitable object shapes and materials. The insulation performance of the press dome is influenced by many factors the most prominent of which include: the thermal conductivity λ, the surface emissivity ε, the insulation thickness t, the density ρ, and the specific heat capacity R, of the wall materials.

The insulating capability of the press dome was measured with thermal conductivity. Low thermal conductivity is equivalent to high insulating capability. The heat energy of the press dome body flows from high energy density towards its surroundings with lower energy density than the dome body. This heat loss process occurs through several mechanisms, namely: convection, conduction and radiation.

Convection is the heat energy transferred through saturated steam into the inside surface of the press dome wall. The rate of energy transferred dependents on the surface area of contact and the density of the saturated steam. ***Conduction*** is basically the transfer of heat energy into and throughout the press dome wall materials. The rate of heat energy transferred is dependent upon the surface area of contact and the conductivity of the press dome wall materials. ***Radiation*** is the electromagnetic energy emitted by the outside-wall surface of the press dome in the form of photons and waves. The radiation heat loss is related to the amount of energy released within the press dome body into its surroundings.

In every steam heating process, a certain percentage of steam heat energy is assumed to be the losses due to insulation inefficiencies. Fourier's law states that the rate of flow of heat through a single homogenous solid material is directly proportional to the area of the section at right angles to the direction of heat flow, and to the change of temperature with respect to the length of the path of the heat flow, dt/dx (Eastop and McConckey, 2006). **Figs. 4.60-61** show the press dome wall materials.

Fig. 4.60: The galvanized dome covers.

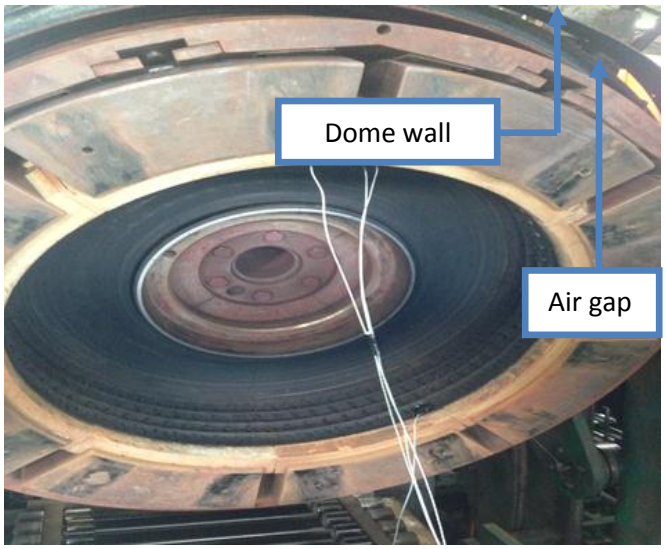

Fig. 4.61: The dome wall and air gap insulation.

(**Figs 4.60-61** are a Courtesy from Apollo-Dunlop tyres)

4.2.1 The heat-loss through convection-conduction

Fourier's law of convection and conduction was applied to determine the heat losses due to insulation inefficiency. Eastop and McConckey (2006) demonstrated the Fourier's law of conduction and conduction. In which a thin slab of material of thickness dx and surface area A has one force at a certain temperature and the other at a temperature $(t + dt)$ to determine rate of heat flow in the direction of x using Fourier's law. Demonstration of the Fourier's law in convection and conduction heat transfer through a solid slab is given as follows:

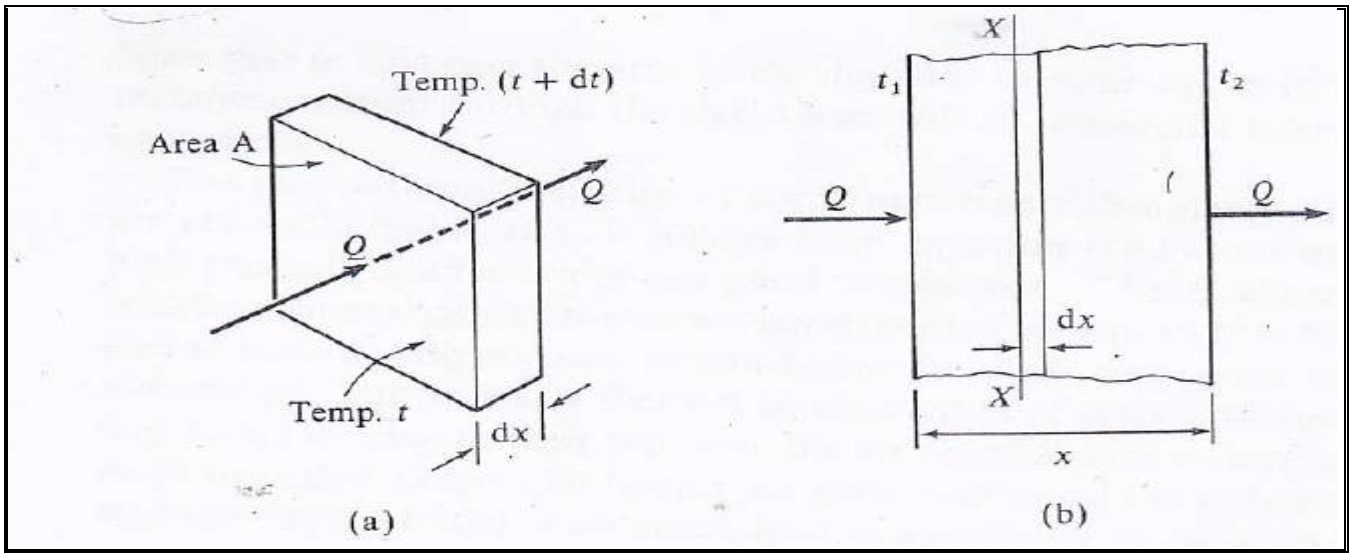

Fig. 4.62 (a and b): The heat flow through a thin slab of material (Eastop and McConckey, 2006)

The rate of the transferred heat is represented as,

$$\dot{Q} = \propto A \frac{dt}{dx} \tag{4.24}$$

$$Or\ \dot{Q} = -\lambda A \frac{dt}{dx} \tag{4.25}$$

We have,

$$\dot{Q} = -\lambda A \frac{dt}{dx} \text{ Or } \dot{Q}(dx) = -\lambda A\,(dt), \tag{4.26}$$

Then integrating,

$$\int_0^x \dot{Q}(dx) = -\int_{t_1}^{t_2} \lambda A\,(dt) \tag{4.27}$$

$$Or \dot{Q}(x) = -A\int_{t_1}^{t_2} \lambda\,(dt) \tag{4.28}$$

This equation can be solved when the variation of thermal conductivity λ with the temperature t are known. Now for most solids the value of thermal conductivity is approximately constant over various temperatures, therefore, λ can be considered as constant,

$$\dot{Q}(x) = -\lambda A \int_{t_1}^{t_2} (dt) \tag{4.29}$$

$$Or\ \dot{Q}(x) = -\frac{\lambda A}{x}(t_2 - t_1) = \frac{\lambda A}{x}(t_1 - t_2) \quad (4.30)$$

Newton's law of cooling states that the heat transfer of a solid surface area (A), at a temperature t_w, to a fluid of a temperature (t), is given by:

$$\dot{Q} = \propto A\ (t_w - t) \quad (4.31)$$

Where $\propto$ is the heat transfer coefficient.

Fig. 4.63 shows the heat transfer taking place from fluid A to fluid B through a dividing wall of thickness x, thermal conductivity λ and a temperature variation.

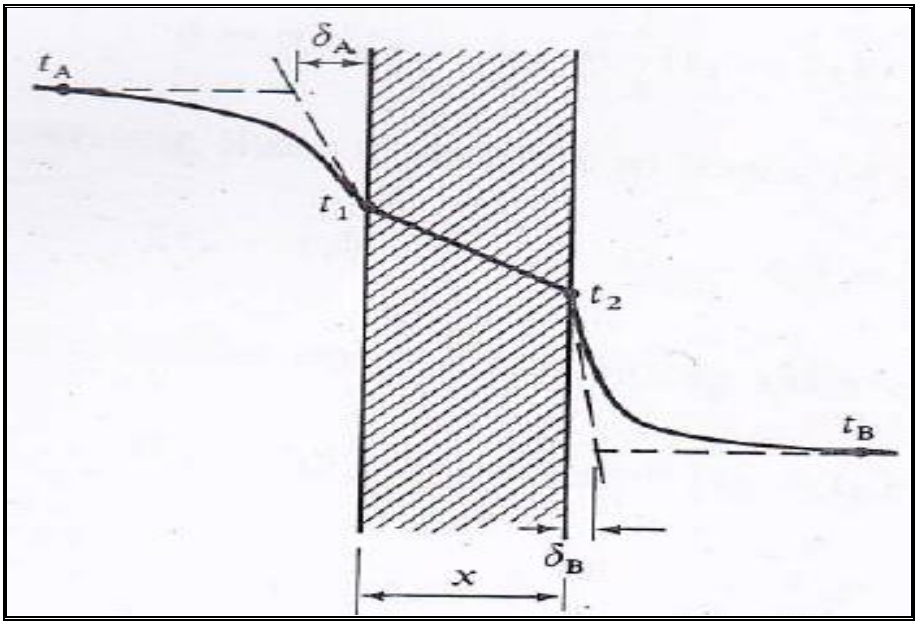

Fig. 4.63: Temperature variation of the heat energy from fluid A to B

(Eastop and McConckey, 2006)

In fluid A, the temperature decreases rapidly from t_A to t_1 in the region of the wall and similarly, in fluid B the temperature decreases rapidly from t_2 to t_B in the region of the wall. In most practical cases the fluid temperature is approximately constant through its bulk, apart from a thin film near the solid surface bounding the fluid. The thickness of the fluid film is given by δ_A for

fluid A and δ_B for fluid B. This is shown by the dotted line on **Fig. 4.63**. The heat transfer in these films is by conduction only, hence applying equation (4.30), considering unit surface area from A to the wall.

The overall heat transfer coefficient equation is derived as follows:

$$\dot{q} = \frac{\lambda_A}{\delta_A} (t_A - t_1) \qquad (4.32a)$$

From the wall to fluid B:

$$\dot{q} = \frac{\lambda_B}{\delta_B} (t_2 - t_B) \qquad (4.32b)$$

Also from equation (4.31), from fluid A to the wall:

$$\dot{q} = \propto_A \ (t_A - t_1) \qquad (4.32c)$$

From the wall to fluid B:

$$\dot{q} = \propto_B \ (t_2 - t_B) \qquad (4.32d)$$

Comparing (a) and (c) and equations (b) and (d), it can be noticed that

$$\propto_A = \frac{\lambda_A}{\delta_A} \quad \text{And} \quad \propto_B = \frac{\lambda_B}{\delta_B} \qquad (4.33)$$

In general, $\propto = \frac{\lambda}{\delta}$ where δ is the thickness of the stagnant film of fluid on the surface. The heat flow through the wall in **Fig. 4.61** is given by equation (4.30) for unit surface area

$$\dot{q} = \frac{\lambda}{x}(t_1 - t_2) \qquad (4.34)$$

For steady-state heat transfer, the heat flowing from fluid A to the wall is equal to the heat flowing through the wall which is also equal to the heat flowing from the wall to fluid B. Therefore,

$$\dot{q} = \propto_A (t_A - t_1) = \frac{\lambda}{x}(t_1 - t_2) \ = \propto_B \ (t_2 - t_B) \qquad (4.35)$$

Rewriting these equations in terms of the temperatures we arrive at,

$$\frac{\dot{q}}{\propto_A} = (t_A - t_1); \quad \frac{\dot{q}x}{\lambda} = (t_1 - t_2); \quad \frac{\dot{q}}{\propto_B} = (t_2 - t_B) \tag{4.36}$$

Hence adding the corresponding sides of the three equations

$$(t_A - t_1) + (t_1 - t_2) + (t_2 - t_B) = \frac{\dot{q}}{\propto_A} + \frac{\dot{q}x}{\lambda} + \frac{\dot{q}}{\propto_B} \tag{4.37}$$

Therefore,

$$(t_A - t_B) = \dot{q}(\frac{1}{\propto_A} + \frac{x}{\lambda} + \frac{1}{\propto_B}) \tag{4.38}$$

$$\dot{q} = \frac{(t_A - t_B)}{\left(\frac{1}{\propto_A} + \frac{x}{\lambda} + \frac{1}{\propto_B}\right)} \tag{4.39}$$

By analogy with equation (4.31) the above can be written down as:

$$\dot{q} = U(t_A - t_B) \tag{4.40}$$

Or

$$\dot{Q} = UA(t_A - t_B) \tag{4.41}$$

Where

$$\frac{1}{U} = \frac{1}{\propto_A} + \frac{x}{\lambda} + \frac{1}{\propto_B} \tag{4.42}$$

U is called the overall heat transfer coefficient and it has the same units as $\propto$ the heat flow is caused by the temperature difference whereas the current flow is caused by the potential difference V. Hence, it is possible to postulate a thermal resistance analogous to an electrical resistance. From Ohm's law we have

$$V = IR \quad \text{Or} \quad I = \frac{V}{R} \tag{4.43}$$

Where V is the potential difference, I is the current and R is the resistance. Comparing the above equations with equation (4.30) results in,

$$R = \frac{x}{\lambda A} \tag{4.44}$$

Where R is the thermal resistance, $\dot{Q}$ is analogous to I and $t_1 - t_2$ is analogous to V. To find the resistances of the fluid film it is necessary to compare Ohm's law with equation (4.31) i.e. thermal resistance of the fluid film is,

$$R = \frac{1}{\alpha A} \tag{4.45}$$

The press dome is composed of a cylinder and an oblate spheroid shape. Therefore, it is split into two shapes where the heat flow through each shape is determined (See **Fig. 4.57**).

4.2.1.1 The heat-loss through the cylindrical section.

The heat flow resistance equation through the cylindrical wall is derived as follows:

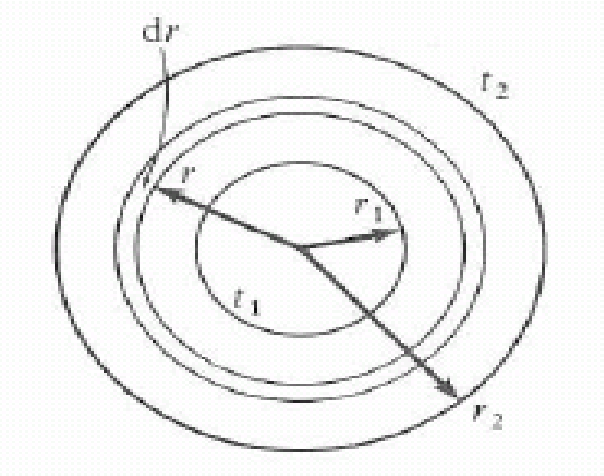

Fig. 4.64: The cross-section area through the cylinder (Eastop and McConckey, 2006).

When applying a unit length of the cylinder in the axial direction on equation (4.25), we arrive at:

$$\dot{Q} = -\lambda A \frac{dt}{dx} = -\lambda(2\pi r \; x \; 1)\frac{dt}{dr} \tag{4.46}$$

$$\dot{Q}\frac{dr}{r} = -2\pi\lambda \, dt \tag{4.47}$$

Integrating through the wall thickness,

$$\dot{Q} \int_{r_1}^{r_2} \frac{dr}{r} = -2\pi\lambda \int_{t_1}^{t_2} dt \tag{4.48}$$

Where $\dot{Q}$ and λ are both constants,

$$\dot{Q}\, ln\frac{r_2}{r_1} = -2\pi\lambda\,(t_2 - t_1) = 2\pi\lambda\,(t_1 - t_2) \tag{4.49}$$

$$\dot{Q} = \frac{2\pi\lambda(t_1 - t_2)}{\ln(r_2/r_1)} \tag{4.50}$$

Now from equation (4.30),

$$\dot{Q} = \frac{\lambda A}{x}(t_1 - t_2) \tag{4.51}$$

Substituting a mean area A_m in this equation, and also substituting for the thickness $x = (t_1 - t_2)$ leads to,

$$\dot{Q} = \frac{\lambda A_m(t_1 - t_2)}{(r_2 - r_1)} \tag{4.52}$$

Equations (4.50) and (4.52) gives:

$$\dot{Q} = \frac{\lambda A_m(t_1 - t_2)}{(r_2 - r_1)} = \frac{2\pi\lambda(t_1 - t_2)}{\ln(r_2/r_1)}$$

Therefore,

$$\frac{A_m}{(r_2 - r_1)} = \frac{2\pi}{\ln(r_2/r_1)} \tag{4.53}$$

$$A_m = \frac{2\pi(r_2 - r_1)}{\ln(r_2/r_1)} = \frac{(A_2 - A_1)}{\ln(r_2/r_1)} \tag{4.54}$$

Therefore the solution can be achieved by substituting the logarithmic mean area A_m into equation (4.30). The logarithmic mean area formula also shows that a logarithmic mean radius can be given by as follows,

$$r_m = \frac{(r_2 - r_1)}{\ln(r_2/r_1)} \tag{4.55}$$

In the case of a composite cylinder (e.g. a metal pipe with several layers of lagging) the most convenient approach is again that of the electrical analogy by using equation (4.35).

$$R = \frac{x}{\lambda A_m} \tag{4.56}$$

Where the thickness of a layer is x and A_m is the logarithmic mean area for that layer. From equation (4.37), applying the electrical analogy (I = V/R), It can be seen that,

$$R = \frac{\ln(r_2/r_1)}{2\pi\lambda} \tag{4.57}$$

The fluid film on the inside and outside surfaces can be treated as before using equation (4.36).

$$R_{outside} = \frac{1}{\alpha_0 A_0} \tag{4.58}$$

Where A_0 is the outside surface area, $2\pi r_2$, referring to **Fig. 4.62** and α_0 is the heat transfer coefficient for the outside surface.

$$R_{inside} = \frac{1}{\alpha_i A_i} \tag{4.59}$$

Where A_i is the inside surface area, $2\pi r_1$ and α_i is the heat transfer coefficient for the inside surface. It can be seen from equation (4.37).

$$\dot{Q} = \frac{2\pi\lambda(t_1 - t_2)}{\ln(r_2/r_1)} \tag{4.60}$$

The heat transfer rate depends on the ratio of the radii, r_2/r_1 and not on the difference $(r_2 - r_1)$. The smaller the ratio r_2/r_1 the higher is the heat flow for the same temperature difference.

4.2.1.2 The heat-loss through the oblate spheroid section

The heat flow resistance equation of a spherical wall is derived as follows:

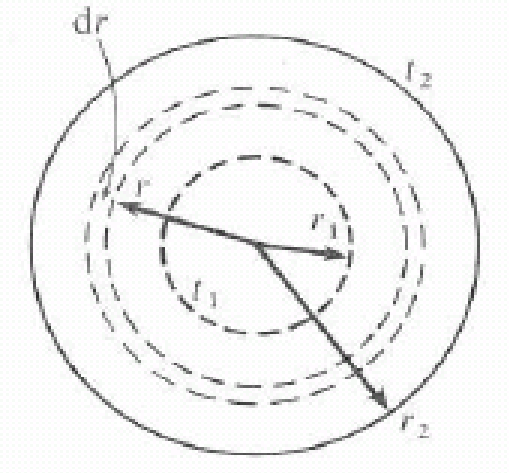

Fig. 4.65: The cross-section area of the hollow sphere (Eastop and McConckey, 2006)

Considering **Fig. 4.65**, the outside radius is r_2 and the internal radius the hollow sphere. The inside and outside temperature of the hollow sphere is taken as t_1 and t_2, respectively. The thermal conductivity is represented as λ, consider the arbitrary radius to be r and the small element thickness to be dr. The spherical element area is shown to be given by $4\pi r^2$.

Then using equation (4.25):

$$\dot{Q} = -\lambda A \frac{dt}{dr} = -4\lambda\pi r^2 \frac{dt}{dr} \tag{4.61}$$

Integrating equation (4.61):

$$\dot{Q} \int_{r_1}^{r_2} \frac{dr}{r^2} = -4\lambda\pi \int_{t_1}^{t_2} dt \tag{4.62}$$

Therefore,

$$-\dot{Q}\left(\frac{1}{r_2} - \frac{1}{r_1}\right) = -4\lambda\pi\,(t_2 - t_1) \tag{4.63}$$

$$\dot{Q}\left(\frac{r_2 - r_1}{r_1 r_2}\right) = 4\lambda\pi\,(t_1 - t_2)$$

$$\dot{Q} = \left(\frac{4\lambda\pi r_1 r_2 (t_1 - t_2)}{r_2 - r_1}\right) \tag{4.64}$$

Hence applying the electrical analogy, $I = V/R$, gives:

$$R = \left(\frac{r_2 - r_1}{4\lambda\pi r_1 r_2}\right) \tag{4.65}$$

If a mean area, A_m is introduced. Then from equation (2),

$$\dot{Q} = \frac{\lambda A_m}{x}(t_1 - t_2) = \left(\frac{\lambda A_m (t_1 - t_2)}{r_2 - r_1}\right) \tag{4.66}$$

Equating equation (4.64) and (4.66) gives:

$$A_m = 4\pi r_1 r_2 \tag{4.67}$$

The mean radius r_m can be defined as,

$$A_m = 4\pi {r_m}^2 = 4\pi r_1 r_2 \tag{4.68}$$

Therefore,

$$r_m = \sqrt{r_1 r_2} \tag{4.69}$$

From equation (4.69) it can be seen that r_m is a geometric mean radius.

4.2.2The heat-loss through radiation

The thermal radiation that occurs during the tyre compression mould warm up process is a direct result of the random movements of saturated steam atoms and molecules. The saturated steam atoms and molecules are composed of charged protons and electrons. Hence, the random movement of the protons and electrons results in the electromagnetic radiation being emitted. This carries energy away from the press dome to the environment surroundings. The press dome is considered to be a gray body because it is a hypothetical source that radiates as a black body

but with an emissivity being less than one and with a constant wavelength. The press dome does not absorb all the incident radiation but emits the radiation in constant proportion to the corresponding black-body radiation. According to Eastop and McConckey (1993) the fourth power of a black body is directly proportional to the emissive power of its absolute temperature. This principle is as follows,

$$\dot{E}_B = \sigma T^4 \tag{4.70}$$

The value of σ is $5.67x10^{-8}\,{}^{W}/_{m^2(k)^4}$, this value is a constant. The rate of energy emitted by a non-black body is then given by:

$$\dot{E} = \varepsilon\sigma T^4 \tag{4.71}$$

Where ε is the emissivity of the non-black body.

Considering body one of emissivity ε_1 at a temperatureT_1 that is completely surrounded by the black surroundings at a lower temperature T_2. The energy leaving body one is completely absorbed by the surroundings and from equation (4.71). Therefore, the rate of energy emission is given by:

$$\varepsilon_1\sigma {T_1}^4 \tag{4.72}$$

The rate of energy emitted by the black surroundings is given by equation (4.70):

$$\dot{E} = \varepsilon\sigma {T_2}^4 \tag{4.73}$$

Now the fraction of this energy which is absorbed by body one depends on the absorption of body one. For a grey body $\alpha = \varepsilon$ at all temperatures and hence,

$$\text{Rate of energy absorption} = \varepsilon\sigma {T_2}^4 = \varepsilon A {T_2}^4$$

In this case, the press dome surroundings area where the emitting of radiation heat transfer occurs was assumed to be as equal to the press dome area. Therefore, the net radiation loss rate of the press dome radiating energy to its cooler surroundings can be expressed as:

$$\dot{Q} = \varepsilon_1 \sigma A {T_1}^4 - \varepsilon_2 \sigma A {T_2}^4 \quad (4.74)$$

4.3 Steam heat-loss across the press dome insulation

Four bars saturated steam is fed into the press dome at 151^0C to pressurize the dome before the high conduction heat transfer between the steam and prismatic container occurs. The dome wall is composed of a 25 mm thick Grade350WA mild steel and 10 mm galvanized outside cover. Both components are separated by 30 mm air gap. However, not 100% heat energy of saturated steam will be conductively transferred to the prismatic container. This is because heat energy is considered to be heat loss due to insulation inefficiency in every heat transfer process. **Fig. 4.66** illustrates a schematic drawing of the materials in the press dome wall.

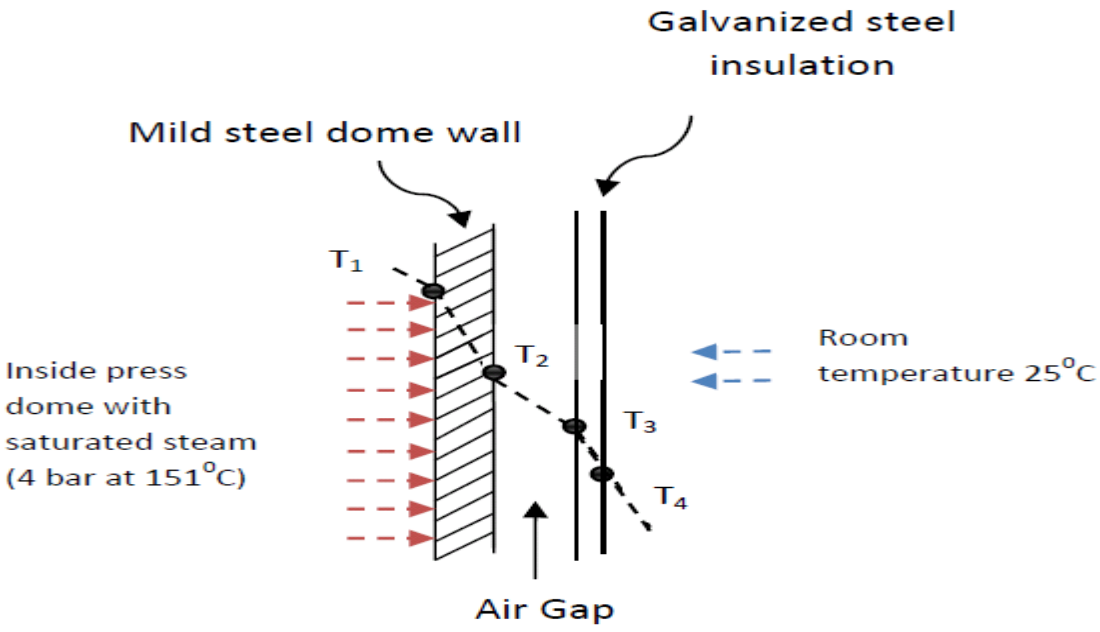

Fig. 4.66: The schematic drawing of the materials in the press dome wall.

4.3.1 The heat loss across the cylindrical section

The heat resistance across the cylindrical shape of the press dome is given by:

$$R = \frac{\ln(r_2/r_1)}{2\pi\lambda}$$

Where (r_1) is the internal radius and (r_2) is the outside surface radius. The thermal conductivity is represented by λ. The heat energy first flows through dome wall, then flows through the air gap and finally through the galvanized outside cover, before it is radiated into the dome surroundings.

4.3.1.1 The press-dome wall

The press dome is made of carbon steel (contains 1% carbon) and has a 25 mm thickness. The temperature of the press dome wall during the warm up process is normally 151^0 C. Therefore, the thermal conductivity was interpolated to be 42 $^{W}/_{m\,K}$, (see ***Appendix H*** for a thermal conductivity table). The dome-wall heat flow resistance is found to be:

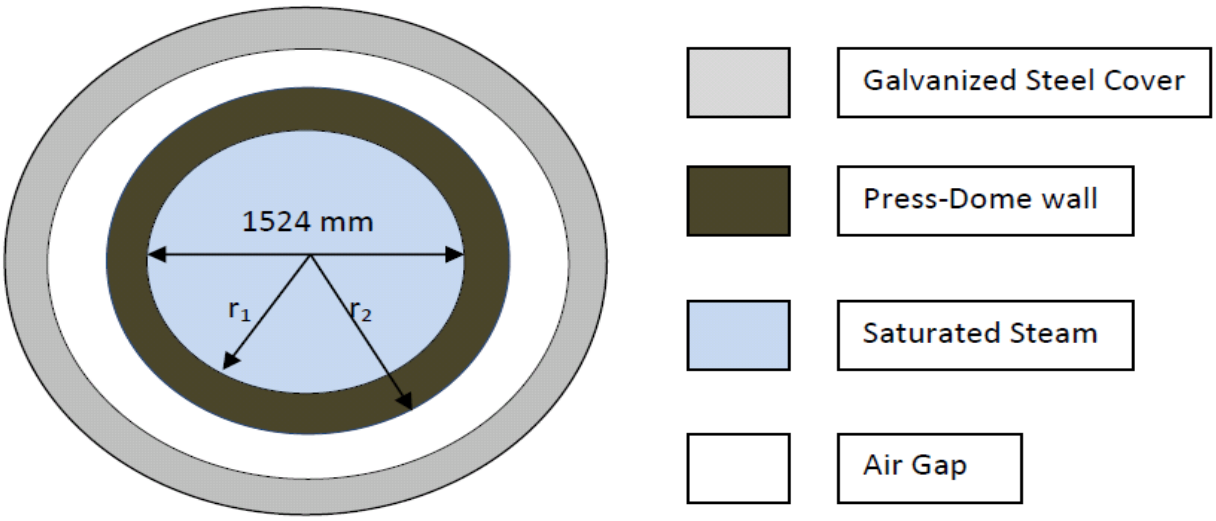

Fig. 4.67: The cross sectional area of the press dome wall

$$R_{PD\,WALL} = \frac{\ln(r_2/r_1)}{2\pi\lambda} \tag{4.75}$$

$$R_{PD\,WALL} = \frac{\ln(0.787/0.762)}{2\pi(42)} = 0.000123\ {}^{K}/_{W}$$

4.3.1.2 The air gap

The air gap has a 30 mm thickness and the thermal conductivity is found to be 0.035 ${}^{W}/_{m\,K}$ at 151^{0}C curing press operational temperature (see ***Appendix I*** for the thermo-physical properties graph).Therefore, the air gap heat flow resistance is found to be:

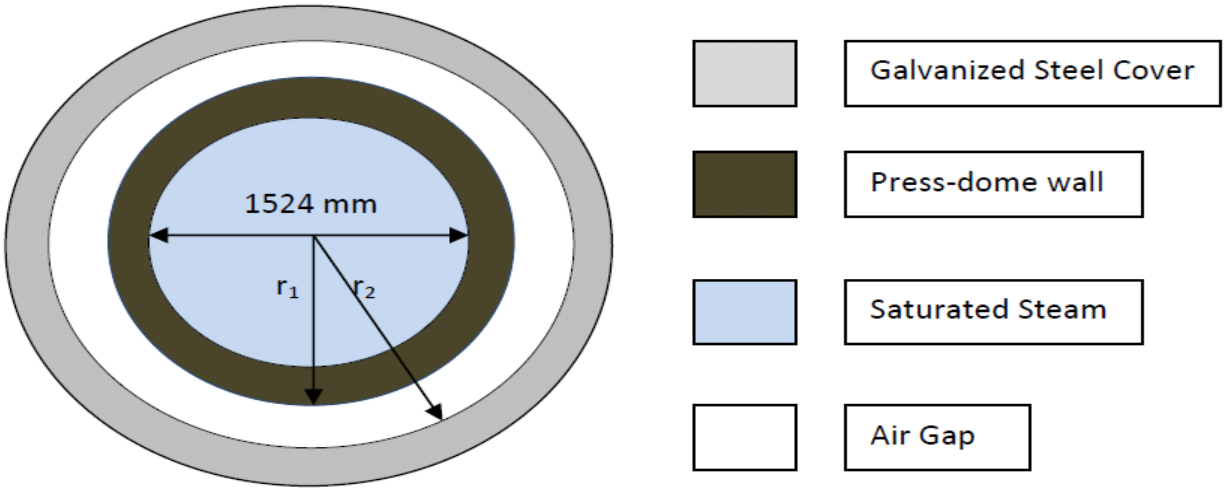

Fig. 4.68: The cross-sectional area of the air gap

$$R_{AIR\,GAP} = \frac{\ln(r_2/r_1)}{2\pi\lambda} \tag{4.76}$$

$$R_{AIR\,GAP} = \frac{\ln(0.817/0.787)}{2\pi(0.035)} = 0.170\ {}^{K}/_{W}$$

4.3.1.3 The galvanized cover

The galvanized cover has a 10 mm thickness and thermal conductivity is found to be 115 $^{W}/_{m\,K}$ at 151^{0}C curing press operational temperature (see ***Appendix H*** for a thermal conductivity table). Therefore, the galvanised cover heat flow resistance is found to be:

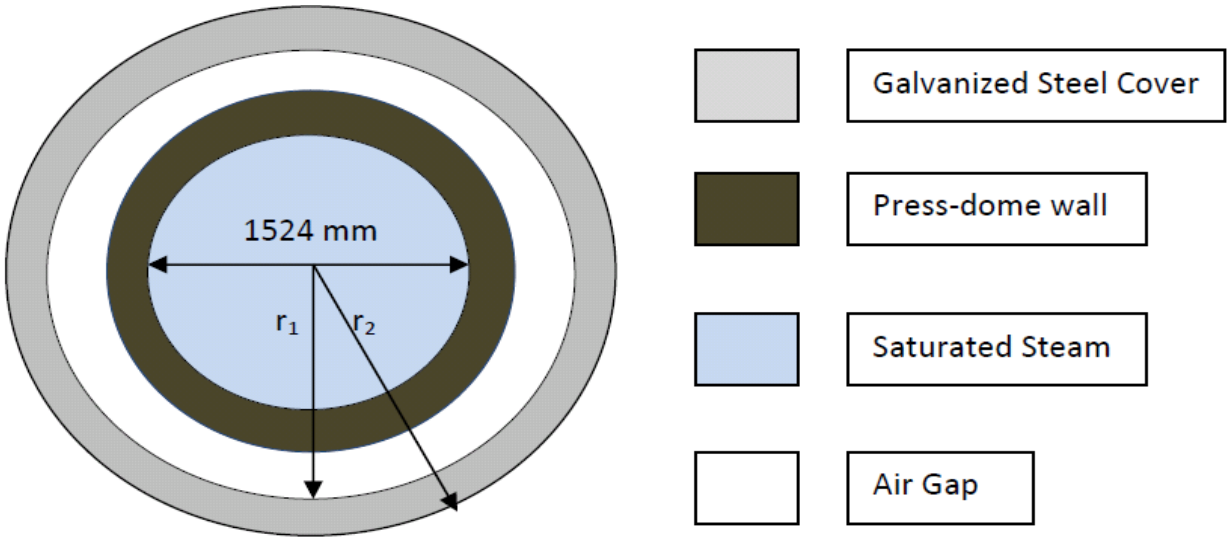

Fig. 4.69: Cross-sectional area of the galvanised sheet

$$R_{GALV\ COVER} = \frac{\ln(r_2/r_1)}{2\pi\lambda} \tag{4.77}$$

$$R_{GALV\ COVER} = \frac{\ln(0.827/0.817)}{2\pi(115)} = 0.00001684\ {}^{K}/_{W}$$

4.3.1.4 The steam film on the inside surface

The steam film on the inside of the press dome has a very low heat flow resistance because the heat coefficient of the saturated steam is significantly high. Therefore, steam film heat-flow resistance inside the press dome is negligible.

4.3.1.5 The air film on the outside surface

The heat energy is transferred from the outside wall surface into the dome surroundings through natural convection. The heat-transfer coefficient was found to be 3.46 W/m^{2}K (see ***Appendix J*** for the convection heat transfer coefficients calculations). Therefore, the air film heat flow resistance is found to be:

$$R_{AIR\ FILM} = {}^{1}/_{\alpha A} \tag{4.78}$$

$$R_{AIR\ FILM} = {}^{(1)}/_{(3.46)(2\pi)(0.827)(1)} = 0.0556\ {}^{K}/_{W}$$

Therefore, the total heat-flow resistance can be given as follows:

$$R_T = R_{PD\ WALL} + R_{AIR\ GAP} + R_{GALV\ COVER} + R_{AIR\ FILM} \tag{4.79}$$

$$R_T = 0.000123 + 0.170 + 0.00001684 + 0.0556 = 0.2257\ {}^{K}/_{W}$$

The cylinder height distance is 1m, therefore, the rate of heat loss per meter length of the cylindrical dome shape can be determined as follows:

$$\dot{Q}_1 = \frac{(t_1 - t_4)}{R_T} = \frac{(151 - 25)}{0.2257} = 558.26\ W \tag{4.80}$$

Therefore, the heat loss across the cylinder section of the press dome insulation is

$$\dot{Q}_1 = 558.26\ W.$$

4.3.2 The heat loss across the oblate spheroid section

4.3.2.1 The press-dome wall

The press dome has a 25 mm thickness and the thermal conductivity is found to be 42 $^{W}/_{m\,K}$ (see ***Appendix H*** for the thermal conductivity table).Therefore, the dome-wall heat flow resistance through the spherical section is found to be as follows:

The sphere area must be divided by two because the heat loss evaluation is for the press dome with a hemispherical top-half. See **Fig. 4.67** for the cross sectional area of the press dome wall.

$$A_m = (4\pi {r_m}^2)/(\frac{1}{2}) = 2\pi r_1 r_2 \tag{4.81}$$

Therefore,

$$R_{PD\,WALL} = \frac{r_2 - r_1}{2\lambda\pi r_1 r_2} \tag{4.82}$$

$$R_{PD\,WALL} = \frac{(0.787 - 0.762)}{2(42)\pi(0.762)(0.787)} = \ 0.000158\ {}^{K}/_{W}$$

4.3.2.2 The air gap

The air gap has a 30 mm thickness and the thermal conductivity is found to be 0.035 $^{W}/_{m\,K}$ at 151^0C curing press operational temperature (see ***Appendix I*** for the thermo-physical properties graph). See **Fig. 4.68** for the cross sectional area of the air gap. The heat flow resistance through the spherical section is found to be:

$$R_{AIR\,GAP} = \frac{r_2 - r_1}{2\lambda\pi r_1 r_2} \tag{4.83}$$

$$R_{AIR\ GAP} = \frac{(0.817 - 0.787)}{2(0.035)\pi(0.787)(0.817)} = 0.212\ {}^{K}/_{W}$$

4.3.2.3 The galvanized steel cover.

The galvanised cover has a 10 mm thickness and thermal conductivity is found to be 115 ${}^{W}/_{m\ K}$ at 151^{0}C curing press operational temperature (see ***Appendix H*** for the thermal conductivity table). Therefore, the galvanised cover heat flow resistance is found to be:

See **Fig. 4.69** for the cross sectional area of the galvanised steel cover.

$$R_{GALV\ COVER} = \frac{r_2 - r_1}{2\lambda\pi r_1 r_2} \tag{4.84}$$

$$R_{GALV\ COVER} = \frac{(0.827 - 0.817)}{2(115)\pi(0.817)(0.827)} = 0.0000205\ {}^{K}/_{W}$$

4.3.2.4 The steam film on the inside surface

The steam film on the inside of the press dome has a very low heat flow resistance because the heat coefficient of the saturated steam is significantly high. Therefore, steam film heat-flow resistance inside the press dome is negligible.

4.3.2.5 The air film on outside surface

The heat energy is transferred from the outside wall surface into the dome surroundings through natural convection. The heat-transfer coefficient was found to be 2.2 W/m^{2}K (see ***Appendix J*** for the convection heat transfer coefficients calculations). Therefore, the air film heat flow resistance is found to be:

$$R_{AIR\ FILM} = {}^{1}/_{\alpha A} \tag{4.85}$$

$$R_{AIR\ FILM} = {}^{(1)}\!/_{(2.2)(2\pi)(0.827)^2} = 0.1058\ {}^{K}\!/_{W}$$

Therefore, the total heat-flow resistance can be given as follows:

$$R_T = R_{PD\ WALL} + R_{AIR\ GAP} + R_{GALV\ COVER} + R_{AIR\ FILM}$$

$$R_T = 0.000158 + 0.212 + 0.0000205 + 0.1058$$

$$R_T = 0.317\ W$$

The rate of the heat loss through the hemispherical dome shape can be determined as follows,

$$\dot{Q}_2 = \frac{(t_1 - t_4)}{R_T} = \frac{(151 - 25)}{0.317} = 397.47\ W$$

4.3.3 The heat loss through radiation

The press dome cover is made of a galvanized steel sheet with an emissivity of $\varepsilon = 0.23$ as per ***Appendix K***. According to Nahle (2004) the total emissivity of a mixture of gases in the atmosphere at 25^0C is found to be $\varepsilon = 0.31$. The surface temperature of the galvanized steel cover is 50^0C. The heat loss can be determined by using equation (4.86):

$$\dot{Q} = \varepsilon_1 \sigma A_{Dome} {T_1}^4 - \varepsilon_2 \sigma A_{surr} {T_2}^4 \qquad (4.86)$$

Where,

$$\varepsilon_1 = 0.23, \varepsilon_2 = 0.31$$

$$A_{Dome} = A_{cylinder} + A_{hemisphere} = 2\pi(\mathrm{r})(\mathrm{L}) + \frac{2\ \pi \mathrm{r}^2}{1} = 2\pi(0.762)(1) + \frac{2\ \pi(0.762)^2}{1} = 8.436 m^2$$

$$A_{surr} = (A_{Dome}) = 8.436\ m^2$$

$$\sigma = 5.67x10^{-8}\ {}^{W}\!/_{m^2(k)^4}$$ (Stefan – Boltzmann constant)

$$T_1 = 50 + 273 = 323\ K$$

$$T_2 = 25 + 273 = 298\ K$$

Therefore, the heat loss due to the radiation is as follows:

$$\dot{Q}_3 = \varepsilon_1 \sigma A_{Dome} {T_1}^4 - \ \varepsilon_2 \alpha A_{surr} {T_2}^4$$

$$\dot{Q}_3 = (0.23)(5.67x10^{-8})(8.436)(323^4) - \ (0.31)(5.67x10^{-8})(8.436)(298^4)$$

$$\dot{Q}_3 = 1457.8 - 1169.4 = \ 288.4W$$

4.3.4. Total heat and steam Losses

The total heat loss through the three heat transfer mechanisms that occurs during the tyre compression mould warm up process is found to be:

$$\dot{Q}_T = \ \dot{Q}_1 + \ \dot{Q}_2 + \dot{Q}_3 \tag{4.87}$$

$$\dot{Q}_T = \ 558.26 + \ 397.47 + 288.4 = 1244.13 = 1.24\ kW$$

Therefore, the quantity of steam losses can be determined by dividing the heat energy loss $\dot{Q}_T$ by the enthalpy difference $(h_1 + \ h_2)$. The temperature of the condensate formed when saturated steam lose heat energy is found to be 80 ^{0}C. This was measured using a temperature probe on the condensate drain line. Graph 2 illustrates the latent and sensible heat energy during the warm up process.

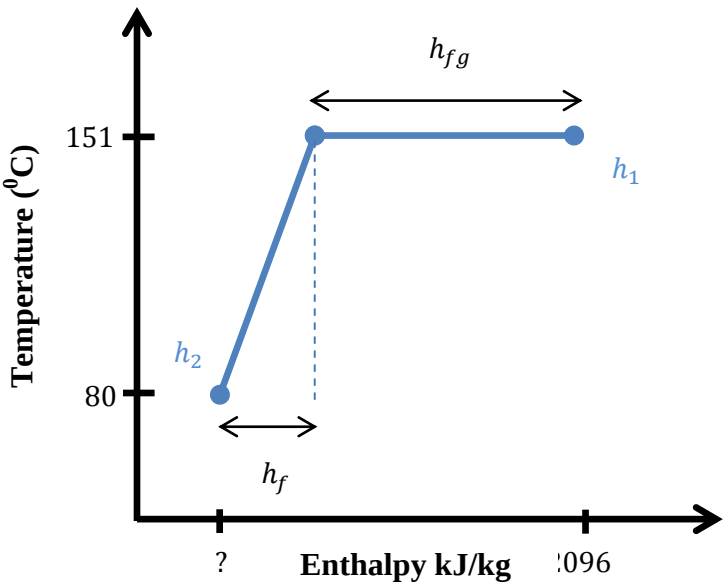

Graph 2: Sensible and latent heat energy during the warm up process.

$$\Delta h_f = C_P\,(T_1 - T_2) \tag{4.88}$$

$$\Delta h_f = 4.19\,(151 - 80)$$

$$\Delta h_f = 298.2\,{}^{kJ}/_{kg}$$

$$\Delta h_f = h_2 \tag{4.89}$$

Therefore, the steam quantity lost due to insulation inefficiencies is found to be:

$$\dot{Q}_T = 1.24\,kW = 1.24\,{}^{kJ}/_{s}$$

$$\dot{m}_s = \frac{\dot{Q}_T}{h_1 - h_2} \tag{4.90}$$

$$\dot{m}_s = \frac{1.24}{2107 - 298.2} = 0.00068\,{}^{kg}/_{s}$$

The proposed warm up duration is 3 hours (see chapter 5), this means the required steam quantity for the heat losses due to insulation inefficiencies during the 3 hours tyre compression mould warm up is:

$$m_s = (\dot{m}_s)(hours)(seconds) = (0.00068)(3)(3600) = 7.34\ kg$$

The heat losses during the warm up process are considered to be part of the total heat energy required to preheat the tyre compression mould to the operational temperature. Hence, the minimal total steam quantity required for the 3 hours warm up process of the tyre compression mould is given by:

M_T = (steam required to warm press dome internals + steam losses due to insulation inefficiencies)

$$M_T = 274.8 + 7.34 = 282.14\ kg$$

Each curing press is composed of two press domes, hence, required steam quantity per curing press is:

$$M_T = (282.14)(2) = 564.28\ kg$$

4.4 Numerical results and discussion

The numerical analysis was carried out to investigate the minimum required steam quantity to warm up the tyre compression mould from the ambient t_1 to the operational temperature t_2. Based on the above numerical predictions, a significant difference was found between the analysed required steam quantity and the steam volume that Apollo-Dunlop tyres utilise during the warm up process. Apollo-Dunlop tyres use 0.875 tons of saturated steam on each curing press during the warm up process, however, the required saturated steam to warm up the compression moulds in a curing press is found to be 0.564 tons via numerical analysis. It is now obvious that Apollo-Dunlop tyres are using excessive steam to warm up the tyre compression mould to the operational temperature.

Steam waste is costly in both an environmental and financial sense and, therefore, this needs a prompt attention in order to ensure that the steam system is working at its optimum efficiency with a minimum impact on the environment. This study provides the proper association needed between processes and products so that energy is utilised as efficiently and effectively as possible around the tyre moulding factory. The numerical analysis proved that the warm process duration must be reduced, since, excessive steam is wasted. The reduction of the warm up process duration will eventually reduce fuel costs, emission surcharges, and maximise process efficiency.

However, the numerical analysis of thermodynamics mainly focuses on systems in a steady state and is concerned with the amount of heat energy required to change a system from initial or ambient condition to operational temperatures. Thermodynamics does not provide a solution to "how fast" a temperature change of an object is accomplished. This can only be answered by the science of heat transfer. Therefore, an experiment to determine "how fast" the tyre compression mould reach the operational temperature must be carried out.

5. Experimental evaluations

This chapter contains the vital information on the type of experiments conducted at Apollo–Dunlop tyre manufacturing plant. It also shows the procedure of obtaining experimental data which is the basis for this research. Two warm up experiments were conducted to investigate "how fast" the tyre compression mould would take to reach the operational temperature. The heat transfer seeks to determine the rate at which energy is transferred between bodies as a result of the temperature differences. The concept of transfer rate is the basic difference between heat transfer and thermodynamics. Thermodynamics does not answer the question of "how fast" a change is accomplished, but it can provide a solution to a system in equilibrium. This solution provides with the steam amount required to warm up the tyre compression mould to reach the operational temperature. Therefore, experimental analysis has been used to determine "how fast" the tyre compression mould reach the operational temperature during the warm up process.

5.1 Determining the appropriate warm up technique

Condensate is formed in the press dome during the tyre compression mould warm up process as the result of saturated steam losing heat energy, known as latent heat, to the dome internals. In this case, press dome internals such as the platen, the prismatic container and the tyre compression mould are the equipment consuming latent heat from saturated steam. Steam condenses into water when the latent heat of steam is transferred to heat the press dome internals. The condensate contains a significant amount of sensible heat that can account for about 10% to 30% of the initial heat energy contained in the steam. This sensible heat is considered as useful energy because it is used for heating purposes in the factory.

Apollo-Dunlop tyres are experiencing problems with the condensate recovery system of the curing presses. There are excessive heat energy losses that occur when draining the condensate during the warm up process of the tyre compression mould. Apollo-Dunlop tyres use the recovered high-temperature condensate as part of the boiler feed-water, this maximize the boiler's output temperature because less heat energy is required to convert water into steam. These heat energy losses can negatively affect the warm up experiments, since the steam amount required to warm up the tyre compression mould to the operational temperatures will not be a true reflection because of the occurring losses. **Fig. 5.70** illustrates a 10-15 minutes condensate draining period.

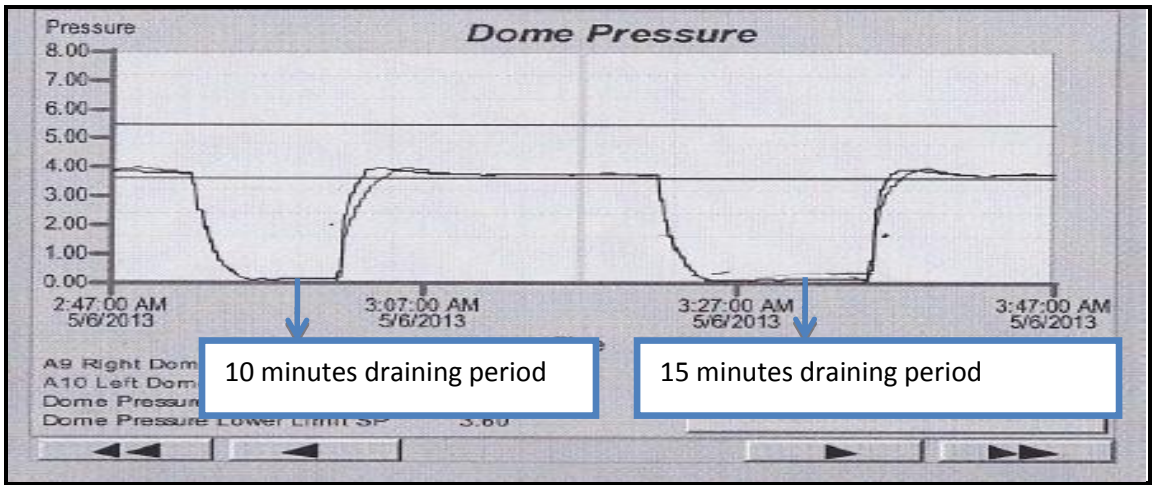

Fig. 5.70: A 10-15 minutes condensate draining period.

(**Fig. 5.70** is a Courtesy from Apollo-Dunlop tyres)

It was found that there are excessive heat energy losses in the press dome during the condensate draining period**. Fig. 5.70** shows that the dome pressure drops from four to zero bars for 10 and 15 minute periods due to steam trap inefficiencies. An energy-intensive steam distribution and condensate recovery system becomes a necessity in times of rising energy costs. A steam trap is an essential part of any steam distribution system. It releases hot condensate from the process for

recovery or for use elsewhere in the plant. A steam trap is a product of over 100 years of development and it is more reliable now than ever before, however, failures occur inevitably. Typically, a condensate load is increased by heat energy losses that normally occur due to the radiation from the steam trap. These losses are directly related to the size and shape of the steam trap.

Apollo-Dunlop tyres use thermostatic steam traps in the drain system of the curing presses. Under normal operating conditions, the thermostatic trap holds back condensate until it has cooled to a certain temperature. However, the saturated steam was able to reach the main control valve which resulted in some wastage of steam. Water logging in a plant can lead to reduced output. The thermostatic trap is lagged to minimise heat losses due to radiation, but this resulted in a long delay during the opening and closing of the trap. This resulted in water logging.

A meeting was held with process engineers at Apollo-Dunlop tyres to discuss possible optimization of the existing condensate recovery system on the curing presses, since, there were excessive steam losses. Permission was granted to optimise the existing condensate recovery system, after lengthy discussions with Apollo-Dunlop tyres engineers. Two trials on the tyre compression mould warm up process were carried out after a brief research on condensate recovery systems. ***The 1st trial:*** a mechanical steam trap was used instead of a thermostatic trap. The mechanical trap (float-thermostatic trap) operates on both density and temperature principles. A lever connects the ball float to the valve and seat. Once the condensate reach a certain level in the trap the float rises, opening the orifice and draining the condensate. The float-thermostatic trap was lagged to reduce heat losses and this did not affect its operation.

Fig.5.71 illustrates a float-thermostatic steam trap with a five minutes condensate draining period.

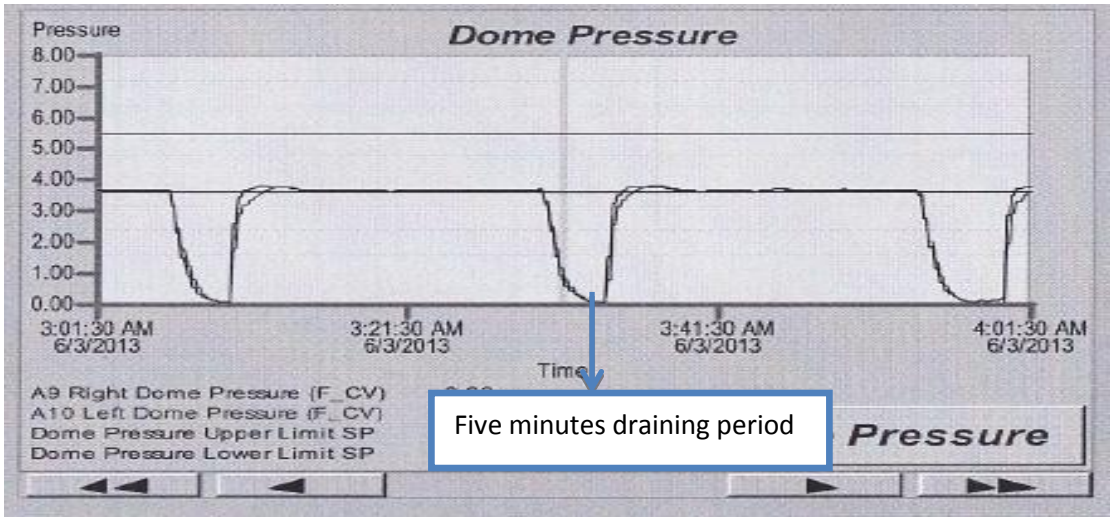

Fig. 5.71: A float-thermostatic condensate draining period (Courtesy from Apollo-Dunlop tyres).

As shown in **Fig. 5.71**, the steam pressure still drops inside the press dome. However, the drop only occurs for five minutes when the float-thermostatic drains the condensate. The usage of steam as a heating media has become extremely expensive because of South Africa experiencing power blackouts and continuous oil price fluctuations, therefore, energy saving is very important.

The 2nd trial: the mechanical steam trap was replaced by a thermodynamic steam trap. This type of trap has become more popular under the heading of steam savings. The thermodynamic steam trap utilises a dynamic effect of flash steam as it goes through the trap. This occurs with condensate on the upstream side and again the flooded valve minimises the losses through the trap. **Fig. 5.72** illustrates a thermodynamic steam trap with a five minutes condensate draining period.

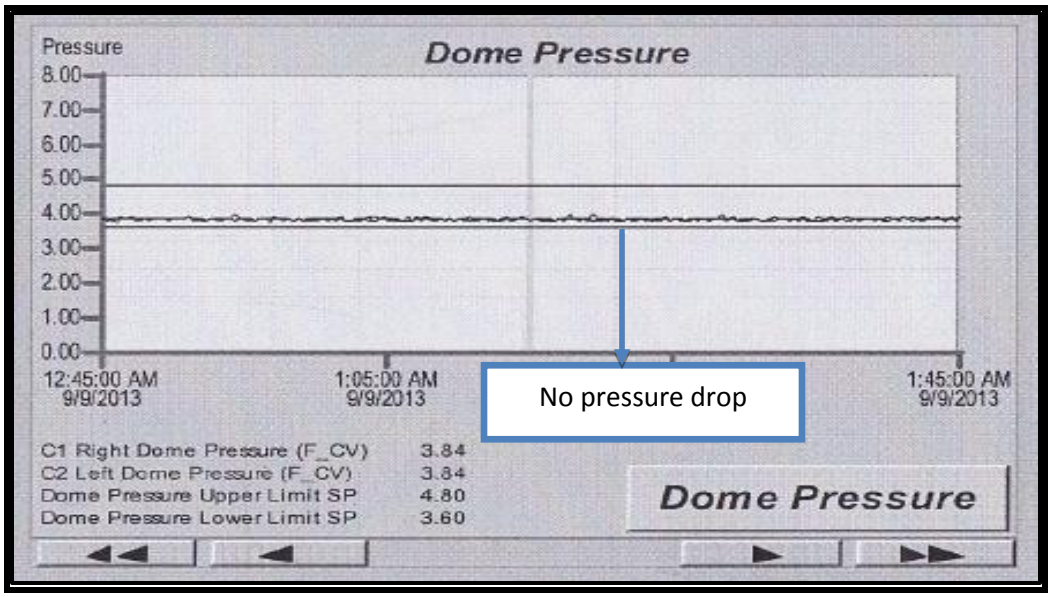

Fig. 5.72: A thermodynamic steam trap with a five minutes condensate draining period.

(**Fig. 5.72** is a Courtesy from Apollo-Dunlop tyres)

As shown in **Fig. 5.72**, the thermodynamic steam trap was able to prevent steam losses during condensate draining periods. The steam pressure drop did not occur in the press dome throughout the warm up process. Steam is an essential resource of many industries. It often provides convinient, reliable and cost effective energy. As such an indispensable tool, it is economical friendly to run a steam system at its optimum efficiency. Therefore, reducing the steam loss due to the condensate draining can lead to considerable savings in terms of energy and water resources. This optimization reduces the boiler fuel consumption by 10 to 20% and minimises the plant's carbon footprint. Therefore, with the condensate draining system now working optimally and efficiently it is convenient to carry out the warm up time evaluations of the tyre compression mould.

5.2 Experimental Setup

Two experiments have been carried out on the upper and bottom half-mould of the tyre compression moulds. The upper half mould consists of the tread sectors and the sidewall plate. The bottom half mould consists of the sidewall plate.

A Personal DAQ 55^{TM} unit was used in addition to a general programming interface bus (GPIB) data link, prismatic container, K-227 pelican thermocouple wires, Butyl rubber, raw cover and a laptop notebook. Together, all these components allowed for mould thermal evaluation at elevated temperatures. This unit accurately recorded the results and automatically generated computer graphs of the temperature versus time. The Personal DAQ 55^{TM} unit logged data from all thermocouples and transferred it through the GPIB data link to a laptop notebook. A custom labview program (DAQ_menu2.m) is developed to save the results and chart the data as acquired. **Fig.5.73** illustrates the data acquisition (DAQ) and the control system of the warm up evaluation experiments.

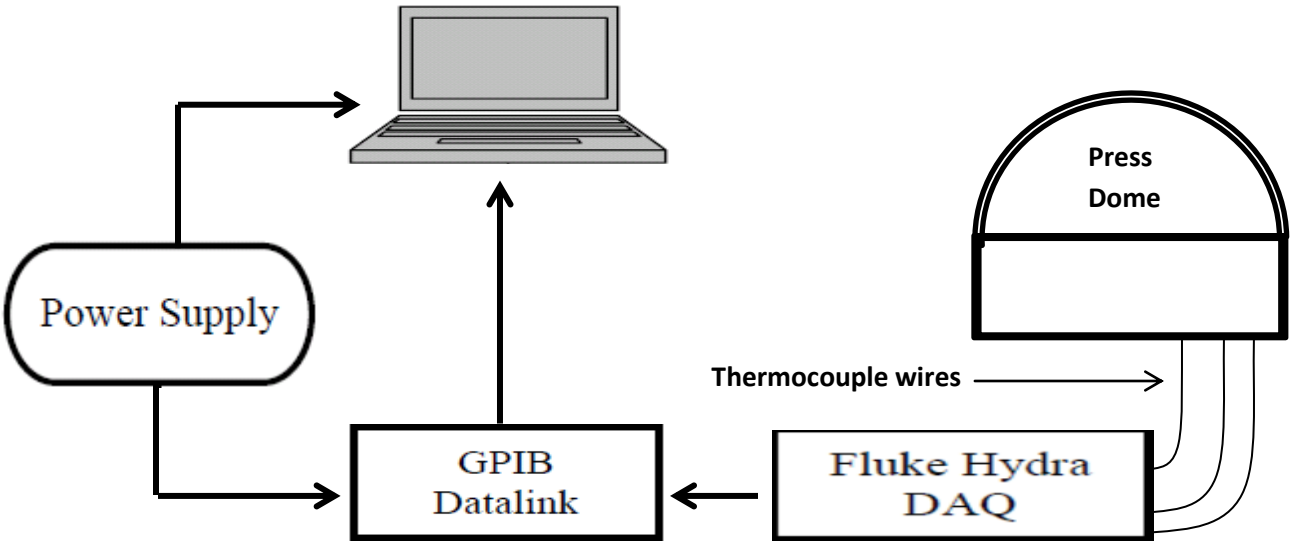

Fig. 5.73: Schematic drawing of the warm up evaluation experiments.

A 275-344 Regal tyre compression mould was used for this warm-up evaluation, due to its enormous size. The 275-344 Regal compression mould has a small tyre volume, but the rest of the mould volume is filled with the steel material. In order to obtain accurate temperature measurements inside the compression mould (Grade350WA mild steel), 3.5 x 45 mm vent holes were drilled on the 275-344 Regal tyre compression mould critical points, the critical points are thickest parts of the mould. The vent holes were drilled into the sidewalls and the tread sectors, the vent hole diameter and depth were determined by the K-227 pelican thermocouple wire diameter and the tyre compression mould thickness. The K-227 pelican thermocouple wires were used because they are designed for durability and reliability in high temperature application of up to 1500^{0}C. These thermocouple wires can withstand molten rubber due to their variety of insulations and sheath material. The upper and lower sidewalls had six K-227 pelican thermocouple wires deep connected to them through vent holes. **Fig. 5.74** illustrates the K-227 pelican thermocouple wires co-ordinated on the tread sectors and upper sidewall mould.

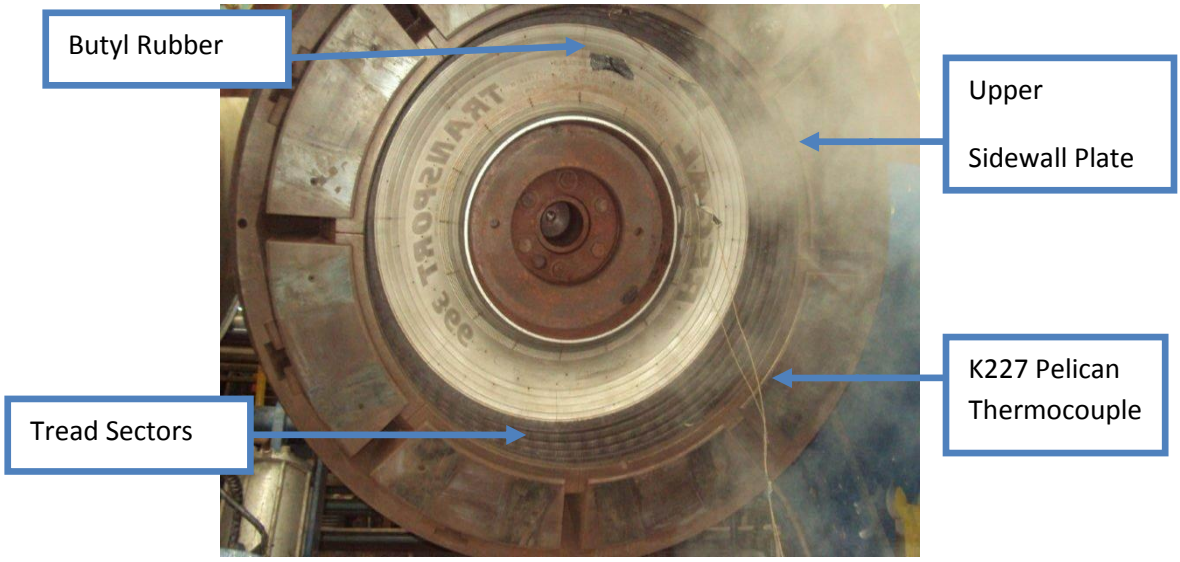

Fig. 5.74: Thermocouple wires co-ordination on tread sectors and upper sidewall mould.

(**Fig. 5.74** is a Courtesy from Apollo-Dunlop tyres)

Thermocouple wires had movement allowance because they were not constrained to avoid strain application to thermocouple wires when closing curing press. A SMR10 Butyl rubber was used to constrain thermocouple wires onto the lower sidewall surface and to prevent condensate to wire contact. The SMR10 Butyl rubber was used due to its excellent impermeability and long polyisobutylene segments of its polymer chains give it good flex properties. Butyl rubber is normally manufactured for airtight sealing and adhesiveness. **Fig. 5.75** illustrates the K-227 pelican thermocouple wires co-ordinated on the lower sidewall mould.

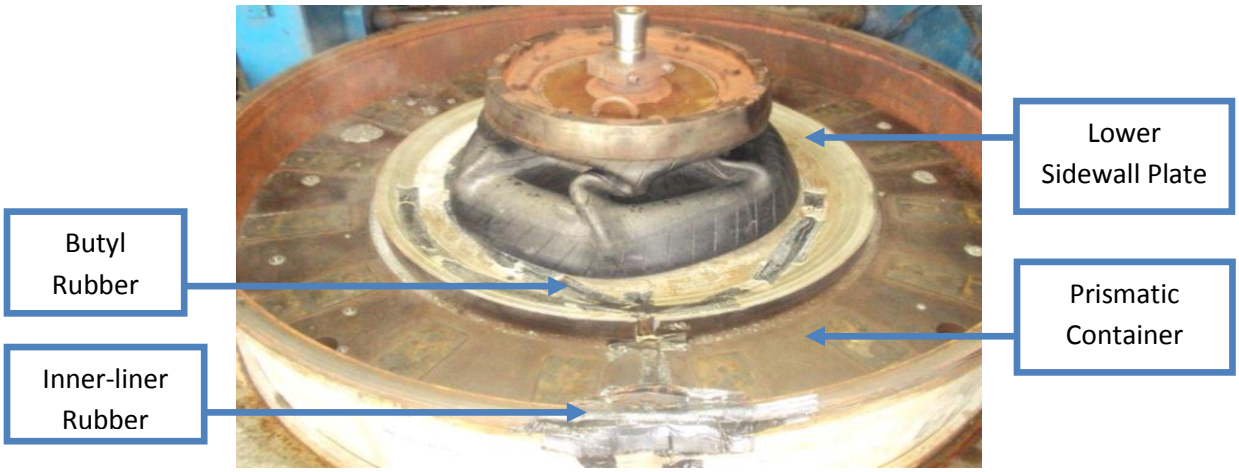

Fig. 5.75: K-227 pelican thermocouple wires co-ordination on the lower sidewall mould.

(**Fig. 5.75** is a Courtesy from Apollo-Dunlop tyres)

In order to avoid squashing of thermocouple wires an inner-liner rubber and Prismatic container were used over the AZ container. The Prismatic container does not have a groove for a seal lip as compare to an AZ container, the lip seal squashes and damages thermocouple wires when the curing press is closed. **Figs. 5.76-77** illustrate the difference between the prismatic and AZ containers.

Fig. 5.76: The AZ container.

Fig. 5.77: The prismatic container.

(**Figs. 5.76-77** are a Courtesy from Apollo-Dunlop tyres)

The Personal DAQ 55™ unit was activated after K-227 thermocouple wires were accurately and safely connected on thickest parts of the tyre compression mould. Thickest parts of the tyre compression mould were treated as critical points, since, the heat transfer rate is lower through them, due to their cavities and large thickness. **Figs. 5.78-79** illustrate the K-227 thermocouple wires connected to programming interface bus (GPIB) data link (Personal DAQ 55– USB).

Fig. 5.78: Personal DAQ 55–USB with thermo-wires.

Fig. 5.79: The DAQ system setup.

(**Figs. 5.78-79** are a Courtesy from Apollo-Dunlop tyres)

An extra thermocouple wire was added to monitor the temperature profile of the atmospheric air. After the experiment setup was complete, a warm up session was loaded into the Personal DAQ 55^{TM} system and saturated steam was introduced into the dome at four bars and 151^0C. The temperature feedback rate was set to be at 30 seconds interval and to save data per 10 minutes. Summarized experimental procedure was as follows:

1. Select a suitable tyre compression mould and prismatic container;
2. Identify the tyre compression mould critical points;
3. Drill vent holes and connect the K-227 thermocouple wires onto the tyre compression mould;
4. Connect the thermocouple wires into the Fluke hydra data acquisition unit;
5. Connect the Fluke Hydra output to the Personal DAQ 55– USB device;
6. Setup the Daqview evaluation system using required parameters;
7. Trigger run the evaluation as soon as the saturated steam inlet valve is opened;
8. Save results, use ten minutes save-interval.

5.3 Experiments Results

This section presents the results and the outcomes of the experimental work performed at Apollo-Dunlop tyre manufacturing plant. The heat transfer in the press dome was first analysed numerically to determine the steam quantity required for the tyre compression mould to warm up from 25^0C to 151^0C operational temperatures. The heat losses due to insulation inefficiencies have also been investigated.

5.3.1 Warm up evaluation on lower sidewall plate

There were no thermocouple wire cuts on the lower sidewall plate purely because the lower mould is on a fixed position. The Personal DAQ 55^{TM} unit logged data from all thermocouples and transferred it through the GPIB data link to a laptop notebook. A custom LABVIEW program (DAQ_menu2.m) was developed to save the results and chart the data as it was acquired. Table 2 shows the initial temperature profile of the lower sidewall plate before saturated steam was introduced into the press dome.

Table 2: The bottom Sidewall Plate mould initial temperatures.

Warm up Evaluation on Bottom Sidewall Plate						
Press	F3 and 4					
Sat Steam Pressure	4 bar (gauge pressure)					
Sat Steam Temperature	151^0C					
Warm-up Evaluation Time	5 hours					
Date	20th Sep 2013					
Cure	N1					
		1	**2**	**3**	**4**	**5**
Time, s	**Time, min**	**Vent Hole**	**Vent Hole**	**Vent Hole**	**Sidewall Surface**	**Ambient**
0	0	33.8	33.3	33.9	33.7	29.2

As shown above, the K-227 thermocouple wires mounted on different points of the tyre compression mould show initial temperatures across the mould (see ***Appendix* L** for full results). Table 3 shows the bottom sidewall plate final temperatures after 1.8 hours.

Table 3: The bottom Sidewall Plate mould temperature after 108 minutes (1.8 hours)

Time, s	Time, min	Vent Hole	Vent Hole	Vent Hole	Sidewall Surface	Ambient
6480	108	148.5	149.1	149.7	149.7	27.0
6510	108.5	148.3	149.1	149.8	149.7	26.9
6540	109	147.8	148.1	149.9	149.6	27.5
6570	109.5	148.1	149.0	150.0	149.	27.6
6600	110	148.3	149.1	149.7	149.6	27.1

The bottom sidewall plate initial temperature gradually increased from 34 to 149.5^0 C within 108 minutes (1.8 hours) of warm up session. The final temperature of the sidewall plate was already expected to be within a range of 147 to 149^0 C, since the saturated steam was fed into the press dome at 151^0 C. The five hour warm up evaluation was aborted two hours earlier to avoid wasting steam for three hours since the lower sidewall plate reached the operational temperature within 1.8 hours (see ***Appendix L*** for full results). Graph 3 shows the lower sidewall plate temperature versus time relationship during warm up session (see ***Appendix L*** for the labview graph).

Graph3: Lower sidewall plate warm up process

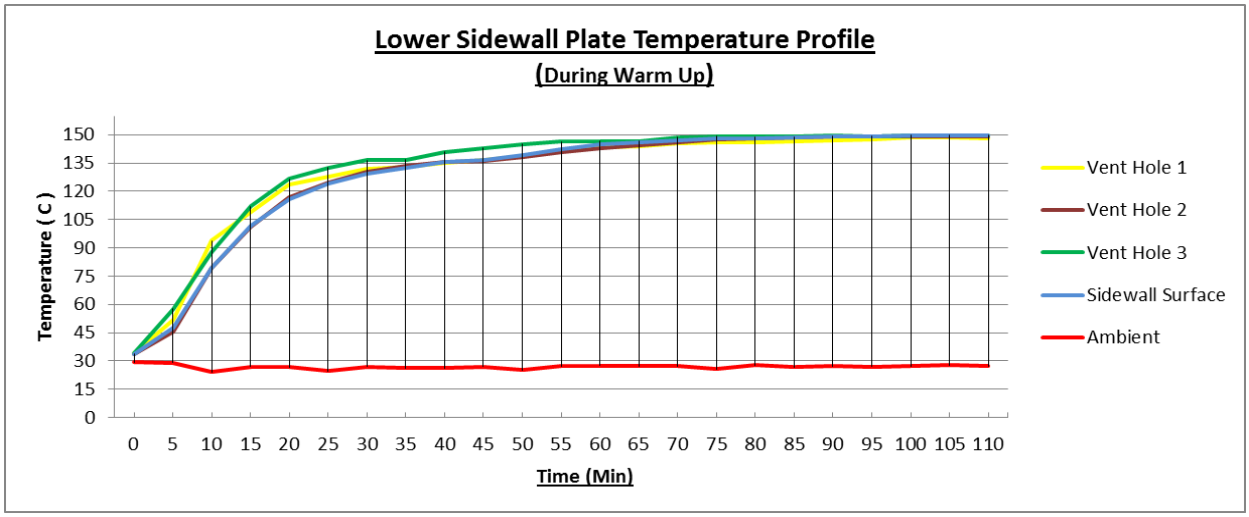

The graph clearly shows that saturated steam had to first fill up and pressurize 1.274 m^3 press dome volume before forced high conventionally heat transfer rate take place between four bar saturated steam and the press dome internals. The high heat transfer rate occurred during the first 50 minutes due to the high temperature difference between the press dome internals and the saturated steam. The latent heat energy of the saturated steam was transferred to the press dome internals through convectional heat transfer, and then it was transferred from the prismatic container to the tyre compression mould through lattice vibrations and random motions of free electrons, this is supported by Fourier's law (Eastop and McConckey, 2006). The ambient air temperature change around the press dome is not significant during the warm up duration due to press dome insulation.

5.3.2 Warm up evaluation on tread sectors and upper sidewall plate

It was found to be difficult to connect K-227 pelican thermocouple wires onto the upper sidewall because two of the six K-227 pelican thermocouple wires were cut-off during the closing of the tyre compression mould. The thermocouple wires cut-off occurred relatively because the upper mould is connected to the curing press that is hydraulic driven, for the closing and opening of the tyre compression mould. Therefore, two thermocouples wires were stretched and cut when the tyre compression mould closed. However, the four remaining thermocouple wires were sufficient to carry out the temperature evaluation on the tread sectors and upper sidewall mould. Table 4 shows the initial temperature profile of the tread sectors and upper sidewall plate before saturated steam was introduced into the press dome.

Table 4: The tread sectors and upper sidewall plate mould initial temperature

Warm up Evaluation on Tread Sectors and Top Sidewall plate							
Dome Pressure	4 bar (gauge pressure)						
Warm up Evaluation Time	5 hours						
Date	21st Sep 2013						
Cure	N1						
		1	2	3	4	5	6
Time, s	**Time, min**	**Tread**	**Tread**	**Sidewall Surface**	**Sidewall Surface**	**Tread**	**Ambient**
0	0	21.3	24.1	22.9	22.7	22.4	19.2

The top half-mould of the tyre compression mould consists of tread sectors and an upper sidewall plate. This experiment was carried out on a cold day. The initial temperature table clearly shows that the initial temperature across the tyre compression mould was ± 23^0 C and the ambient temperature was recorded as 19 ^{0} C (see ***Appendix M*** for full results). Table 5 shows that the tread sectors and the upper sidewall plate reached the operational temperature within 2.3 hours of the warm up evaluation duration.

Table 5: The tread sectors and an upper sidewall plate temperature after 138 minutes (2.3 hours)

Warm up Evaluation on Top Sidewall plate and Sectors							
Dome Pressure	4 bar (gauge pressure)						
Warm up Time	5 hours						
Date	20th Sep 2013						
Cure	N1						
		1	2	3	4	5	6
Time, s	**Time, min**	**Tread**	**Tread**	**Tread**	**Sidewall Surface**	**Sidewall Surface**	**Ambient**
8280	138	149.6	149.0	150.1	87.4	43.4	21.2
8310	138.5	149.6	149.2	150.2	143.2	43.6	19.8
8340	139	149.6	149.3	149.4	143.2	143.4	19.3

Damaged thermocouple wire

Two sidewall surface wires were damaged due to the tension exerted in the thermocouple wires during the closing of the press dome. The tread sectors and the upper sidewall plate initial temperature gradually increased from 22 to 149 ^{0} C within 138 minutes (2.3 hours) since the start of the warm up session. The warm up evaluation was set for four hours, but it was aborted within 2.3 hours of the five hours warm up session to avoid the waste of steam (see ***Appendix M*** for full results). Graph 4 shows the relationship between the temperatures of the tread sectors/upper sidewall plate versus time during the warm up session.

Graph 4: Tread sectors and upper sidewall plate warm up

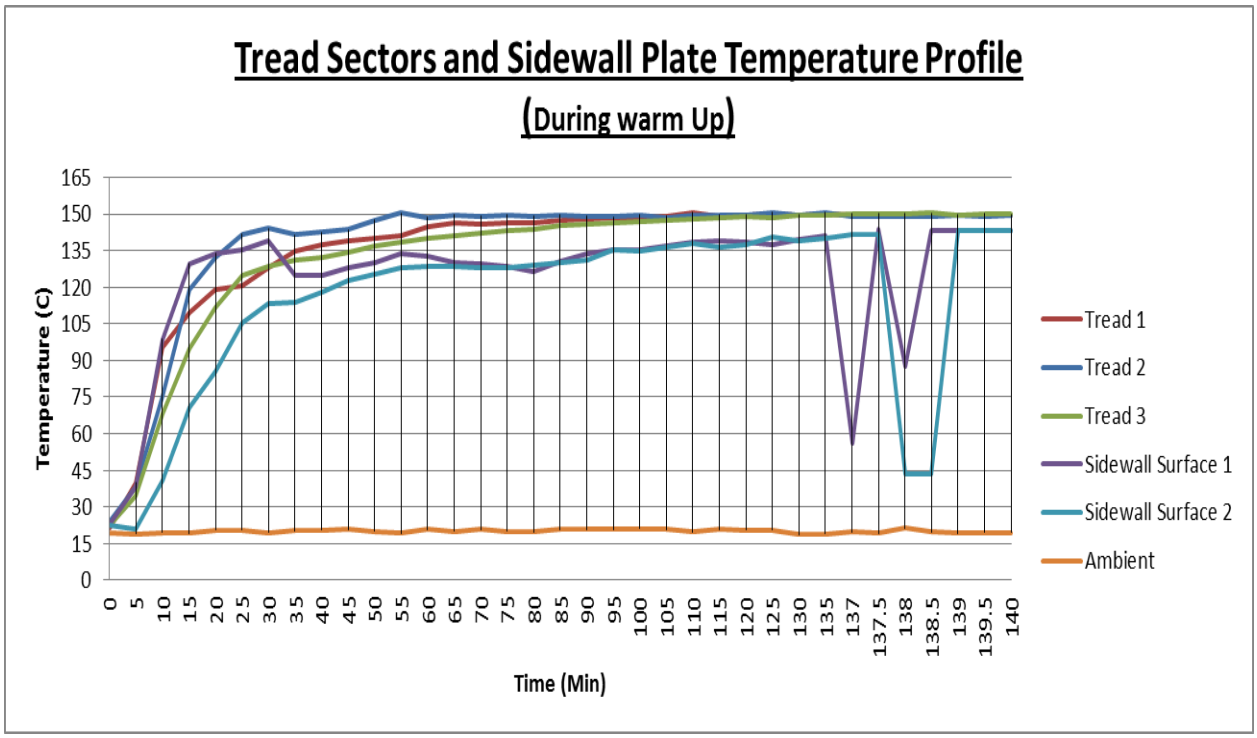

The high heat transfer rate occurred during the first 80 minutes due to the high temperature difference between the press dome internals and the saturated steam. The tread sectors and sidewall plate took longer to warm up as compared to the bottom sidewall plate because the steam inlet is closer to the bottom of the prismatic container.

5.4 Discussion of experimental results

The heat transfer in the tyre compression mould was first analysed numerically by determining the required amount of saturated steam to warm up the compression mould from the ambient temperature of 25 to 151^0C operational temperature. However, even with required steam quantity, the duration of the accomplished temperature change had to be investigated. Thermodynamics can determine the amount of heat energy required to warm up the tyre compression mould. However, it cannot provide a solution as to 'how fast' the tyre compression mould take to reach the operational temperature. Hence, experimental evaluations had been carried out to investigate the time it takes for the tyre compression mould to reach the operational temperature.

As expected, the initial warm up process evaluation conducted at Apollo-Dunlop tyres manufacturing plant illustrated that the lower sidewall plate require 108 minutes (1.8 hours) to warm up from 25 to 149^0C. The lower sidewall plate is close to the steam inlet of the press dome. Hence, it was expected to reach the operational temperature faster than the tread sectors and upper sidewall plate. The top mould-half consisting of tread sectors and upper sidewall plate reached operational temperature, 149^0C, within 138 minutes (2.3 hours) of the five hours warm up session. The tread sectors and upper sidewall took longer to reach operational temperature as compared to the lower sidewall plate since the tread sectors and upper sidewall plate are the thickest parts of the tyre compression mould. However, an extra 0.7 hours was added to the 2.3 hours in order to account for unforeseen steam losses, therefore the total warm up time is 3 hours. These results proved that the truck-tyre compression moulds require a reduced warm up session. Reducing the warm up time would help to produce high quality tyres with a reduced production cost.

6. Performance Evaluation

The new proposed warm up process had to be rigorously tested before implementation, to avoid waste of time and money should the idea become a dud. The sample tyre cured with the compression mould that was heated using the proposed warm process was tested to evaluate whether it meets the required performance standards. The performance test was composed of evaluation of the tyre's durability (wear resistance/life span) and effectiveness (braking ability) through quantitative tests carried out in testing lab.

6.1 Method

6.1.1 Braking ability

A 3.58 tons load was exerted onto the axle of the tyre while running at 120 km/h and a brake was applied suddenly. This was carried out determine the duration it takes for a tyre to maintain traction and braking performance on wet roads surfaces before it completely stops after brakes are applied.

6.1.2 Durability (wear resistance and life span)

A hydraulic driven indoor wear tester was used to test the sample tyre's durability at high speeds of up to 250 km/h varies road conditions such as acceleration, cornering, load range of $(0-4.26)$ tons and temperature range of $(25\text{-}38^{0}C)$ were simulated to reproduce what a tyre experiences on the road. The radial load and lateral force were measured through strain gauge sensors for the ability to control lateral force by slip angle motion.

6.2 Results Discussion

The testing process demonstrated that the 275/344 sample tyre meets Apollo-Dunlop tyres performance criteria (see ***Appendix B*** for the results). The sample tyre ran for 71 hours under 120% of the required load (4.26 tons). The minimum required performance standards are as follows, 47 hours run time and load of 3.58 tons. The sample tyre exceeded the required run time by 51% and the required load by 20%. The results were captured while the sample tyre was still running to save time and energy. This result proves that reduced warm up process increases the tyre performance and life span. Overheating the rubber material of the tyre reduces its durability, therefore reducing the heat energy usage during the warm up session will maximise the tyre safety and reliability.

7. Cost analysis

Cost reduction is a vital factor in modern tyre manufacturing business sector. Identifying cost saving opportunities can help Apollo-Dunlop tyres to increase profits by reducing outflows. Every decision in the tyre development process affects the production cost, therefore process optimization is the driving force to company savings. The need to save energy is now necessary due to recent increase of fuel and energy costs. The market strategy of Apollo-Dunlop tyre factories is to be one of the low cost tyre producers in order to maintain the global competitiveness. However, Apollo-Dunlop tyre has found it very difficult to maintain the global competitiveness due to the significant rise of fuel and energy cost. Thus, optimising the energy efficiency of the tyre factory provides a very high potential to reduce the tyre price whilst maintaining the quality. The tyre price becomes a differentiator in the market, low cost manufacturing makes the product very competitive in the tyre manufacturing business sector.

It currently costs Apollo – Dunlop tyres ***R506.00*** to produce 1 ton of saturated steam. Hence, it becomes a necessity to reduce the warm up duration for the tyre compression mould. Graph 5 shows the cost of producing one ton of steam over a period of six production months.

Graph 5: Steam cost vs. Production months (Courtesy from Apollo-Dunlop tyres).

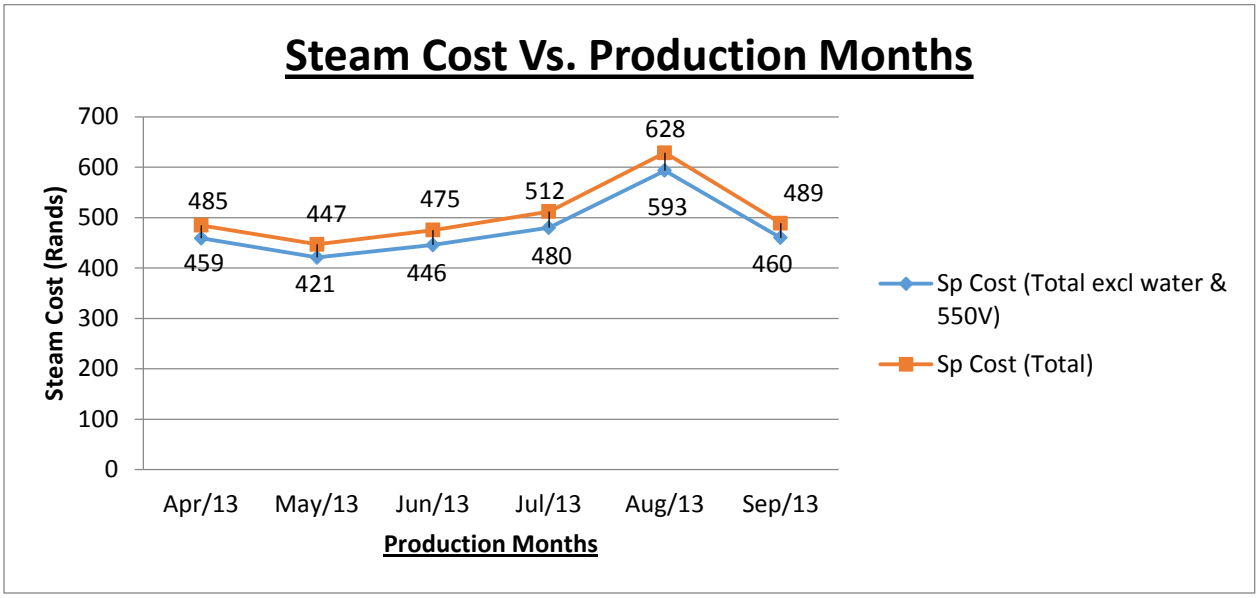

As shown above, the cost of producing saturated steam using HFO boilers is very high. This negatively affects the business in terms operations and maintenance budget, with the national fuel price frequently increasing. Apollo-Dunlop tyres utilises 0.875 tons of saturated steam to warm up the tyre compression moulds on each curing press. Thus, the cost to produce 0.875 tons of saturated steam is $(R\ 506\ x\ 0.875) = R\ 442.75$.

The current tyre compression moulds warm up cost in terms of steam usage is R442.75 per curing press, each curing press is composed of two tyre compression moulds. However, numerical analysis shows that the curing press requires 0.564 tons of steam to warm up the tyre compression moulds. Therefore, by knowing the current steam cost and the usage, the cost for the proposed usage was calculated to be $(R\ 442.75\ x\ 0.564)/0.875\ =\ \boldsymbol{R\ 285.38}$

As determined above, it will cost Apollo - Dunlop tyres ***R285.38*** per curing press, to warm up the tyre compression moulds from the initial temperature t_1 to the operational temperature t_2 should the warm up duration be reduced from five to three hours. Apollo - Dunlop tyres utilises 85 curing presses to carry out the tyre curing process. This entails that steam-cost savings can be

achieved across all the curing presses, since, they are composed of two press domes with one tyre compression mould each. Steam-cost savings per press were found to be:

$$Current\ warm\ up\ cost – Proposed\ warm\ up\ cost\ = Savings\ per\ curing\ press$$

$$R442.75 – R285.38 = \boldsymbol{R\ 157.4}$$

This clearly shows that reducing the tyre compression mould warm up duration from 5 to 3 hours will save Apollo - Dunlop tyres ***R 157.4*** per warm up session.

7.1 Weekly Savings

Apollo – Dunlop tyres carry out warm up sessions once a week before the production start-up. The start-up warm up is carried out on Monday morning after a Sunday production stop. Therefore, weekly savings are given as follows:

$$(Savings\ per\ press)(Number\ of\ presses)(Number\ of\ warm\ up\ sessions) = Weekly\ savings$$

$$(R\ 157.4)x\ (85)x\ (1) = \boldsymbol{R\ 13\ 379}$$

7.2 Monthly savings

Apollo – Dunlop tyres carry out the warm up sessions four times a month. Therefore, monthly savings are given as follows:

$$(Savings\ per\ press)(Number\ of\ presses)(Number\ of\ warm\ up\ sessions) = Monthly\ savings$$

$$(R\ 157.4)x\ (85)x\ (4) = \boldsymbol{R\ 53\ 516}$$

7.3 Yearly savings

Apollo – Dunlop tyres carry out the warm up sessions 48 times a year. Therefore, yearly savings are given as follows

$$(Savings\ per\ press)(Number\ of\ presses)(Number\ of\ warm\ up\ sessions) = Yearly\ savings$$

$$(R\ 157.4)(85)(48) = \boldsymbol{R\ 642\ 192}$$

7.4 Cost saving discussion

Apollo – Dunlop tyres will currently save approximately ± 0.64 million in energy usage each year by improving the warm up process of the tyre compression moulds. This study was one of the major findings during the evaluation of the steam usage of the tyre moulding factory. It costs Apollo – Dunlop tyres ***R506.00*** to produce 1 ton of saturated steam. Hence, it becomes possible to reduce the warm up duration for the tyre compression mould. Steam savings are very vital for Apollo – Dunlop tyres, since, most of the heating systems that they utilise are direct steam injection. This means, a large quantity of the sensible heat energy of the steam distributed into the plant is not recovered. Since, steam is instantly blended with the process fluid, resulting in full use of both the latent and sensible heat energy. Therefore, there is a necessity for Apollo-Dunlop tyres to implement this study to save energy and cost.

8. Summary and Conclusions

The aim of the study was to optimize the warm up process of the tyre compression mould. Numerical analysis was developed in order to determine the exact saturated steam required to warm up the tyre compression mould to the operational temperature. Additionally, an experimental evaluation was carried out since the duration of the warm up process is directly proportional to the required steam.

The numerical analysis results proved that Apollo-Dunlop tyres was using excessive steam to warm up the tyre compression moulds to operational temperature. Trials were conducted to evaluate the adjusted warm up time in order to significantly reduce the heating duration of the tyre compression mould. The pneumatic sample tyres moulded with the tyre compression moulds that were heated up with the optimized warm up process performed better than the "normal" tyres. This led to a new warm up process being proposed and implemented at Apollo-Dunlop tyres (see ***Appendix A*** for the specification change form). The steam usage during the warm up process was reduced from 0.875 tons to 0.564 tons per curing press and the heating duration was reduced from five hours to three hours.

Apollo-Dunlop tyres will now currently save approximately ± 0.64 million per year, after implementing the new warm up process. This study was a great success since the steam waste is costly in both an environmental and financial sense. Therefore, this required a prompt attention in order to ensure that the steam system is working at its optimum efficiency with a minimum impact on the environment.

9. Bibliography

Baeyer, H.C. von (1998) *Warmth Disperses and Time Passes — the History of Heat*. New York: The Modern Library. ISBN 0-375-75372-9.

Bergles, A.E. (1986) *Enhancements of convective heat transfer: Newton's legacy pursued*, Dept. Mechanical Engineering, New York 12180-3590: *pp. 53-63*.

Best, B.W. (2004) *Oxford Dictionary of National Biography*, Oxford University Press [online]. Available from: http://www.oxforddnb.com/[Accessed on the: 10-06-2015].

Bolz, G. (2008) "Know how Catalogue - snow-grip," ed: Continental.

Brydson, J.A. (1988) "Rubbery materials and their compounds". London and New York: Elsevier. Science Publishers.

Castle, A. (2000) *Die Heating in Production*, Alan Castle-Service Extrusion Consultants, Gloucester, UK-Ian Avent- Service Aluminium, Gloucester, UK.

Chen, Z. Tu, M. and **Bai, H**. (1995) "Research of tire tread pattern design expert system," Journal of Wuhan University of Technology, Vol. 17, No. 1, pp. 85-88.

Chiu, J.T. Weng, W.C. and **Hung, C.F**. (2002) "Optimization of pitch sequencing for pneumatic tire by Tabu search method," Japan Journal of Industrial and Applied Mathematics, Vol. 19, No. 3, pp. 399-414.

Cheng, X. and **Schulenberg, T**. (2001) *Heat Transfer at Supercritical Pressures-Literature Review and Application to a High Performance Light Water Reactor system,* FZKA 6609: pp.6-9.

Chu, C.H. Song, M.C. and **Luo, V.C**. (2006) "Computer aided parametric design for 3D tire mould production," Computers in Industry, Vol. 57, No. 1, pp. 11-25.

Chu, C.H. and **Séquin, C.H.** (2002) "Developable Bézier patches: properties and design," Computer Aided Design, Vol. 34, No. 7, pp. 511-527.

Chu, C.H. and **Chen, J.T.** (2006) "Automatic tool path generation for 5- axis flank milling based on developable surface approximation," International Journal of Advanced Manufacturing Technology, Vol. 29, No. 7-8, pp. 707-713.

Dalkilic, A.S. and **Wongwises, S.** (2009) *Condensation heat transfer, Condensation pressure drop heat transfer enhancement review inside smooth and enhanced tubes,* Dept.Mech Eng. King Mongkut's University of Technology, Bangkok, International Journal of Heat and Mass Transfer, 52 3409–3426: pp. 10-15.

Dick, J. S. (2006) "Review of common rubber factory problems", Department of Materials Science and Engineering Massachusetts Institute of Technology.

Eastop, T.D. and **McConckey, A.** (1993) *Applied Thermodynamics for engineering technologists*. 5th Ed, ISBN 0-470-21982-3.

Eastop, T.D. and **McConckey, A.** (2006) *Applied thermodynamics for technologists*. 6th edition: p 220-350. University of Glamorgan.

Edwards, D.C. *(2001) Handbook of Elastomers, Second Edition* . Marcel Dekker Inc. 1st edition. pp. 135. ISBN 0-8247-0383-9. Retrieved 8 February 2015.

FardiIlkhchy, A. Varahraam, N. and **Davami, P.** (2011) *Evaluation of pressure effect on heat transfer coefficient at the metal-mould interface for casting of A356 AL alloy.*

Fleming, R.A. (1995) "Tire moulding technology in die casting and venting: an overview," Die Casting Engineer, Vol. 39, No. 5, pp. 111-117.

Garcia, A. and **Ferreira, I.L.** (2005) *Evaluation of heat transfer coefficients during upward and downward transient directional solidification of Al-Si alloys,* Department of Materials Engineering, State University of Campinas.

German, R.M. (2005) *A-Z of Powder Metallurgy*, pp. 103. Elsevier.

Goldstein, R.J. and **Eckert, R.G**. (2005) *Heat transfer—a review of 2002 literature.* Heat Transfer Laboratory, Department of Mechanical Engineering, University of Minnesota, 125 Mechanical Engineering Building,111 Church Street S.E., Minneapolis, MN 55455, United States.

Guerlac, F. and **Henry, M.** (1980) "Black, Joseph". Dictionary of Scientific Biography 2. New York: Charles Scribner's Sons. Pp. 173-183. ISBN 978-0-684-10114-9.

Hsieh, S.T. and **Chu, C.H.** (2012) "Reducing machining error in 5-axis flank milling of ruled surfaces with improved PSO," International Journal of Precision Engineering and Manufacturing, Vol. 13, No. 1, pp. 1-8.

Huang, K. (2006) 'A review of literature on manufacturing systems productivity measurement and improvement', International Journal of Industrial and systems engineering, Vol. 1 No.4, pp. 461-484.

Jung, S.W. Bae, S.W. and **Park, G.T.** (1994) "A design scheme for a hierarchical fuzzy pattern-matching classifier and its application to the tire tread pattern recognition." Fuzzy Sets and Systems, No. 65, No. 2-3, pp. 311-322.

Kulkarni, S.N and **Radhakrishna, K**. (2005) *Evaluation of metal–mould interfacial heat transfer during the solidification of aluminum*, Department of Mechanics, Adhiyamaan College of Engineering, Hosur-635 1009, India.

Laughton, M.A. and **Say, M.G.** (2013) *electrical engineer's reference book, technology and engineering.*

Merril, A.M. (1955) *Plastics Technology, Volume 1*. Rubber/Automotive Division of Hartman Communications, Incorporated.

Messrs, C.J. and **Firestone, H.S**. (1971) *Tyre manufacturing standards*, The Tyre and Rim Association, Incorporated, Akron, Ohio.

Miller, R.C. (1985) *Tires: A Century of Progress*, Popular Mechanics. June 4, pp. 60-64.

Moutee, M. (2006). "Chapter 2: Modeling the creep behavior of wood cantilever". Loaded at free end during drying. Available: http://archimede.bibl.ulaval.ca/archimede/fichiers/ 23 791 /ch03.html. [Accessed on the: 05-04 2013].

Osmond, F. and **Austen, B.** (2012) *Forging grinding balls, (online),* from http://www.goldsteelballs.com/News/n44.html [Accessed on the: 28-05 2013].

Pacejka, H.B. (2006) *Tyre and vehicle dynamics*. SAE International. 2nd edition p. 198. ISBN 978-0-7680-1702-1.

Roylance, D. (2001) "Engineering Viscoelasticity," ed. Department of Materials Science and Engineering, Massachusetts Institute of Technology.

Rumford, S. (1804) *An enquiry concerning the nature of heat and the mode of its communication.* Philosophical Transactions of the Royal Society pp. 77.

Sadiktsis, I. (2012). *"Automobile Tires—A Potential Source of Highly Carcinogenic Dibenzopyrenes to the Environment". Environmental Science & Technology **46**: pp. 3326–1134.*

Simsons, D. Mason, R. and **Gardner, B.** (2004) 'Overall Vehicle Effectiveness' International journal of logistics: research and applications.0:0: pp.1-17.

Sipe, J.F (1923) *Elastic tire and method of making same*, New York, USA

Skaletz, J. (2008) "6D help-list," ed: Continental AG.

Sohnen, D.D. (2005) "Major tread compound components and their influence on tire performance." ed: Continental.

Spiegelhalder, B. (1983) *Occupational nitrosamine exposure. 1. Rubber and tyre industry*. Carcinogenesis 4: pp.1147–1152. doi:10.1093/carcin/4.9.1147.

Tadmor, Z and **Gogos, C.G.** (2006) *Principles of Polymer Processing*. John Wiley and Sons. ISBN 978-0-471-38770-1.

Tayler, G.F. (1933) *Apparatus for Making Hard Metal Compositions*, U.S. Patent 1,896,854, 7

Thomson, W. (1851) *On the Dynamical Theory of Heat, with numerical results deduced from Mr. Joule's equivalent of a Thermal Unit, and M. Renault's Observations on Steam. Excerpts. [§§1-14 & §§99-100], Transactions of the Royal Society of Edinburgh, March 1851; and Philosophical Magazine IV. 1852*, [from Mathematical and Physical Papers, vol. I, art. XLVIII, p. 174].

Thomas, D.G. (1986) *Performance Evaluation of the UMTRl Tire wheel Uniformity Test Machine,* Department of Mechanical Engineering, The University of Michigan Transportation Research Institute.

Todd, R.H. and **Dell, K**. (1993) *Alting Manufacturing Processes Reference Guide*. New York: Industrial P, Incorporated, pp. 219-220.

Tompkins, E. *(1981) Tread Patterns in the Thirties. The History of the Pneumatic Tyre. Dunlop Archive Project. p. 63. ISBN 0-903214-14-8.*

Vlachopoulos, J and **Strutt, D.** (2003) "The Role of Rheology in Polymer Extrusion," ed. Hamilton, Ontario, Canada.

Wang, G. and **Zhao, G**. (2010) *Research of thermal response simulation and mould structure optimization for rapid heat cycle moulding processes, respectively, with steam heating and electric heating.* Materials and Design 31: pp. 382-395. School of Materials Science and Engineering, Shandong University, Jinan, Shandong 250061, China.

White, J.L. (1990) *Principles of Polymer Engineering Rheology*. Wiley-Interscience. p.49.

Williams, A.R. (1984) "Tire design," CHEMTECH, Vol. 14, No. 12, pp. 756-764.

Wood, A. (1994) 'Availability Modelling', Circuits & Devices (IEEE), pp. 22-27.

Wu, P.H. Li, Y.W. and **Chu, C.H.** (2007) "Optimized tool path generation based on dynamic programming for five-axis flank milling of rule surface," International Journal of Machine Tools & Manufacture, Vol. 48, No. 11, pp. 1224-1233.

Xue, P. (2005) "The discussion on development trend of machine manufacturing". An Yang Engineering College Academic Journal, 04. pp. 14-16.

ZAE Bayern, (2000) Division 1: Energy Conversion and Storage, Walther-Meissner-Str. 6, 85748 Garching, Germany.

Zalba, B. and **Marın, J.M.** (2003) *Review on thermal energy storage with phase change: materials, heat transfer analysis and applications.* Applied Thermal Engineering 23: pp. 251–283.

Appendices

Appendix A: Standard specification change.

Apollo Tyres,Technical Department, Durban

STANDARD SPECIFICATION CHANGE

Circulation : S. Makardoij, A.Padayachee, M.Louis , J. Mellem ,T.Govender, G.Horsley , L.Gumbi, S.Reddy, M.Dlamini, R.Nxumalo, W. May, W. Reynolds, C. Walters, U. Mahadeo, A Sheik, N. Govender

CC: C. Anderson

Log no: S11177
Date: 13.02.2014
Effective Date: 13.02.2014

Please effect the following change to existing Spec. or Process no. : TRM16 Issue no:2

SPEC/PROCESS TITLE: **Press warm up procedures**

CHANGE:

1. **Reduction of warm up time.**
   - The warm-up time for a cold mold (not used for a day or shutdown and mold change) to be changed from 240 to 180 min.

Note: 1. Issue no 3 supersedes issue 2

REASON:

1. Energy Saving
2. Cost reduction.
3. Process update
4. GTM/D instructions.

APOLLO TYRES SOUTH AFRICA (PTY) LTD
REG No. 1997/021619/07
P O BOX 925 DURBAN 4000
TEL 031 242 1111
FAX 031 242 1205

RAW MATERIAL EFFECT (To be completed by originator) **Only if applicable to change.**

Industrialisation (Originator to state if Commenced or Completed)						
MILL	EXTRUDERS	FAB.PREP	MAKING	MOULDING	FINISHING	MASS CHANGE
				Commenced		

SAP – BOM CHANGED			
DATE RECEIVED	DATE IMPLEMENTED	NAME	SIGNATURE
	N/A		

	ORIGINATOR	APPROVED BY QTM	AGREED BY GMP
DATE :	13.02.2014	13.02.2014	13.02.2014
NAME :	Happy Tshimbiluni	Thiren Govender	Anand Padayachee
SIGNATURE :	[redacted]	[redacted]	[redacted]
TITLE :	GRADUATE ENGINEER	QTM DIVISION A OR B	GMP DIVISION A OR B

A1: The specification change sheet 1 (courtesy from Apollo-Dunlop tyres).

Appendix A: Standard specification change.

Apollo Tyres,Technical Department, Durban

STANDARD SPECIFICATION CHANGE

GROUP MANAGER TECHNICAL : or **GROUP MANAGER QUALITY :**

AUTHORISED BY :	
DATE :	13/6/2014
SIGNATURE :	[redacted]

ACKNOWLEDGEMENT FOR INFORMATION ONLY

DATE :				
SIGNATURES :				
TITLE	HEAD OF PROD	MAN COST AC	IE MAN	PLAN. MAN

APOLLO TYRES SOUTH AFRICA (PTY) LTD
REG No. 1997/021619/07
P O BOX 925 DURBAN 4000
TEL 031 242 1111
FAX 031 242 1205

A2: The specification change sheet 2 (courtesy from Apollo-Dunlop tyres).

Appendix B: Sample tyre performance results

Table B: Tyre performance results (courtesy from Apollo-Dunlop tyres).

Machine Daily Status
Month FEB.2014

Distributio C Anderson, G. De Lange, P.Cullen, R.Hollister,
P.Frost, W.May, S.Makardoij, C. Walters. A.Padayachee
C.Moyo, M.Ndlovu, B.Moyo, Z.Nyoni P. Cullen
W. Reynold G.Govender, T. Govender,

Machine	Station	STR. No.	Mould No.	Test Code	Revision No.	Temp Range	Actual Temp	DOM	Test	Objective	Size	Distance	Min.Req.	Status	Failure
FMC2	1	13/568-2	LM 1050	D3	6	20'C TO 30'C	30'C	4913	G/S	EVALUATE E8188 (T101) TREAD COMPOUND	315/80 R22.5 (18) T/S 354	5668	8000 KM	RUNNING	
	2														BROKEN BOLTS
ACRON	1	13/540-1	LM 1260	D3	6	20'C TO 30'C	30'C	4813	G/S	EVALUATE LP111 & LP126 WITH ALTERNATIVE COBALT STERATE SUPPLIER	12 R22.5 (16) T/S 811+	2230	8000 KM	RUNNING	
	2	13/151-1	LM 1012	D3	6	20'C TO 30'C	30'C	1713	G/S	PRODUCT MONITOR	315/80 R22.5 (18) T/S 366	2230	8000 KM	RUNNING	
VME TRUCK	1	14/27-1	LM 1258	D5	7	38'C +/- 2.5'C	38'C	0414	EGS	EVALUATE REDUCED WARM-UP	275 R22.5 (16) T/S 344	71 HRS @ 120% = 4260 KG	47 HRS @ 101% = 3585.5 KG	RUNNING	
	2	14/75-1	LM 1111	D5	7	38'C +/- 2.5'C	38'C	4613	EGS	EVALUATE T862 TREAD COMPOUND	315/80 R22.5 (18) T/S 354	71 HRS @ 120% = 4500 KG	47 HRS @ 101% = 3787.5 KG	RUNNING	
HEENAN	1	13/209-1	LM 1024	D3	6	20'C TO 30'C	30'C	1813	G/S	PRODUCT MONITOR	295/80 R22.5 (16) REGAL 465+	8050	8000 KM	RUNNING	
	2														

Appendix C: Cure sheet.

FACTORY TECHNICAL DEPARTMENT, DURBAN

PROCESS TRM7
ISSUE 9
PAGE 1 of 4

CURE CYCLE FOR 63½" BOMS AND 65"BOMS:

Cure cycles may differ from size to size, depending on the shoulder gauge of the tyre. The higher the gauge, the higher the possibility of a longer cure.

A. TABLED BELOW ARE THREE CURE CODES FOR A, B AND C LINE CURING PRESSES

1. **N1** (HP8/N35/T46), **N2** (HP11/N34/T48) **& N3** (HP13/N34/T52)

Breakdown of cure code: **N1 (HP8 / N35/ T46)**

- **Code**
- **High pressure steam time of 8 mins**
- **Nitrogen time of 35 mins**
- **Total time of 46 mins**

	N1 (HP8/N35/T46)		N2 (HP11/N34/T48)		N3 (HP13/N36/T52)	
ACTION	**Time (Sec)**	**Time (Min: sec)**	**Time (Sec)**	**Time (Min: sec)**	**Time (Sec)**	**Time (Min: sec)**
Close Press, Main drain closed	0	0	0	0	0	0
HPS on, HPS drain open (1st purge)						
HPS drain closed	45	45	45	45	45	45
Dome steam on	120	2	120	2	120	2
HPS drain open (2nd Purge)	120	2	120	2	120	2
HPS drain closed	140	2:20	140	2:20	140	2:20
HPS drain open (3rd Purge)	420	7:00	540	9:00	660	11:00
HPS drain closed	435	7:15	555	9:15	680	11:20
HPS off, Nitrogen On	480	8	660	11	780	13
Nitrogen outlet block off closed						
Nitrogen inlet block off closed (Leak test on)	2280	38	2400	40	2640	44
Nitrogen inlet block off open (Leak test off)	2460	41	2580	43	2820	47
Dome steam off, Dome exhaust open	2550	42:30	2670	44:30	2820	47
Nitrogen off, Nitrogen outlet block off open	2580	43:00	2700	45:00	2940	49
Purge drain open	2592	43:12	2712	45:12	2952	49:12
Purge drain close	2712	45:12	2832	47:12	3072	51:12
Main drain open	2714	45:14	2834	47:14	3074	51:14
Main drain closed, Vacuum on	2730	45:30	2850	47:30	3090	51.30
Press opens	2760	46	2880	48	3120	52

C1: The cure sheet 1 (courtesy from Apollo-Dunlop tyres).

Appendix C: Cure sheet.

FACTORY TECHNICAL DEPARTMENT, DURBAN

PROCESS TRM7
ISSUE 9
PAGE 2 of 4

B. TABLED BELOW ARE THREE CURE CODES FOR D ,E and F LINE CURING PRESSES

NOTE: The below cure codes does not apply to press D9 and D10, refer to table A

1. **N1** (HP8/N37/T46.21), **N2** (HP11/N36/T48.21) **& N3** (HP13/N38/T52.21)

ACTION	N1		N2		N3	
	TIME (SEC)	TIME(MIN)	TIME (SEC)	TIME(MIN)	TIME (SEC)	TIME(MIN)
Close Press Main drain closed	0	0:00	0	0:00	0	0:00
HPS on	0	0:00	0	0:00	0	0:00
Dome Steam on, Dome Exhaust on	120	2:00	120	2:00	120	2:00
HPS off, Nitrogen #1 on	480	8:00	660	11:00	780	13:00
Block-off on (Leak test on)	2400	40:00	2520	42:00	2760	46:00
Block-off off (Leak test off) Nitrogen #2 on	2520	42:00	2640	44:00	2880	48:00
Dome Steam off, Dome Exhaust open	2670	44:30	2790	46:30	2940	49:00
Nitrogen off, Purge drain open	2700	45:00	2820	47:00	3060	51:00
Purge drain closed, Main drain open	2736	45:36	2856	47:36	3096	51:36
Vacuum on Press opens	2781	46:21	2901	48:21	3141	52:21

C. TABLED BELOW ARE THREE CURE CODES FOR D ,E and F LINE CURING PRESSES AS DISPLAYED ON PANEL SCREEN

	N1	N2	N3
HP Steam #1	120	120	120
Dome Steam on	0	0	0
HP Steam #2	360	540	660
HP Nitrogen #1	1400	1360	1460
Leak Check	120	120	120
HP Nitrogen #2	670	650	580
Dome deflate Nitrogen on	30	30	120
Slow Deflate	36	36	36
Bladder Drain	45	45	45
Vacuum	0	0	0

C2: The cure sheet 2 (courtesy from Apollo-Dunlop tyres).

Appendix C: Cure sheet.

FACTORY TECHNICAL DEPARTMENT, DURBAN

PROCESS TRM7
ISSUE 9
Page 3 of 4

D. TYRE SIZES AND THEIR RESPECTIVE CURE CODES:
N.B = L.W refers to light weight

	N1	N2	N3
12R22.5 TS 811	N1		
13R22.5 TS811	N1		
315/80R22.5 TS811	N1		
12R22.5TS811 L.W.	N1		
12R22.5 TS822			N3
315R22.5 TS822			N3
12R22.5TS 822 L.W			N3
12R22.5 TS431	N1		
315/80R22.5 TS431		N2	
12R22.5 TS354/357		N2	
315/80R22.5 TS354/357		N2	
295/80R22.5 TS366	N1		
315/80R22.5 TS366		N2	
315/80R22.5 TS367		N2	
385/65R22.5 TS366		N2	
385/65R22.5 TS833		N2	
12R22.5 TS367		N2	
295/80R22.5 TS355	N1		
11R22.5 TS355	N1		
12R22.5 TS355	N1		
315/80R22.5 TS355	N1		
275/80R22.5 TS344	N1		
11R22.5 TS344/ 295R22.5 TS 344	N1		
10R22.5 TS344	N1		
295/80R22.5 TS465	N1		
315/80R22.5 TS465		N2	

C3: The cure sheet 3 (courtesy from Apollo-Dunlop tyres).

Appendix D: The density of plain carbon steel.

Table D1: The density of steel (Huang, 2006).

Materials Sorted By Category Then Density		
Category	**Material**	**Density**
Metal	Steel, tool	7.715
Metal	Wrought Iron	7.75
Metal	Carbon Tool Steel	7.82
Metal	Steel, cold-drawn	7.83
Metal	Carbon Steel	7.84
Metal	Steel, C1020, HR	7.85
Metal	Pure Iron	7.86
Metal	Soft Steel (0.06% C)	7.87
Metal	Stainless Steel, 304	8.03
Metal	Stainless 18Cr-8Ni	8.03

Table D2: The density of steel (Huang, 2006).

Common Name	Density (g/cm^3)
Plain carbon steel AISI-SAE 1020	7.86
Stainless steel type 304	7.9

Appendix E: Volume calculations

Platen adjuster

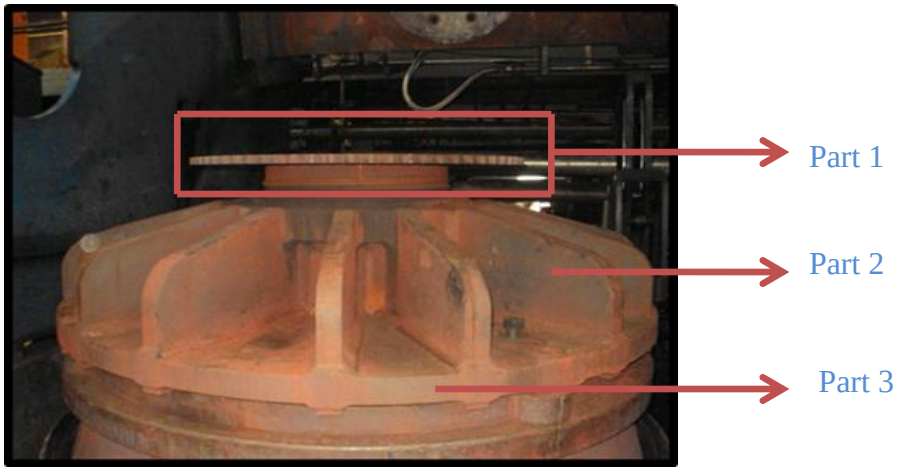

Fig. 4.52: Stripped platen mould adjuster mounted on the prismatic container

(**Fig. 4.52** is a Courtesy from Apollo-Dunlop tyres)

Part 1

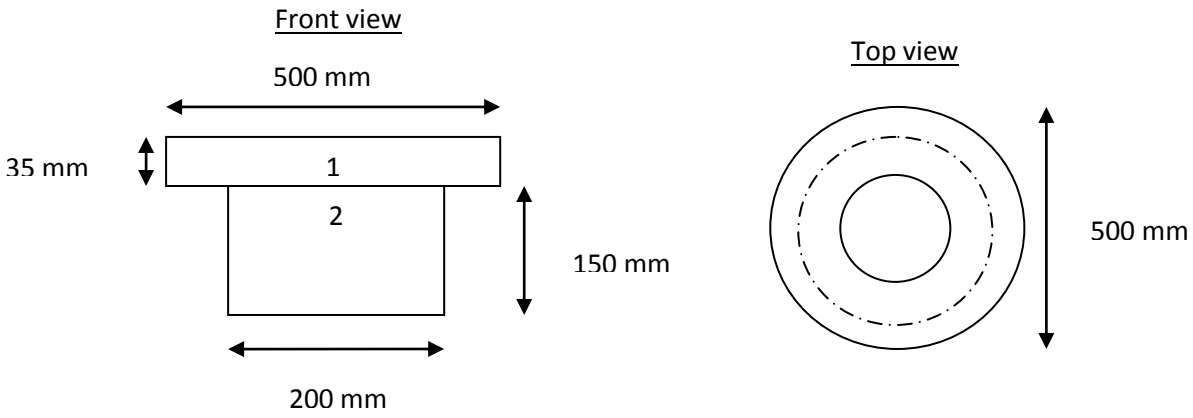

$$V_1 = \frac{\pi {D_1}^2 - {D_2}^2 h}{4} = \frac{\pi\,(0.5^2 - 0.15^2)(0.01)}{4} = 0.00178\ \mathrm{m}^3$$

$$V_2 = \frac{\pi {D_1}^2 - {D_2}^2 h}{4} = \frac{\pi\,(0.2^2 - 0.15^2)(0.15)}{4} = 0.00206\ \mathrm{m}^3$$

$$Part\ 1\ volume = V_1 + V_2 = 0.00384\ \mathrm{m}^3$$

Part 2

Front view

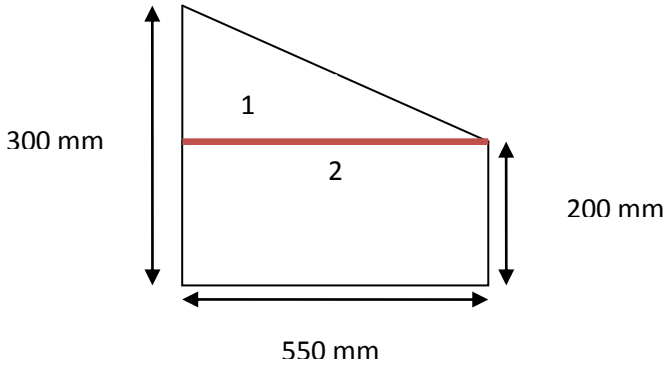

$$V_1 = \frac{(b)(h)(l)}{2} x\ 14 = \frac{(0.1)(0.55)(0.035)}{2} x\ 14 = 0.013\ m^3$$

$$V_2 = (b)(h)(l) x\ 14 = (0.035)(0.2)(0.55) x\ 14 = 0.054\ m^3$$

$$Part\ 2\ volume = V_1 + V_2 = 0.067\ m^3$$

Part 3

Isometric view

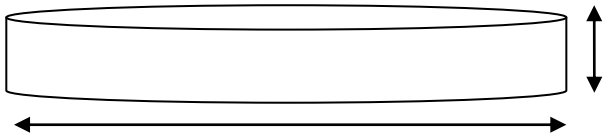

Top view

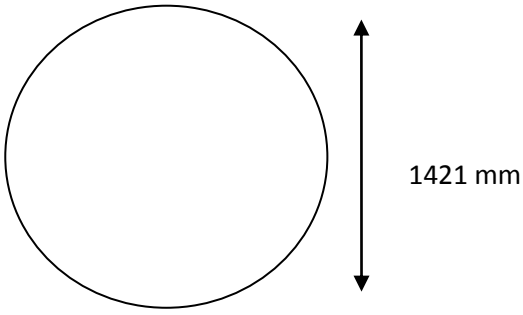

$$V = \frac{\pi D^2 h}{4} = \frac{\pi\ (1.421^2)(0.07)}{4} = 0.111\ m^3$$

$$Part\ 3\ volume = 0.111\ m^3$$

Therefore, the platen volume is given by,

$$Platen_{vol} = P_1 + P_2 + P_3 = 0.182\ m^3$$

Prismatic support bars

Fig. 4.54: Prismatic container support bars

(**Fig. 4.54** is a Courtesy from Apollo-Dunlop tyres)

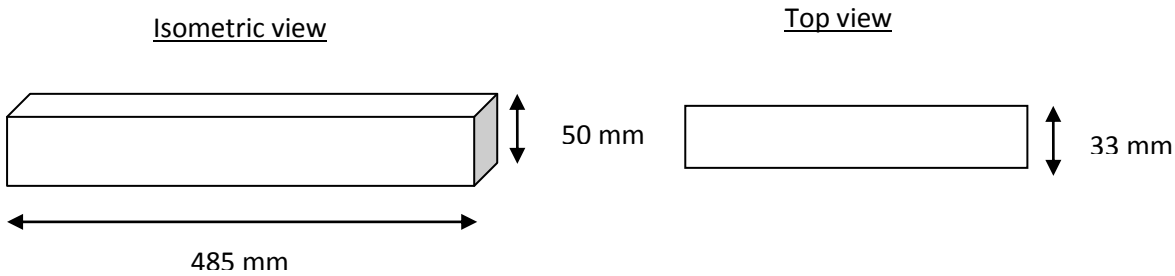

$$V = (b)(h)(l)x\,14 = (0.033)(0.05)(0.485)x\,24 = 0.019\ m^3$$

Press dome volume

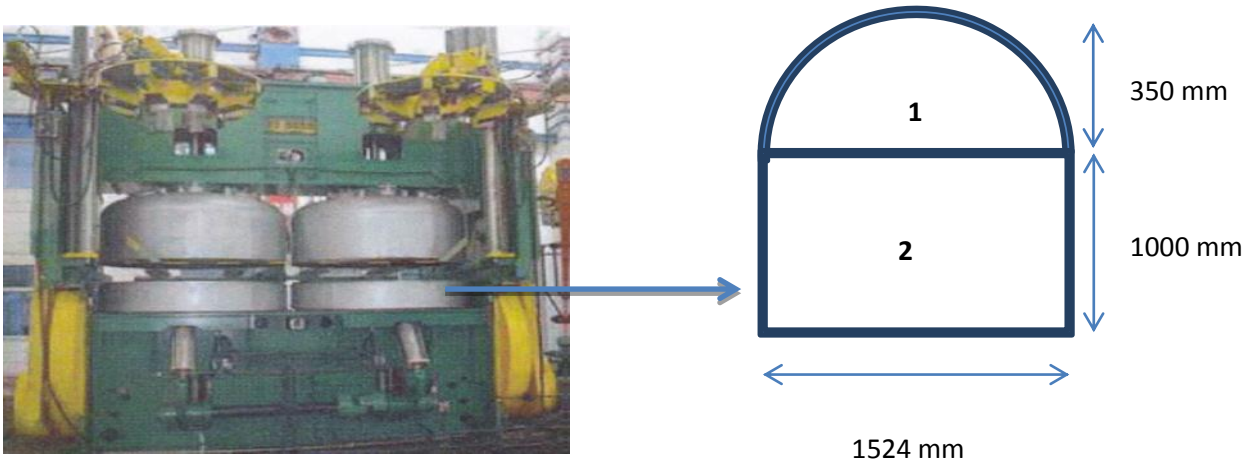

Fig. 4.59: Slightly open press dome (**Fig. 4.59** is a Courtesy from Apollo-Dunlop tyres)

Shape ① is an oblate spheroid, therefore,

$$\text{Volume} = \frac{4\,\pi r^2 h}{3}$$

$$V_1 = \frac{4\,\pi r^2 h}{3} = \frac{4\pi\,(0.762^2)(0.35)}{3} = 0.85\ m^3$$

Shape ② is a cylinder, therefore, volume $= \pi r^2 h$

$$V_2 = \pi(0.762)^2(1) = 1.82\ m^3$$

Therefore, the press dome volume is given by,

$$\text{Press dome}_{Vol} = V_1 + V_2 = 2.67\ m^3$$

Appendix F: The specific heat capacity of plain carbon steel.

Table F: The specific heat capacity of various materials (Huang, 2006).

Metal	Specific Heat - c_p		
	(kJ/kg K)	*(kcal/kg°C)*	*(Btu/lb$_m$°F)*
Aluminum	0.91	0.22	0.22
Antimony	0.21	0.05	0.05
Barium	0.20	0.048	0.048
Beryllium	1.83	0.436	0.436
Bismuth	0.13	0.03	0.03
Cadmium	0.23	0.055	0.055
Calsium	0.63	0.15	0.15
Carbon Steel	0.49	0.12	0.12
Cast Iron	0.46	0.11	0.11
Cesium	0.24	0.057	0.057
Chromium	0.46	0.11	0.11
Cobalt	0.42	0.1	0.1
Copper	0.39	0.092	0.09
Gallium	0.37	0.088	0.088
Germanium	0.32	0.076	0.076
Gold	0.13	0.031	0.03
Hafnium	0.14	0.033	0.033
Indium	0.24	0.057	0.057
Iridium	0.13	0.031	0.31
Iron	0.45	0.108	0.11
Lanthanum	0.195	0.047	0.047
Lead	0.13	0.031	0.03
Lithium	3.57	0.85	0.85
Lutetium	0.15	0.036	0.036
Magnesium	1.05	0.243	0.25
Manganese	0.48	0.114	0.114

Appendix G: The steam table.

Table G: The steam table(Miller, 1985).

Absolute pressure	Boiling point	Specific volume (steam)	Density (steam)	Specific enthalpy of liquid water (sensible heat)		Specific enthalpy of steam (total heat)		Latent heat of evaporization		Specific heat
(bar)	(°C)	(m^3/kg)	(kg/m^3)	(kJ/kg)	(kcal/kg)	(kJ/kg)	(kcal/kg)	(kJ/kg)	(kcal/kg)	(kJ/kg K)
1.8	116.93	0.977	1.023	490.70	117.20	2701.54	645.25	2210.84	528.05	2.1037
1.9	118.62	0.929	1.076	497.85	118.91	2703.98	645.83	2206.13	526.92	2.1124
2	120.23	0.885	1.129	504.71	120.55	2706.29	646.39	2201.59	525.84	2.1208
2.2	123.27	0.810	1.235	517.63	123.63	2710.60	647.42	2192.98	523.78	2.1372
2.4	126.09	0.746	1.340	529.64	126.50	2714.55	648.36	2184.91	521.86	2.1531
2.6	128.73	0.693	1.444	540.88	129.19	2718.17	649.22	2177.30	520.04	2.1685
2.8	131.20	0.646	1.548	551.45	131.71	2721.54	650.03	2170.08	518.32	2.1835
3	133.54	0.606	1.651	561.44	134.10	2724.66	650.77	2163.22	516.68	2.1981
3.5	138.87	0.524	1.908	584.28	139.55	2731.63	652.44	2147.35	512.89	2.2331
4	143.63	0.462	2.163	604.68	144.43	2737.63	653.87	2132.95	509.45	2.2664
4.5	147.92	0.414	2.417	623.17	148.84	2742.88	655.13	2119.71	506.29	2.2983
5	151.85	0.375	2.669	640.12	152.89	2747.54	656.24	2107.42	503.35	2.3289
5.5	155.47	0.342	2.920	655.81	156.64	2751.70	657.23	2095.90	500.60	2.3585
6	158.84	0.315	3.170	670.43	160.13	2755.46	658.13	2085.03	498.00	2.3873

Appendix H: The thermal conductivity table.

Table H1: The thermal conductivity of various materials (Miller, 1985).

Metal	Composition (%)	Properties at 293 K: ρ (kg/m³)	c_v [kJ/(kg °C)]	k [W/(m °C)]	$\alpha \times 10^5$ (m²/s)	Variation of properties with temperature T(K): k [W/(m °C)]/c_v [kJ/(kg °C)] 100	200	400	600	800	1000	1200
Aluminum												
Duralumin	94-96 Al, 3-5 Cu, trace Mg	2787	0.883	164	6.676		163 **0.787**	186 **0.925**	186 **1.042**			
Silumin	87 Al, 13 Si	2659	0.871	164	7.099		165					
Copper												
Aluminum Bronze	95 Cu, 5 Al	8666	0.410	83	2.330							
Bronze	75 Cu, 25 Sn	8666	0.343	26	0.859							
Red brass	85 Cu, 9 Sn, 6 Zn	8714	0.385	61	1.804							
Brass	70 Cu, 30 Zn	8522	0.385	111	3.412	75	95 **0.360**	137 **0.395**	149 **0.425**			
German silver	62 Cu, 15 Ni, 22 Zn	8618	0.394	24.9	0.733							
Constantan	60 Cu, 40 Ni	8922	0.410	22.7	0.512	17 0.237	19 0.362					
Iron												
Cast iron	≈4 C	7272	0.420	52	1.702							
Wrought iron	0.5 C	7849	0.460	59	1.626			56	47	39	34	33
Steel												
Carbon steel	0.5 C	7833	0.465	54	1.474			51	44	43	32	30
	1 C	7801	0.473	43	1.172			43	39	34	30	28
	1.5 C	7753	0.486	36	0.970			36	35	32	29	28

Appendix H: The thermal conductivity table.

Table H2: The thermal conductivity of various materials (Miller, 1985).

Mercury	234	13546					28.9					
Molybdenum	2883	10240	0.251	138	53.7	179 **0.141**	143 **0.224**	134 **0.261**	126 **0.275**	118 **0.285**	112 **0.295**	105 **0.308**
Nickel	1726	8900	0.446	91	22.9	164 **0.233**	106 **0.385**	80.1 **0.487**	65.5 **0.595**	67.4 **0.532**	71.8 **0.564**	76.1 **0.597**
Niobium	2741	8570	0.270	53.6	23.2	55.2 **0.192**	52.6 **0.254**	55.2 **0.279**	58.2 **0.288**	61.3 **0.298**	64.4 **0.307**	67.5 **0.316**
Palladium	1825	12020	0.244	71.8	24.5	76.5 **0.168**	71.6 **0.227**	73.6 **0.251**	79.7 **0.261**	86.9 **0.271**	94.2 **0.281**	102 **0.291**
Platinum	2042	21450	0.133	71.4	25.0	77.5 **0.100**	72.4 **0.125**	71.6 **0.136**	73.0 **0.141**	75.5 **0.146**	78.6 **0.152**	82.6 **0.157**
Potassium	337	860	0.741	103	162		104	52				
Rhenium	3453	21100	0.137	48.1	16.6	58.9 **0.097**	51 **0.127**	46.1 **0.139**	44.2 **0.145**	44.1 **0.151**	44.6 **0.156**	45.7 **0.162**
Rhodium	2233	12450	0.248	150	48.6	186 **0.150**	154 **0.225**	146 **0.258**	136 **0.280**	127 **0.299**	121 **0.317**	115 **0.334**
Rubidium	312	1530	0.348	58.2	109		58.9					
Silicon	1685	2330	0.703	153	93.4	884 **0.256**	264 **0.549**	98.9 **0.780**	61.9 **0.856**	42.2 **0.900**	31.2 **0.934**	25.7 **0.955**
Silver	1234	10500	0.234	427	174	444 **0.187**	430 **0.225**	425 **0.239**	412 **0.250**	390 **0.262**	379 **0.277**	361 **0.292**
Sodium	371	971	0.121	133	114		138					
Tantalum	3269	16600	0.138	57.5	25.1	59.2 **0.108**	57.5 **0.131**	57.8 **0.142**	58.6 **0.144**	59.4 **0.147**	60.2 **0.150**	61 **0.153**
Tin	505	5750	0.227	67.0	51.3	85.2 **0.188**	73.3 **0.215**	62.2 **0.243**				
Titanium	1953	4500	0.522	21.9	9.32	30.5 **0.300**	24.5 **0.465**	20.4 **0.551**	19.4 **0.591**	19.7 **0.633**	20.7 **0.675**	22 **0.620**
Tungsten	3653	19300	0.134	179	69.2	214 **0.088**	197 **0.124**	162 **0.139**	139 **0.144**	128 **0.147**	121 **0.150**	115 **0.154**
Uranium	1407	19070	0.113	27.4	12.7	21.7 **0.092**	25.1 **0.105**	29.6 **0.122**	34 **0.142**	38.8 **0.171**	43.9 **0.175**	49 **0.157**
Vanadium	2192	6100	0.502	31.4	10.3	35.8 **0.265**	31.5 **0.441**	32.1 **0.528**	34.2 **0.554**	36.3 **0.578**	38.6 **0.612**	41.2 **0.662**
Zinc	693	7140	0.385	121	44.0	122 **0.294**	123 **0.363**	116 **0.398**	105 **0.432**			
Zirconium	2125	6750	0.272	22.8	12.8	33.2 **0.200**	25.2 **0.258**	21.6 **0.294**	20.7 **0.315**	21.6 **0.335**	23.7 **0.354**	25.7 **0.336**

Appendix I: The thermal conductivity of air.

Graph I: The air thermal conductivity graph (Zalba and Marın, 2003).

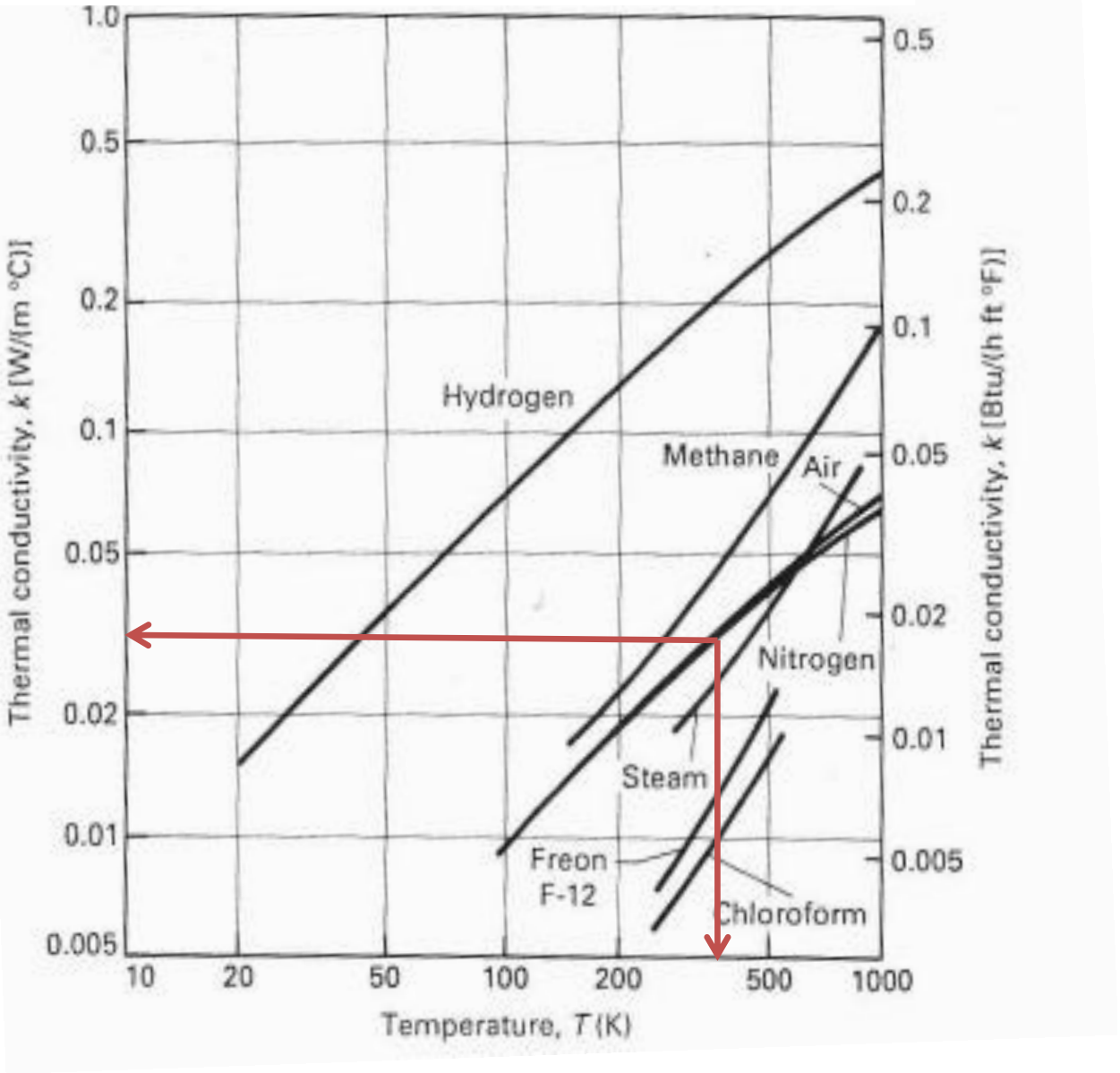

Appendix J: The heat transfer coefficient of air

The dome is divided into two shapes, cylindrical and oblate spheroid, respectively. The total length of the dome is 1350 mm, the cylindrical and oblate shapes are 1000 mm and 350 mm long, respectively. The transition point of the heat transfer from laminar flow to turbulent flow is unknown. The heat energy is transferred into the surroundings of the press dome cover through natural (free) convection. Fig. 58 shows the natural convection of heat energy around the press dome cover.

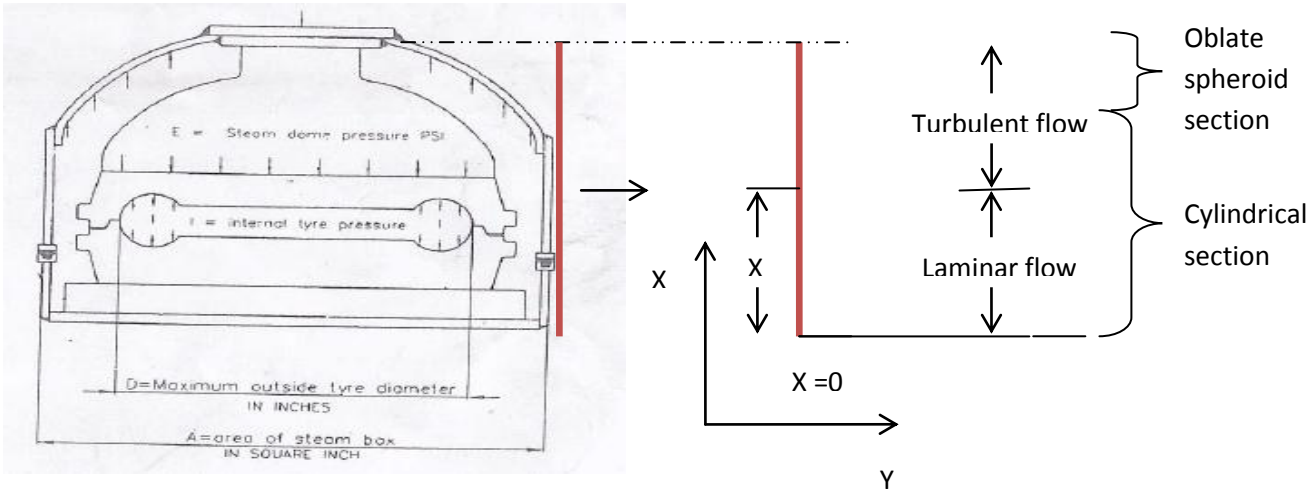

Fig. 4.58: The press steam dome with vacant dome space.

(**Fig. 4.58** is a Courtesy from Apollo-Dunlop tyres).

The empirical correlations for a free convection are given as follows:

The Grashof number, $G_r = \frac{L^3 g \beta \Delta t}{V^2}$ where,

L = characteristics length

$\Delta t = t_s - t_\infty$ where t_s is the surface temperature and t_∞ is the surrounding fluid temperature.

β = the coefficient of thermal expansion, = $\frac{1}{t_f + 273}$

ν = Kinetic viscosity

g = Gravity

The Prandtl number, $P_r = \frac{\mu c_p}{k}$ where

μ = Dynamic viscosity

c_p = Specific heat capacity

K = Thermal conductivity

The galvanized cover of the press done is maintained at 50^0C and the temperature of the surrounding air is 25^0C. the transition point (x) is calculated as follows:

The mean film temperature is given by,

$$t_f = \frac{t_s + t_\infty}{2} = \frac{50 + 25}{2} = 37.5^0\text{C}$$

The thermo-physical properties of air at 37.5^0C were all interpolated (see ***Appendix N***):

$$\nu = 16.74x10^{-6}\, {}^{m^2}/_{s}$$

$$P_r = 0.711$$

$$k = 0.02693\, {}^{W}/_{mK}$$

The coefficient of thermal expansion was found to be,

$$\beta = \frac{1}{t_f - 273} = \frac{1}{37.5 + 273} = 0.0032\ K^{-1}$$

Using Rayleigh number,

$$R_a = Gr_x P_r = 10^9, \left(\frac{x^3 g \beta \Delta t}{V^2}\right)(0.711) = 10^9$$

$$\left(\frac{x^3(9.81)(0.0032)(50-25)}{(16.74x10^{-6})^2}\right)(0.711) = 10^9$$

$$x = 0.7948 = 794.8\,mm$$

Therefore, the heat energy is naturally convected into the surrounding air through a laminar flow for 792.8 mm from the bottom of the press dome cover.

When considering the cylindrical section:

The heat transfer coefficient of the cylindrical section is determined by the sum of laminar and turbulent heat transfer coefficient.

The laminar heat transfer coefficient was found to be:

$$\bar{h}_1 = 1.42(\frac{\Delta t}{L})^{\frac{1}{4}}$$

$$\bar{h}_1 = 1.42(\frac{(50-25)}{0.7948})^{\frac{1}{4}}$$

$$\bar{h}_1 = 3.36\ {}^{W}/_{m^2\mathrm{C}}$$

The turbulent heat transfer coefficient was found to be:

$$\bar{h}_2 = 1.32(\Delta t)^{\frac{1}{3}} = \ 1.32(50-25)^{\frac{1}{3}} = 3.86\,{}^{W}/_{m^2\mathrm{C}}$$

Therefore, the overall heat transfer co-efficient of the cylindrical section was found to be:

$$\bar{h}_{cylindrical\ section} = (x)(\bar{h}_1) + (x)(\bar{h}_2)$$

$$\bar{h}_{cylindrical\ section} = (0.7948)(3.36) + (1-0.7948)(3.86) = \mathbf{3.4}\ {}^{\boldsymbol{W}}/_{\boldsymbol{m^2\mathrm{C}}}$$

When considering the oblate spheroid section:

$$G_r = \left(\frac{D^3 g\beta\Delta t}{V^2}\right) = \left(\frac{(1.524)^3(9.81)(0.0032)(50-25)}{(16.74x10^{-6})^2}\right) = 9.9x10^9$$

Therefore, the heat transfer co-efficient of the oblate spheroid section was found to be:

$$\bar{h}_{oblate\ spheroid} = 2 + 0.392(G_r)^{\frac{1}{4}}\left(\frac{k}{D}\right)$$

$$\bar{h}_{oblate\ spheroid} = 2 + 0.392(9.9x10^9)^{\frac{1}{4}}\left(\frac{0.02693}{1.524}\right) = \mathbf{2.2}\ {}^{\boldsymbol{W}}/_{\boldsymbol{m^2C}}$$

Appendix K: The radiation emissivity coefficients table

Table K1: The radiation emissivity coefficients of various materials (William, 1984).

Surface Material As a guideline the emmisivities below are based on temperature 300 K.	Emissivity Coefficient - ε -
Rubber, hard glossy plate	0.94
Rubber, natural hard	0.91
Rubber, natural oft	0.86
Salt	0.34
Sand	0.76
Sandstone	0.59
Sapphire	0.48
Sawdust	0.75
Silica	0.79
Silicon Carbide	0.83 - 0.96
Silver Polished	0.02 - 0.03
Soil	0.38
Steel Oxidized	0.79

Appendix K: The radiation emissivity coefficients table.

Table K2: The radiation emissivity coefficients of various materials (William, 1984).

Surface Material As a guideline the emmisivities below are based on temperature 300 K.	Emissivity Coefficient - ε -
Stainless Steel, weathered	0.85
Stainless Steel, polished	0.075
Stainless Steel, type 301	0.54 - 0.63
Steel Galvanized Old	0.88
Steel Galvanized New	0.23

Appendix L: The warm up evaluation results of the bottom sidewall plate.

Press	F3 & 4					
Saturated Steam Pressure	4 bar		**Warm Up Evaluation Bottom Sidewall Plate**			
Saturated Steam Temperature	151 C					
Warm up Evaluation Time	5 hours					
Date	20-Sep-13					
Cure	N1					
		#DIV/0!	#DIV/0!	#DIV/0!	#DIV/0!	#DIV/0!
Units	Units	°C	°C	°C	°C	
		67,22	58,42	66,68	59,12	26,96
		1	2	3	4	16
Time, s	**Time, min**	**Vent Hole**	**Vent Hole**	**Vent Hole**	**Sidewall Surface**	**Ambient**
0	0,0	33,87	33,31	33,97	33,70	29,26
30	0,5	34,253	33,758	34,138	33,819	28,875
60	1,0	34,091	33,549	33,937	33,686	28,487
90	1,5	34,128	33,627	34,511	33,765	28,399
120	2,0	34,623	33,841	36,298	34,167	27,812
150	2,5	35,808	34,473	39,129	35,064	28,079
180	3,0	37,969	35,492	42,532	36,641	28,828
210	3,5	40,959	37,004	46,257	38,757	28,284
240	4,0	44,069	39,274	50,266	41,443	25,832
270	4,5	48,022	41,855	53,952	44,264	26,119
300	5,0	51,544	45,459	57,621	47,389	29,074
330	5,5	55,740	48,090	61,041	50,156	28,705
360	6,0	60,310	50,738	63,025	52,799	27,631
390	6,5	67,773	54,499	67,185	57,036	27,415
420	7,0	75,074	66,352	72,080	61,196	27,591
450	7,5	80,224	68,709	77,835	66,201	24,906
480	8,0	86,530	70,542	79,886	70,436	24,421
510	8,5	90,643	72,685	82,874	73,265	26,277
540	9,0	89,773	74,921	83,863	74,403	25,033
570	9,5	89,217	77,112	85,661	76,794	27,828
600	10,0	93,926	79,163	87,728	79,424	24,052
630	10,5	96,081	82,337	89,803	82,181	26,501
660	11,0	97,266	83,859	92,437	84,864	27,057
690	11,5	99,254	85,699	95,244	87,661	27,417
720	12,0	100,830	87,612	98,332	90,148	25,311
750	12,5	102,382	89,758	101,446	92,552	24,054
780	13,0	103,936	92,125	104,400	94,650	27,607
810	13,5	105,494	94,300	106,213	96,629	27,382
840	14,0	106,919	96,392	108,471	98,515	25,173
870	14,5	108,230	98,203	110,234	100,324	26,963
900	15,0	109,091	101,001	112,087	101,982	26,851
930	15,5	110,823	105,654	112,875	104,030	26,962
960	16,0	114,610	105,996	115,459	105,806	27,321
990	16,5	117,568	107,574	117,298	107,112	26,888
1020	17,0	117,802	109,440	119,020	108,645	25,327
1050	17,5	119,247	111,126	120,641	110,195	24,319
1080	18,0	120,277	112,584	121,795	111,596	26,200
1110	18,5	120,724	114,018	123,145	112,939	26,394
1140	19,0	121,692	114,945	124,374	114,050	25,817
1170	19,5	122,457	115,784	125,528	115,136	28,000
1200	20,0	123,823	116,640	126,610	116,020	26,556
1230	20,5	125,065	117,504	127,466	117,074	26,598
1260	21,0	125,095	118,350	128,424	118,122	26,604
1290	21,5	125,466	119,393	129,367	119,054	25,668
1320	22,0	125,910	120,250	130,159	120,060	25,073
1350	22,5	126,380	121,154	130,753	120,657	26,652
1380	23,0	127,328	122,001	131,076	121,338	27,314
1410	23,5	127,418	122,843	131,526	122,098	26,170
1440	24,0	127,320	123,481	131,823	122,637	26,706
1470	24,5	127,181	124,123	132,309	123,355	25,722
1500	25,0	128,009	124,732	132,647	124,233	24,466
1530	25,5	128,096	125,405	133,148	124,899	25,615
1560	26,0	128,437	126,063	134,012	125,437	27,709
1590	26,5	128,955	126,560	134,913	125,954	27,479
1620	27,0	129,051	126,958	135,412	126,428	26,511
1650	27,5	129,456	127,553	135,580	126,933	25,624
1680	28,0	130,349	128,160	135,902	127,488	27,306

Time, s	Time, min	Vent Hole	Vent Hole	Vent Hole	Sidewall Surface	Ambient
1710	28,5	132,798	128,701	136,051	128,001	27,249
1740	29,0	131,374	129,179	136,120	128,409	26,233
1770	29,5	131,215	129,695	136,382	129,032	23,816
1800	30,0	131,756	130,138	136,559	129,324	26,870
1830	30,5	132,880	130,631	136,625	129,932	24,966
1860	31,0	132,988	131,959	136,399	130,068	25,579
1890	31,5	131,257	132,063	134,760	129,892	25,806
1920	32,0	131,327	131,914	134,775	130,089	26,902
1950	32,5	134,011	132,085	135,181	130,514	25,080
1980	33,0	132,577	132,423	134,802	130,818	23,749
2010	33,5	132,998	132,713	135,443	131,237	24,638
2040	34,0	133,824	132,973	135,302	131,823	26,019
2070	34,5	132,912	132,996	135,865	132,092	27,021
2100	35,0	132,834	133,287	136,824	132,563	26,091
2130	35,5	134,295	133,552	136,659	132,777	27,773
2160	36,0	133,455	133,745	137,717	133,029	27,742
2190	36,5	133,254	133,925	137,707	133,364	26,104
2220	37,0	134,288	134,087	138,396	133,621	26,245
2250	37,5	135,374	134,213	138,766	134,086	25,587
2280	38,0	134,358	134,374	139,920	134,314	25,965
2310	38,5	134,100	134,706	140,445	134,591	23,958
2340	39,0	134,487	134,792	140,736	134,963	25,182
2370	39,5	134,775	135,143	140,691	135,129	23,736
2400	40,0	135,059	135,459	140,909	135,598	26,268
2430	40,5	135,090	135,401	140,967	135,689	26,434
2460	41,0	136,581	135,552	141,766	135,865	26,656
2490	41,5	136,780	135,617	142,090	135,867	26,907
2520	42,0	137,025	135,723	141,973	136,007	27,028
2550	42,5	137,189	135,810	141,826	136,150	26,949
2580	43,0	137,034	135,877	142,476	136,220	26,861
2610	43,5	137,053	135,888	142,801	136,389	25,591
2640	44,0	136,972	135,897	142,698	136,504	26,539
2670	44,5	136,804	136,145	142,915	136,786	25,780
2700	45,0	136,704	136,212	142,971	136,573	26,929
2730	45,5	136,667	136,282	143,193	136,722	26,887
2760	46,0	136,542	136,324	143,035	136,811	26,845
2790	46,5	136,955	136,561	143,421	136,914	27,217
2820	47,0	136,688	136,639	143,534	137,115	24,399
2850	47,5	137,214	136,833	144,195	137,577	24,764
2880	48,0	137,396	137,017	144,501	137,842	26,678
2910	48,5	137,602	137,054	144,506	138,061	27,212
2940	49,0	137,790	137,334	144,622	138,404	26,500
2970	49,5	138,192	137,570	144,857	138,758	25,281
3000	50,0	138,733	138,021	145,206	139,229	25,084
3030	50,5	139,212	138,302	145,533	139,682	24,233
3060	51,0	139,774	138,670	145,889	140,159	26,406
3090	51,5	139,939	138,946	146,074	140,440	26,879
3120	52,0	140,311	139,402	146,134	141,008	24,610
3150	52,5	140,657	139,709	146,213	141,305	26,235
3180	53,0	141,093	139,908	146,450	141,690	27,380
3210	53,5	141,346	140,212	146,385	141,969	27,247
3240	54,0	141,556	140,480	146,265	142,229	27,190
3270	54,5	141,763	140,692	146,271	142,427	27,092
3300	55,0	141,947	140,925	146,308	142,565	27,220
3330	55,5	142,107	141,064	146,598	142,783	25,659
3360	56,0	142,273	141,275	146,272	143,157	24,354
3390	56,5	142,587	141,519	145,884	143,553	25,252
3420	57,0	142,854	141,785	146,142	143,733	27,291
3450	57,5	142,974	142,022	146,535	143,973	26,306
3480	58,0	143,035	142,279	146,623	144,269	24,170
3510	58,5	142,961	142,548	146,767	144,445	26,886
3540	59,0	143,029	142,334	146,810	144,617	26,859
3570	59,5	143,045	142,489	146,791	144,688	27,523
3600	60,0	143,146	142,758	146,745	144,789	27,382
3630	60,5	143,199	142,750	146,420	144,852	27,135
3660	61,0	143,227	142,919	146,516	144,919	27,424
3690	61,5	143,417	142,798	146,523	144,988	27,257
3720	62,0	143,462	142,961	146,694	145,111	25,740
3750	62,5	143,283	143,262	146,701	145,341	26,277
3780	63,0	143,527	143,261	146,917	145,448	26,006
3810	63,5	143,682	143,528	146,902	145,511	27,380
3840	64,0	143,793	143,841	146,890	145,603	24,800
3870	64,5	143,955	144,166	146,866	145,761	26,006
3900	65,0	144,121	144,513	146,748	145,945	27,288
3930	65,5	144,268	144,794	146,979	146,139	27,553
3960	66,0	144,361	144,852	147,491	146,163	26,839
3990	66,5	144,439	145,082	147,452	146,332	27,154

4020	67,0	144,864	145,198	148,313	146,512	27,468
Time, s	**Time, min**	**Vent Hole**	**Vent Hole**	**Vent Hole**	**Sidewall Surface**	**Ambient**
4050	67,5	145,068	145,434	148,431	146,618	26,007
4080	68,0	145,113	145,539	148,622	146,734	26,811
4110	68,5	145,260	145,784	148,823	146,914	27,678
4140	69,0	145,459	145,889	148,896	147,075	26,750
4170	69,5	145,432	145,999	148,859	147,160	27,377
4200	70,0	145,501	146,158	148,771	146,953	27,265
4230	70,5	145,624	146,224	149,080	147,024	27,183
4260	71,0	145,587	146,324	149,119	147,089	27,523
4290	71,5	145,513	146,315	148,680	147,082	26,865
4320	72,0	145,645	146,516	148,609	147,238	27,067
4350	72,5	145,668	146,550	148,974	147,368	24,993
4380	73,0	145,658	146,699	149,014	147,475	26,609
4410	73,5	145,757	146,857	149,173	147,533	27,093
4440	74,0	145,776	147,005	149,264	147,599	26,159
4470	74,5	145,807	147,195	149,193	147,700	23,907
4500	75,0	145,863	147,434	149,183	147,855	25,715
4530	75,5	145,958	147,521	149,123	148,009	25,228
4560	76,0	145,811	147,546	149,131	148,027	27,890
4590	76,5	145,829	147,620	149,106	148,037	27,645
4620	77,0	145,806	147,652	148,983	148,020	25,558
4650	77,5	145,916	147,826	149,028	147,943	24,391
4680	78,0	145,568	147,884	148,371	147,352	23,946
4710	78,5	146,283	148,050	149,177	147,787	25,789
4740	79,0	146,366	148,056	149,190	147,913	27,301
4770	79,5	146,266	148,009	148,928	147,901	28,232
4800	80,0	146,250	148,031	148,928	147,869	27,677
4830	80,5	146,375	148,147	149,211	148,030	27,729
4860	81,0	146,541	148,292	148,374	148,268	26,812
4890	81,5	146,509	148,339	148,354	148,329	27,343
4920	82,0	146,663	148,459	148,640	148,463	27,649
4950	82,5	146,767	148,586	148,515	148,544	26,320
4980	83,0	146,902	148,647	148,622	148,624	27,076
5010	83,5	146,859	148,685	148,685	148,597	27,527
5040	84,0	146,822	148,747	148,623	148,695	27,566
5070	84,5	146,748	148,771	148,535	148,584	26,707
5100	85,0	146,678	148,830	148,900	148,667	26,646
5130	85,5	146,763	148,919	149,123	148,767	25,408
5160	86,0	146,842	148,987	149,118	148,886	26,404
5190	86,5	146,789	149,004	149,431	148,932	27,278
5220	87,0	146,742	148,985	149,495	148,896	27,517
5250	87,5	146,748	148,941	149,470	148,865	25,419
5280	88,0	146,772	148,885	149,466	148,882	26,890
5310	88,5	146,711	148,800	149,453	148,854	26,883
5340	89,0	146,733	148,807	149,464	148,868	25,519
5370	89,5	146,924	148,870	149,470	148,844	27,239
5400	90,0	146,974	148,870	149,447	148,859	27,067
5430	90,5	146,883	148,782	149,332	148,686	26,861
5460	91,0	146,943	148,796	149,412	148,747	27,224
5490	91,5	146,975	148,795	149,368	148,728	27,359
5520	92,0	147,071	148,839	149,337	148,786	25,934
5550	92,5	146,966	148,759	149,269	148,781	27,358
5580	93,0	146,804	148,485	149,223	148,873	27,457
5610	93,5	146,480	148,487	149,368	148,686	27,036
5640	94,0	147,489	148,726	149,327	148,815	26,210
5670	94,5	147,808	148,844	149,370	149,015	25,045
5700	95,0	147,686	148,904	149,370	149,073	26,997
5730	95,5	147,779	149,014	148,583	149,173	28,150
5760	96,0	147,905	149,014	148,329	149,084	27,084
5790	96,5	148,284	149,079	148,489	149,173	27,498
5820	97,0	148,573	148,817	149,169	149,389	27,222
5850	97,5	148,609	148,864	149,402	149,440	27,152
5880	98,0	148,626	148,846	149,640	149,584	27,420
5910	98,5	148,680	148,879	149,438	149,589	27,157
5940	99,0	148,742	148,875	149,689	149,728	27,245
5970	99,5	148,834	148,931	149,702	149,784	27,419
6000	100,0	148,812	149,279	149,803	149,837	27,293
6030	100,5	148,833	149,264	149,923	149,834	27,335
6060	101,0	148,798	149,244	150,032	149,886	26,933
6090	101,5	148,691	149,264	150,026	149,851	26,182
6120	102,0	148,602	149,217	149,961	149,786	27,243
6150	102,5	148,582	149,095	149,852	149,724	27,445
6180	103,0	148,487	149,129	149,822	149,667	27,524
6210	103,5	148,396	148,953	149,778	149,563	27,152
6240	104,0	148,508	149,154	149,830	149,662	26,836
6270	104,5	148,415	149,091	149,764	149,554	27,473
6300	105,0	148,415	149,074	149,806	149,604	27,775

6330	105,5	148,451	149,069	149,817	149,537	27,766
Time, s	**Time, min**	**Vent Hole**	**Vent Hole**	**Vent Hole**	**Sidewall Surface**	**Ambient**
6360	106,0	148,474	149,075	149,819	149,548	27,429
6390	106,5	148,514	149,126	149,768	149,605	27,587
6420	107,0	148,539	149,121	149,783	149,630	27,590
6450	107,5	148,462	149,057	149,714	149,641	27,252
6480	108,0	148,508	149,120	149,789	149,752	27,079
6510	108,5	148,309	149,125	149,817	149,704	26,935
6540	109,0	147,821	148,167	149,925	149,682	27,552
6570	109,5	148,174	149,042	150,011	149,680	27,677
6600	110,0	148,302	149,163	149,761	149,635	27,129

Appendix L: The warm up evaluation results of the bottom sidewall plate.

Graph L: The temperature profile of the bottom sidewall plate (courtesy of Apollo-Dunlop tyres).

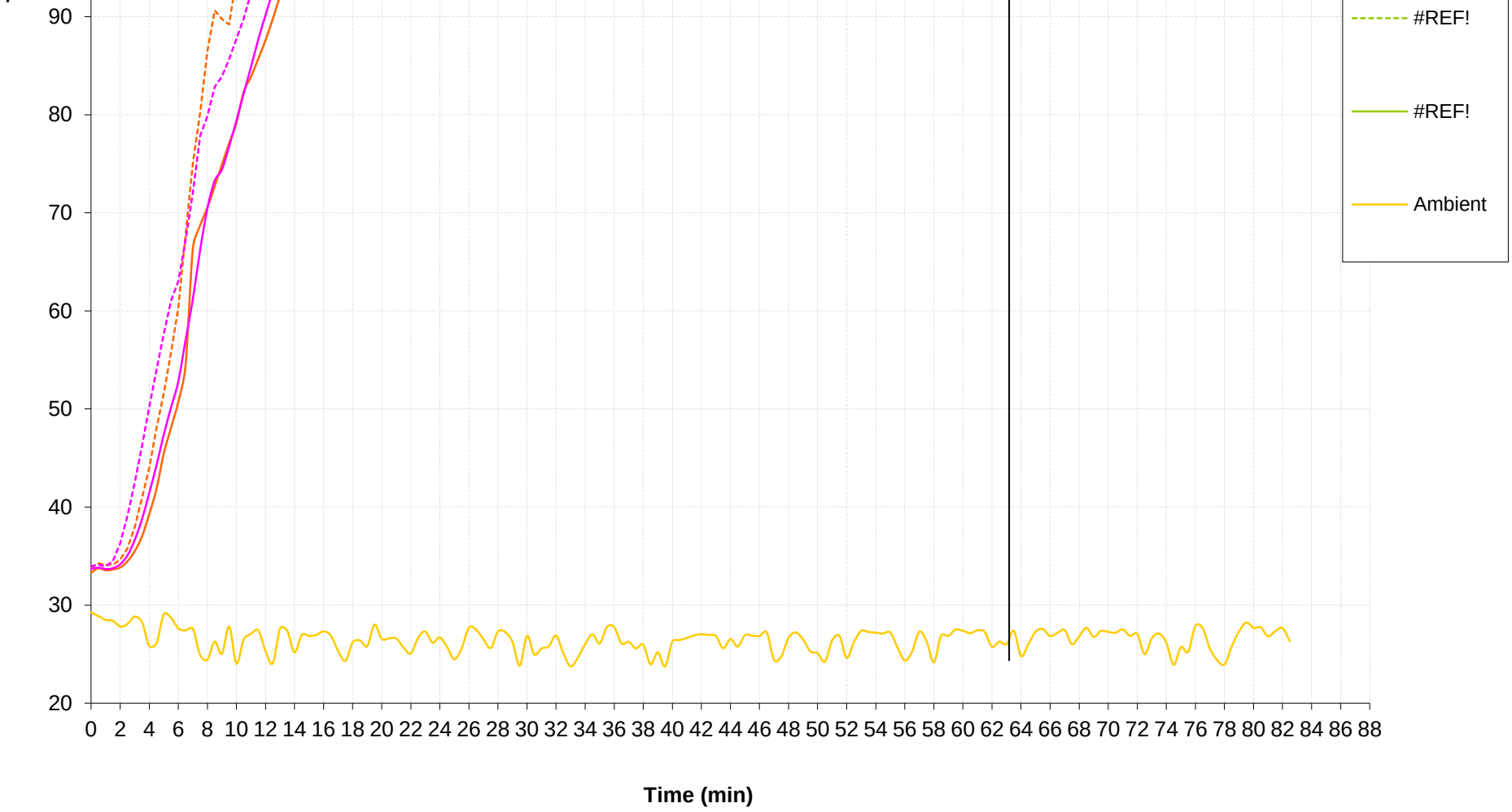

Appendix M: The warm up evaluation results of the top sidewall plate and tread sectors.

Press	F3 & 4						
Dome Pressure	4 bar						
Warm up Evaluation Time	5 hours		Warm up Evaluation Top Sidewall plate and Sectors				
Date	20-Sep-13						
Cure	N1						
		#DIV/0!	#DIV/0!	#DIV/0!	#DIV/0!	#DIV/0!	#DIV/0!
Units	Units	°C	°C	°C	°C	°C	°C
							19,32
		1	2	3	4	5	6
Time, s	**Time, min**	**Tread**	**Tread**	**Tread**	**Sidewall Surface**	**Sidewall Surface**	**Ambient**
0	0,0	21,4	24,2	22,4	22,9	22,8	19,2
30	0,5	25,4	24,5	22,3	22,8	22,2	20,3
60	1,0	23,5	24,0	21,8	22,7	21,8	20,7
90	1,5	26,9	22,3	21,8	22,5	21,4	20,8
120	2,0	25,4	24,6	22,2	22,0	21,5	20,4
150	2,5	27,8	24,1	23,3	22,5	22,0	19,6
180	3,0	29,4	27,3	25,0	28,4	22,2	18,1
210	3,5	33,2	32,5	26,9	32,4	21,8	18,6
240	4,0	33,7	32,9	29,2	34,2	21,0	18,3
270	4,5	35,9	37,1	31,9	34,2	21,3	18,4
300	5,0	40,1	38,3	34,6	38,4	21,0	19,0
330	5,5	42,9	41,7	37,6	45,6	22,1	19,3
360	6,0	45,9	46,6	42,1	57,4	22,4	19,9
390	6,5	45,2	49,1	53,6	60,0	30,8	19,1
420	7,0	48,6	51,5	56,4	67,9	34,1	18,5
450	7,5	53,8	55,5	58,1	73,0	26,7	18,7
480	8,0	58,4	58,1	62,1	79,8	24,7	18,5
510	8,5	60,8	62,0	61,6	86,5	16,8	18,8
540	9,0	73,7	66,6	62,7	90,7	8,8	18,9
570	9,5	83,2	71,7	64,6	95,7	0,3	18,7
600	10,0	95,3	75,7	68,0	98,9	5,4	19,6
630	10,5	104,8	80,5	70,8	106,7	13,7	19,9
660	11,0	109,5	84,5	74,5	108,7	21,7	20,0
690	11,5	111,8	87,8	77,2	112,4	30,0	20,1
720	12,0	112,5	91,8	78,7	115,7	36,9	19,2
750	12,5	108,8	95,7	82,1	117,2	43,9	19,4
780	13,0	106,3	100,4	83,9	116,5	48,7	18,7
810	13,5	105,5	106,1	86,6	115,5	52,8	18,7
840	14,0	105,0	111,7	88,9	121,9	59,6	18,4
870	14,5	104,5	115,2	91,3	124,1	64,3	18,6
900	15,0	109,4	119,0	94,9	129,7	70,8	19,2
930	15,5	112,4	117,7	96,3	128,3	72,4	19,6
960	16,0	112,1	118,8	98,3	128,9	74,9	19,9
990	16,5	111,4	120,2	99,7	128,3	75,6	20,4
1020	17,0	109,5	122,0	101,2	126,4	75,0	19,4
1050	17,5	110,9	124,4	102,7	126,1	77,0	20,2
1080	18,0	109,5	126,3	104,5	128,0	77,9	20,4
1110	18,5	110,5	127,6	106,5	126,5	79,0	20,3
1140	19,0	115,1	129,3	108,1	126,9	81,4	20,4
1170	19,5	116,3	131,1	109,9	131,5	83,7	20,7
1200	20,0	119,3	132,3	111,5	133,8	85,6	20,6
1230	20,5	120,3	133,8	113,1	135,4	87,3	20,2
1260	21,0	121,4	134,8	114,3	133,7	88,5	20,4
1290	21,5	121,7	136,2	115,6	139,9	91,7	20,5
1320	22,0	120,8	136,2	116,8	140,1	92,6	20,4
1350	22,5	120,3	137,1	117,9	137,4	97,2	20,3
1380	23,0	120,7	139,0	119,2	135,2	99,1	20,4
1410	23,5	121,0	140,3	120,3	137,1	100,9	20,4
1440	24,0	120,6	140,8	121,1	135,5	107,2	20,4
1470	24,5	120,9	141,5	125,0	136,4	104,9	20,4
1500	25,0	120,5	141,9	125,1	135,3	105,2	20,5
1530	25,5	120,9	142,0	125,2	133,6	106,5	20,5
1560	26,0	119,5	140,9	125,3	133,6	105,0	20,7
1590	26,5	121,1	142,3	125,9	133,9	102,9	19,7
1620	27,0	121,1	142,7	126,3	133,7	105,1	20,2
1650	27,5	122,5	143,0	126,8	133,2	111,3	20,5

Time, s	Time, min	Tread	Tread	Tread	Sidewall Surface	Sidewall Surface	Ambient
1680	28,0	123,8	143,1	127,3	133,2	118,7	20,8
1710	28,5	124,8	143,3	127,5	133,7	121,2	19,5
1740	29,0	126,1	143,7	127,6	133,8	123,6	20,7
1770	29,5	127,2	143,8	128,3	137,7	115,9	18,5
1800	30,0	128,1	144,2	128,3	139,2	113,4	19,5
1830	30,5	130,1	144,1	128,9	134,2	112,8	18,7
1860	31,0	130,6	142,4	129,2	134,0	112,2	18,9
1890	31,5	131,3	141,2	129,5	131,1	112,3	19,1
1920	32,0	131,8	141,7	129,4	128,9	111,9	20,4
1950	32,5	132,5	141,6	129,5	127,9	112,6	20,6
1980	33,0	132,7	140,3	129,7	126,9	112,5	18,6
2010	33,5	133,2	140,7	129,8	126,5	112,8	19,4
2040	34,0	133,7	141,0	130,7	125,6	113,0	20,1
2070	34,5	134,3	141,5	130,8	125,6	113,5	20,6
2100	35,0	134,7	141,5	131,1	124,7	113,7	20,3
2130	35,5	135,1	141,6	131,3	124,4	113,9	20,0
2160	36,0	135,5	141,4	131,1	124,1	114,2	20,6
2190	36,5	135,9	141,6	131,6	123,9	114,2	20,3
2220	37,0	135,9	142,2	131,7	123,2	114,6	20,1
2250	37,5	135,6	142,1	131,8	122,8	114,8	20,0
2280	38,0	135,8	142,2	132,0	122,1	115,4	19,2
2310	38,5	136,4	142,4	131,3	123,1	116,0	20,3
2340	39,0	136,6	142,5	131,5	123,5	116,5	20,3
2370	39,5	137,2	142,6	131,6	124,0	117,2	20,5
2400	40,0	137,5	142,5	132,1	124,6	117,8	20,6
2430	40,5	137,8	142,5	132,5	124,9	118,4	20,5
2460	41,0	138,0	141,9	132,6	125,1	118,7	20,7
2490	41,5	138,0	142,6	132,8	125,1	119,2	20,7
2520	42,0	138,4	142,6	133,1	125,8	119,6	19,6
2550	42,5	138,5	142,8	133,3	126,1	120,2	18,2
2580	43,0	138,6	143,1	133,7	126,5	120,9	18,8
2610	43,5	139,0	143,4	134,0	127,1	121,6	20,1
2640	44,0	139,1	143,5	134,2	127,4	122,1	19,2
2670	44,5	139,1	143,6	134,3	127,7	122,6	20,7
2700	45,0	139,0	143,6	134,5	127,9	122,9	20,9
2730	45,5	139,1	143,6	134,7	128,1	123,3	19,0
2760	46,0	137,5	143,4	134,5	128,0	122,8	18,3
2790	46,5	138,1	144,1	135,3	128,7	124,4	17,8
2820	47,0	139,3	145,0	135,6	128,8	124,6	17,9
2850	47,5	139,8	145,5	135,9	129,2	124,7	19,7
2880	48,0	140,5	146,0	136,1	129,5	125,0	20,6
2910	48,5	140,3	146,3	136,3	130,1	125,0	20,7
2940	49,0	140,0	146,5	136,5	130,0	124,9	20,6
2970	49,5	139,9	146,9	136,6	130,1	125,3	18,6
3000	50,0	140,2	147,6	136,7	130,2	125,4	20,1
3030	50,5	140,4	148,0	136,9	130,6	125,5	20,7
3060	51,0	140,3	148,1	137,1	130,9	125,4	20,9
3090	51,5	140,4	148,5	137,3	131,5	125,8	19,9
3120	52,0	139,2	149,0	137,4	132,6	126,2	20,0
3150	52,5	140,0	149,4	137,5	132,9	126,7	19,0
3180	53,0	140,7	149,7	137,8	133,2	127,1	18,9
3210	53,5	141,1	150,0	138,0	133,4	127,4	18,8
3240	54,0	141,1	150,0	138,6	133,7	127,4	19,4
3270	54,5	141,3	150,3	138,4	133,5	127,9	18,5
3300	55,0	141,2	150,5	138,6	133,8	128,1	19,3
3330	55,5	141,5	150,8	138,9	134,4	128,7	19,4
3360	56,0	141,4	150,7	139,0	134,8	129,2	18,7
3390	56,5	140,9	150,3	139,0	134,6	129,2	20,5
3420	57,0	144,1	149,0	139,2	134,3	129,2	20,6
3450	57,5	144,4	149,1	139,3	134,3	129,1	20,8
3480	58,0	144,3	149,4	139,6	133,8	128,9	20,8
3510	58,5	143,5	149,6	139,5	133,4	128,9	18,8
3540	59,0	144,4	149,8	139,7	133,2	128,7	20,1
3570	59,5	144,8	150,0	140,0	132,9	128,8	20,4
3600	60,0	144,7	148,5	140,2	132,6	128,6	20,9
3630	60,5	144,1	148,4	140,3	132,4	128,6	20,8
3660	61,0	144,0	149,2	140,3	132,1	128,3	20,2
3690	61,5	143,0	149,4	140,2	133,2	129,0	19,3
3720	62,0	143,7	149,4	140,0	134,7	130,7	19,4
3750	62,5	144,8	149,5	140,3	133,7	130,4	19,9
3780	63,0	145,5	149,5	140,4	132,4	130,0	19,5
3810	63,5	145,9	149,6	140,6	131,2	129,7	20,0
3840	64,0	145,9	149,5	140,9	130,5	129,3	20,7
3870	64,5	146,0	149,6	141,0	130,0	128,6	21,0
3900	65,0	146,2	149,7	141,3	129,9	128,6	20,0
3930	65,5	146,3	149,6	141,2	129,9	128,5	19,9
3960	66,0	146,2	149,7	141,3	129,6	128,3	19,9

3990	66,5	144,6	149,7	141,6	129,8	128,4	20,6
4020	67,0	145,4	149,8	141,6	129,5	128,3	19,9
Time, s	**Time, min**	**Tread**	**Tread**	**Tread**	**Sidewall Surface**	**Sidewall Surface**	**Ambient**
4050	67,5	145,7	149,8	141,8	129,0	128,0	20,2
4080	68,0	145,9	150,0	141,8	128,6	128,0	20,4
4110	68,5	146,0	150,2	141,9	129,6	128,2	20,6
4140	69,0	145,8	150,1	142,0	129,6	128,3	20,5
4170	69,5	145,9	150,2	142,2	129,4	128,1	20,9
4200	70,0	145,8	149,2	142,2	129,3	128,0	20,9
4230	70,5	145,9	149,4	142,4	129,2	127,8	20,8
4260	71,0	145,9	149,4	142,3	128,8	127,9	21,1
4290	71,5	145,8	149,5	142,5	128,6	128,0	20,8
4320	72,0	146,0	149,5	142,7	128,4	127,9	21,0
4350	72,5	145,9	149,6	142,6	128,2	127,9	20,7
4380	73,0	146,0	149,5	142,7	128,3	128,1	20,8
4410	73,5	146,0	149,6	143,0	128,3	128,1	20,9
4440	74,0	146,1	149,7	142,9	128,3	128,2	21,0
4470	74,5	146,1	149,6	142,9	128,6	128,3	20,8
4500	75,0	146,2	149,7	143,0	128,7	128,2	20,1
4530	75,5	146,3	149,7	143,3	129,0	128,3	20,1
4560	76,0	146,5	149,8	143,4	128,9	128,3	20,8
4590	76,5	146,5	149,8	143,2	128,8	128,2	21,0
4620	77,0	146,3	150,0	142,5	130,3	130,7	20,7
4650	77,5	145,8	150,2	142,2	131,9	130,0	19,9
4680	78,0	146,8	150,1	142,7	130,3	127,6	20,8
4710	78,5	147,0	149,6	143,0	129,8	129,1	21,1
4740	79,0	147,0	149,5	143,4	129,3	130,0	20,5
4770	79,5	146,7	149,6	143,4	128,3	129,7	21,1
4800	80,0	146,5	149,2	143,8	126,7	129,3	19,9
4830	80,5	146,4	149,4	144,0	128,1	129,3	20,6
4860	81,0	146,5	149,4	144,2	127,8	129,4	19,5
4890	81,5	146,6	149,5	144,5	129,0	129,6	20,5
4920	82,0	146,8	149,5	144,7	129,4	129,8	20,9
4950	82,5	146,9	149,6	144,5	129,6	129,9	20,9
4980	83,0	147,2	149,5	144,7	130,0	130,3	20,8
5010	83,5	147,3	149,6	144,7	130,3	130,1	21,0
5040	84,0	147,4	149,7	144,9	130,5	130,5	20,7
5070	84,5	147,4	149,6	144,8	130,7	130,1	20,7
5100	85,0	147,5	149,7	145,1	130,8	129,8	20,8
5130	85,5	147,6	149,7	145,2	130,7	129,8	20,8
5160	86,0	147,7	148,5	145,1	131,1	130,0	20,9
5190	86,5	147,9	148,7	145,3	131,1	129,9	20,8
5220	87,0	147,9	148,7	145,4	131,3	130,0	20,6
5250	87,5	147,9	148,8	145,4	131,8	130,1	20,8
5280	88,0	147,9	148,8	145,4	132,4	130,4	21,0
5310	88,5	147,9	148,9	145,6	132,4	130,5	20,9
5340	89,0	148,0	148,9	145,7	132,8	130,8	20,8
5370	89,5	148,0	149,0	145,7	133,1	130,8	20,7
5400	90,0	147,9	149,1	145,8	133,8	131,2	20,7
5430	90,5	147,9	149,2	145,8	133,9	131,4	21,1
5460	91,0	147,9	148,1	146,1	134,1	132,3	20,9
5490	91,5	147,9	147,5	146,2	135,1	132,1	21,0
5520	92,0	148,1	148,1	146,2	135,2	132,1	20,7
5550	92,5	145,6	148,3	145,4	133,2	135,9	20,7
5580	93,0	144,4	148,5	145,0	135,0	137,3	20,8
5610	93,5	147,5	148,7	145,6	135,2	136,4	19,5
5640	94,0	148,6	148,8	146,0	135,5	135,6	20,9
5670	94,5	148,6	148,8	146,2	135,5	135,4	20,8
5700	95,0	148,3	148,9	146,4	135,3	135,3	20,9
5730	95,5	148,2	148,9	146,4	135,7	135,5	20,8
5760	96,0	148,2	149,0	146,5	135,8	135,6	20,9
5790	96,5	148,3	149,1	146,5	136,1	135,8	20,8
5820	97,0	148,3	149,2	146,6	136,1	135,8	20,6
5850	97,5	148,3	149,4	146,7	136,4	136,3	20,8
5880	98,0	148,4	149,4	146,8	136,3	136,2	20,8
5910	98,5	148,3	149,5	146,8	135,8	135,5	20,3
5940	99,0	148,3	149,5	146,8	135,6	135,3	20,9
5970	99,5	148,4	149,6	146,8	136,0	134,9	20,5
6000	100,0	148,3	149,5	146,9	135,1	134,8	21,2
6030	100,5	148,4	149,6	146,9	135,5	134,7	20,7
6060	101,0	148,6	149,7	147,0	134,0	134,9	20,5
6090	101,5	148,5	149,6	147,1	135,0	134,9	20,8
6120	102,0	148,7	149,7	147,1	135,4	135,0	20,9
6150	102,5	148,9	149,7	147,2	135,7	135,0	19,8
6180	103,0	148,9	149,8	147,3	135,3	135,2	20,4
6210	103,5	148,9	149,8	147,4	135,1	135,1	20,9
6240	104,0	148,8	150,0	147,4	136,1	135,9	21,4
6270	104,5	148,9	148,6	147,5	136,4	136,1	21,0

6300	105,0	149,0	148,3	147,6	136,8	136,1	20,8
6330	105,5	149,1	148,2	147,5	136,9	136,1	20,1
6360	106,0	149,4	148,2	147,7	137,9	137,0	19,3
Time, s	**Time, min**	**Tread**	**Tread**	**Tread**	**Sidewall Surface**	**Sidewall Surface**	**Ambient**
6390	106,5	149,6	148,3	147,9	138,2	137,5	18,1
6420	107,0	149,8	149,0	148,0	138,5	137,5	20,0
6450	107,5	150,0	149,1	148,0	138,8	137,6	19,5
6480	108,0	148,5	149,2	147,2	140,7	139,1	18,9
6510	108,5	148,4	149,4	146,6	140,0	139,4	20,2
6540	109,0	150,1	149,4	147,3	140,2	138,1	19,4
6570	109,5	150,5	149,5	147,6	140,1	138,5	19,4
6600	110,0	150,7	149,5	147,8	138,7	138,1	19,8
6630	110,5	150,8	149,6	147,9	138,6	138,1	20,4
6660	111,0	150,8	149,5	148,0	138,2	137,7	18,4
6690	111,5	150,8	149,6	148,1	137,7	137,4	20,6
6720	112,0	150,9	149,7	148,1	138,8	137,3	20,8
6750	112,5	150,9	149,6	148,1	139,0	137,0	21,1
6780	113,0	148,8	149,7	148,0	139,1	136,9	21,0
6810	113,5	148,9	149,7	148,1	139,2	136,7	20,8
6840	114,0	148,9	149,5	148,2	139,0	136,7	19,1
6870	114,5	149,0	149,5	148,2	138,6	136,6	20,8
6900	115,0	149,1	149,6	148,3	138,8	136,4	20,8
6930	115,5	149,2	149,5	148,3	138,5	136,4	20,8
6960	116,0	149,4	149,6	148,3	139,8	136,7	20,8
6990	116,5	149,4	149,7	148,4	137,7	136,7	20,8
7020	117,0	149,5	149,6	148,4	138,1	136,4	20,8
7050	117,5	149,5	149,7	148,5	138,8	136,6	20,7
7080	118,0	149,6	149,7	148,6	138,1	136,3	20,7
7110	118,5	149,5	149,8	148,5	138,9	136,4	20,6
7140	119,0	149,6	149,8	148,7	138,8	137,0	20,7
7170	119,5	149,7	150,1	148,7	139,0	137,1	20,4
7200	120,0	149,6	149,6	148,8	138,5	137,4	20,6
7230	120,5	149,7	149,5	148,8	138,5	137,2	20,6
7260	121,0	149,7	149,6	148,9	138,7	137,3	20,7
7290	121,5	149,8	149,7	148,9	138,7	137,3	20,7
7320	122,0	149,8	149,6	149,0	138,8	137,2	20,6
7350	122,5	150,0	149,7	149,1	138,9	137,4	19,4
7380	123,0	150,2	150,5	149,2	139,2	138,4	20,4
7410	123,5	150,1	150,7	148,1	138,5	139,2	20,9
7440	124,0	149,0	150,8	147,5	139,3	141,8	20,4
7470	124,5	149,5	150,8	148,1	138,8	141,3	20,5
7500	125,0	150,0	150,8	148,3	137,2	140,7	20,6
7530	125,5	150,5	150,9	148,5	137,9	140,3	20,6
7560	126,0	148,9	150,9	148,7	138,0	139,2	18,3
7590	126,5	148,9	148,8	148,8	138,3	138,8	20,6
7620	127,0	149,0	148,9	148,8	138,1	138,6	21,0
7650	127,5	149,1	148,9	148,9	138,3	138,9	20,2
7680	128,0	149,2	149,0	148,9	138,2	138,8	20,7
7710	128,5	149,4	149,1	149,0	138,6	138,5	20,7
7740	129,0	149,4	149,2	149,1	138,6	138,5	20,5
7770	129,5	149,5	149,4	149,2	138,5	138,8	18,0
7800	130,0	149,5	149,4	149,4	139,5	139,0	18,8
7830	130,5	149,6	149,5	149,4	139,8	139,1	20,7
7860	131,0	149,5	149,5	149,5	139,9	139,3	20,8
7890	131,5	149,6	149,6	149,5	140,0	139,4	20,3
7920	132,0	149,7	149,5	149,6	140,1	139,2	21,0
7950	132,5	149,6	149,6	149,5	140,2	139,2	21,0
7980	133,0	149,7	149,7	149,6	140,1	138,9	20,4
8010	133,5	149,7	149,6	149,7	140,4	139,0	20,9
8040	134,0	149,8	149,7	149,6	140,7	139,7	20,9
8070	134,5	149,8	149,7	149,7	140,9	139,3	20,9
8100	135,0	150,0	149,7	149,7	141,1	140,1	19,1
8130	135,5	150,2	148,8	149,8	140,9	139,9	20,4
8160	136,0	150,1	148,8	149,8	141,9	140,3	18,9
8190	136,5	149,6	148,9	150,0	143,1	141,3	18,5
8220	137,0	149,5	148,9	150,2	56,0	141,6	19,8
8250	137,5	149,6	149,0	150,1	143,8	141,7	19,2
8280	138,0	149,7	149,1	150,2	87,5	43,4	21,2
8310	138,5	149,6	149,2	150,3	143,3	43,6	19,8
8340	139,0	149,6	149,4	149,5	143,3	143,5	19,3
8370	139,5	149,5	149,2	150,2	143,3	143,5	19,5
8400	140,0	149,7	149,4	149,8	143,3	143,5	19,5

Appendix M: The warm up evaluation results of the top sidewall plate and tread sectors.

Graph M: The temperature profile of the top sidewall plate (courtesy of Apollo-Dunlop tyres).

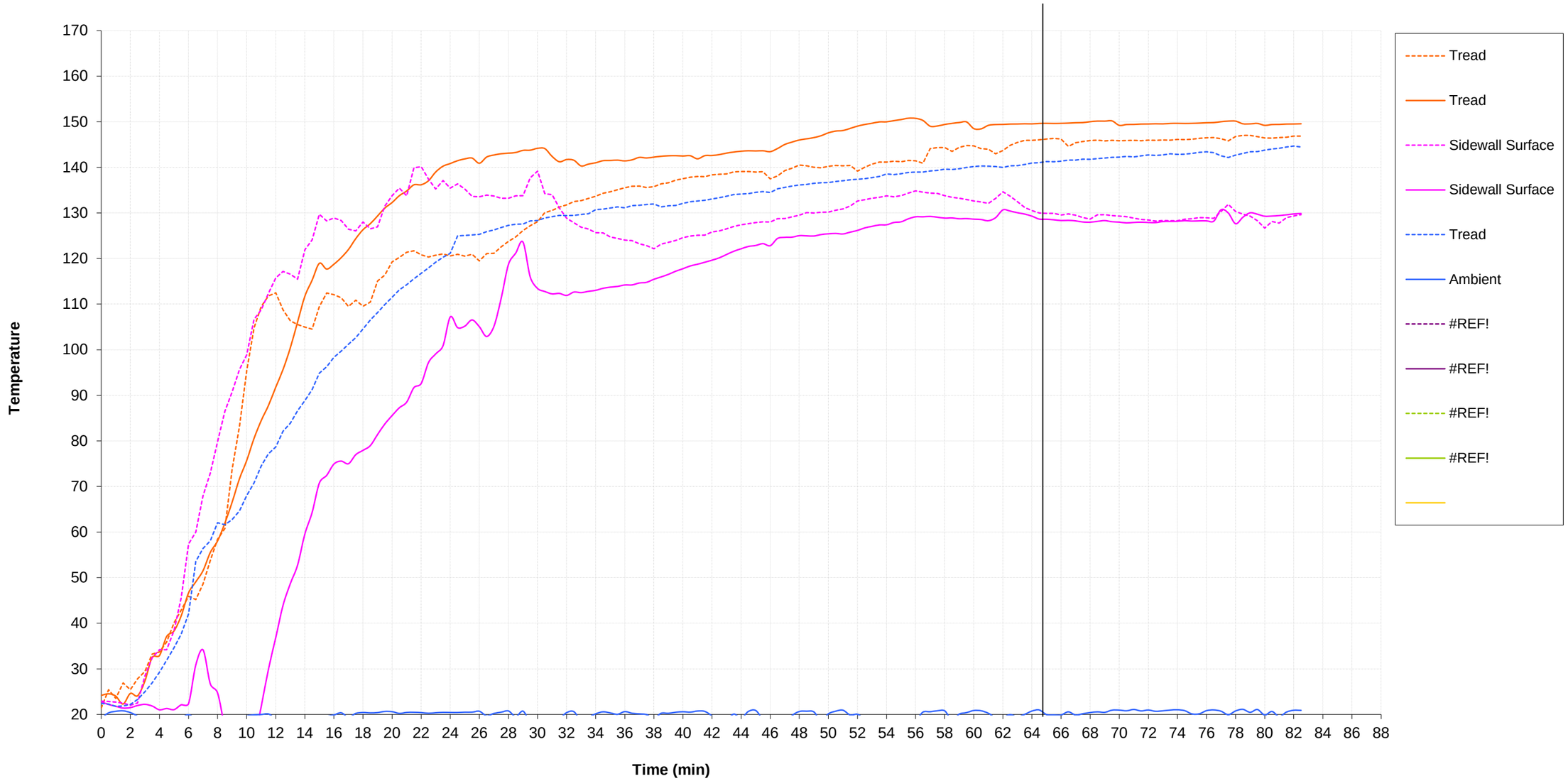

Appendix N: Simplified free convection heat transfer correlations for air.

Table N: The free convection correlations for air (Williams, 1984).

S.No.	Surface and its orientation	Laminar	Turbulent
1.	Vertical plate or cylinder	$\bar{h} = 1.42 \left(\frac{\Delta t}{L}\right)^{1/4}$ $(10^4 < Gr.Pr < 10^9)$	$\bar{h} = 1.32 (\Delta t)^{1/3}$ $(10^9 < Gr.Pr < 10^{13})$
2.	Horizontal cylinder	$\bar{h} = 1.32 \left(\frac{\Delta t}{D}\right)^{1/4}$ $(10^4 < Gr.Pr < 10^9)$	$\bar{h} = 1.25 (\Delta t)^{1/3}$ $(10^9 < Gr.Pr < 10^{12})$
3.	Horizontal plate: Heated surface facing up	$\bar{h} = 1.32 \left(\frac{\Delta t}{L}\right)^{1/4}$ $(10^5 < Gr.Pr < 2 \times 10^7)$	$\bar{h} = 1.67 (\Delta t)^{1/3}$ $(2 \times 10^7 < Gr.Pr < 3 \times 10^{10})$
	Heated surface facing down	$\bar{h} = 0.59 \left(\frac{\Delta t}{L}\right)^{1/4}$ $(3 \times 10^5 < Gr.Pr < 3 \times 10^{10})$	
4.	Spheres	$\bar{h} = [2 + 0.392 (Gr)^{1/4}] \frac{k}{D}$ $(1 < Gr < 10^5)$	

Appendix O: Process Flow Diagram (Steam Distribution).

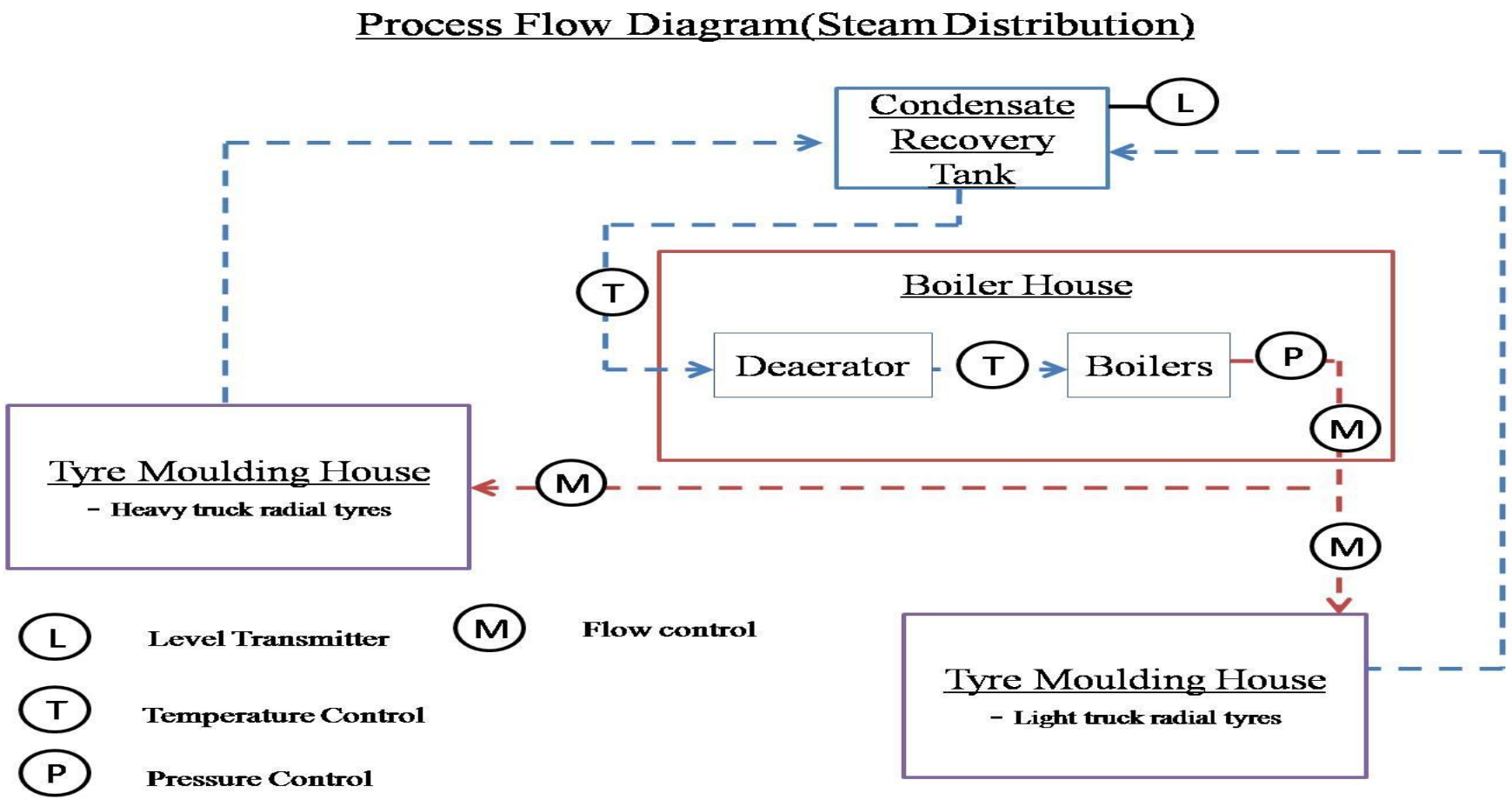

Fig. O1: Process flow diagram (steam distribution).